

Numerical Study on Debris Flow Behavior with Two Sabo Dams

A dissertation submitted in partial fulfillment for the requirement
Doctoral Degree in Civil and Earth Resources Engineering

by

Namgyun KIM

Supervised by Prof. Hajime NAKAGAWA



Disaster Prevention Research Institute

River Disaster Prevention Systems Laboratory

Department of Civil and Earth Resources Engineering

Kyoto University

Japan

2015

Abstract

Debris flows are very dangerous phenomenon in mountainous areas throughout the world. Debris flows involve the fluidized flow of earth, rocks, vegetation etc. In addition to causing significant morphological changes along riverbeds and mountain slopes, every year, debris flows also continue to ruin lives and damage properties.

Debris flow is the flow of a mixture water and solids, in which the solids are an assemblage of widely distributed grains. Therefore, an essential model of the mechanics of flow should simultaneously be considered. The rheological debris flow model depends on a variety of factors, such as sediment distribution, cohesive components, grain friction, and sediment concentration. Numerical models of debris flow based on the conservation of mass and momentum of the flow have been proposed by several researchers. These models can be classified as: the Bingham model, Dilatant model, Newtonian model, and non-linear viscoplastic models. However, the existing discrete element models that are suitable for discussing individual particle motion cannot treat solid-fluid interaction well, and more importantly, they cannot predict the macro behaviors, which is required in practice.

Numerical simulations are important for ensuring that countermeasures will be efficient before construction. Countermeasures designed to reduce debris flow disasters can be classified into structural and non-structural measures. Structural measures include Sabo dams, guide levees and training channels. Sabo dams are commonly used to mitigate debris flows and they are effective countermeasures against debris flow disasters. On the other hand, non-structural measures include warning systems, proper land use in areas, reinforcement of houses, etc.

To prevent or mitigate debris flow disaster, many efforts are made by the scientific and engineering communities in designing proper devices able to capture the debris flow volume. Sabo dams are an effective structural countermeasure for debris flow control. In fact, there are a many kinds of dams such as the closed-type, grid-type, slit-type, etc. In the closed-type Sabo dam, it is difficult to prevent it from losing its capturing capacity unless sediment is continuously removed. On the other hand, the open-type dam may keep its trapping capacity without sediment having to be removed.

Design consideration of a Sabo dam is very important in deciding dam construction. The control function of such Sabo dams have been reported through a number of studies. In order to

develop measures to increase the effectiveness of a Sabo dam, its control functions and design have been reported. In recent studies, experimental and numerical works have been performed in order to determine the general design criteria of Sabo dams. Nevertheless, there are few studies discussing the arrangement of Sabo dams.

The main objective of this study is to study the debris flow reduction effect by a series of Sabo dams. Numerical simulations and experiments have been carried out so as to investigate the debris flow deposition volume of a series of Sabo dams, and also to estimate debris flow discharges at a Sabo dam site using overflow equations. A one-dimensional numerical simulation method of debris flows is presented. Numerical simulations of debris flow were conducted including overflow discharge at the dam point and laboratory experiments were performed to validate the simulation results. Comparisons between the numerical simulation results and laboratory experimental results show reasonable agreement. Application of the numerical model used here is recommended for calculating overflow discharge at Sabo dam sites and evaluating the sediment-capturing effects of Sabo dam arrangements.

Keywords: *debris flow, sabo dam, overflow discharge, discharge coefficient.*

Acknowledgements

I would never complete of my dissertation without the support of many people. I am deeply thankful to them.

I am particularly grateful to my supervisor, Professor Hajime Nakagawa of Disaster Prevention Research Institute (DPRI), Kyoto University, for his valued guidance, advice, support, and encouragement while I carried my research work.

I would also like to deeply grateful to Professor Kenji Kawaike of DPRI at Kyoto University, for his patience, support, caring, and guidance. Especially, he helped me when I had a hard time.

I am deeply grateful to Prof. Hao Zhang and Prof. Masaharu Fujita for their valuable comments, and recommendations to refine the dissertation.

I am also grateful to Ms. Iguchi Natsuyo for her helping when I was in trouble. Also, I grateful to Ms. Himuro Tomoko.

Thanks to all of my colleagues with whom I studied while obtaining my PhD: Dr.Hiroshi Teraguchi, Dr. Hideaki Mizutani, Dr. Seungsoo Lee, Dr. Yeonjoong Kim, Dr. Amir Reza Mansoori, Dr. Masakazu Hashimoto, Mr. Shiro Nakanishi, Mr. Tomouki Ide, Mr. Masatoshi Ogura, Mr. Taichi Tachikawa, Mr. Osamu Kitaguchi, Mr. Shunsuke Hiratsuka, Mr. Nanahiro Tanaka, Mr. Taku Oomoto, Mr. Dongwoo Ko, Mr. Pawan Bhattarai, Mr. Rocky Talchabhadel, Ms. Yu Wang, Ms. Shoko Fujita, Mr. Shogo Harigae, Mr. Kei Nishio, Dr. Wansik Yu, Dr. Mikyung Choi, etc. Thank you for your advice and support.

I am also greatly indebted to my previous supervisor Professor Byonghee Jun, Kangwon National University, Republic Korea for bringing me into this world and always caring me. I am also greatly indebted to prof. Kyewon Jun and prof. Byungsik Kim.

I wish to express my greatest appreciation to the Monbukagakusho (Ministry of Education, Culture, Sports, Science, and Technology in Japan) for the financial support of my PhD study.

The last word of acknowledgement I am sincerely grateful to my mother, Wonjung Choi.

Namgyun KIM

Table of Contents

Abstract	i
1. Introduction	1
1.1 General	1
1.2 Literature Review	5
1.2.1 Classification of Debris Flow	5
1.2.2 Countermeasures	6
1.2.3 Numerical Model of Debris Flow	12
1.2.4 A series of Sabo Dams	12
1.3 Objectives of the Research	14
1.4 Outlines of the Dissertation	14
2. Experiments on Arrangement of Sabo Dams	15
2.1 General	15
2.2 Laboratory Experiments	17
2.2.1 Experiments of Debris flow Deposition by Arrangement of Sabo dams	18
2.2.2 Experiments of Debris flow Discharge by Arrangement of Sabo dams..	22
2.3 Results and Discussions	24
2.3.1 Deposition process by Arrangement of Sabo Dams	24
2.3.2 Discharge and Sediment Concentration without a Sabo Dam	28

2.3.3 Discharge and Sediment Concentration with a Sabo Dam.....	30
2.3.4 Sediment Distributions.....	33
2.4 Summary.....	35
3. Numerical Simulation of Debris Flow with Arrangement of Sabo Dams.....	37
3.1 General.....	37
3.2 Analysis of Debris Flow.....	39
3.2.1 Basic Equations.....	39
3.2.2 Erosion and Deposition Velocity Equations... ..	40
3.2.3 Bottom Shear Stress.....	42
3.3 Analysis of Arrangement of Sabo Dams.....	47
3.3.1 Boundary Conditions of Sabo Dam.....	47
3.3.2 Overflow Equations for Debris flow Discharge.....	48
3.4 Solution Methods.....	50
3.4.1 Calculation Method of Conservation of Momentum.....	50
3.4.2 Calculation Method of Conservation of Mass and Bed.....	53
3.5 Results and Discussions Compared with the Experimental Results.....	53
3.5.1 Debris Flow Deposition.....	54
3.5.2 Debris flow Discharge and Sediment Concentration.....	59
3.6 Summary.....	66
4. Estimation of Discharge Coefficient for Debris Flow	68
4.1 General.....	68

4.2 Experiment for Debris Flow Discharge Coefficient.....	69
4.3 Theoretical Analysis.....	72
4.4 Results and Discussions.....	73
4.4.1 Discharge Coefficient by arrangement of Sabo Dam.....	73
4.4.2 Discharge coefficient by Regression Analysis.....	78
4.5 Summary.....	96
5. Conclusions and Recommendations.....	97
5.1 Conclusions.....	97
5.2 Recommendations for Future Researches.....	99
References.....	101
List of Figures.....	105
List of Tables.....	109
Curriculum Vitae.....	110
Papers Based on the Thesis.....	111

CHAPTER 1

INTRODUCTION

1.1 General

Sediment erosion, and the subsequent transport and deposition cycle is a natural phenomenon. Sediments are caused by localized torrential downpours, earthquakes, volcanic eruptions, and so forth. These sediments are transported by water, wind, or the force of gravity acting on the particles. So, there are many types of sediment movement like landslide, slope failure, rockfall, riverbank collapse, debris flow and so on(Figure 1.1). However, these natural phenomena could be sediment-related disasters. Because urbanization continues to expand in mountainous areas, the risk of sediment-related disasters has increased. Since ancient times there have been many sediment-related disasters. At the same time, we have been controlling sediment-related disasters through countermeasures. However, we cannot protect ourselves from sediment-related disasters to save our properties and lives.

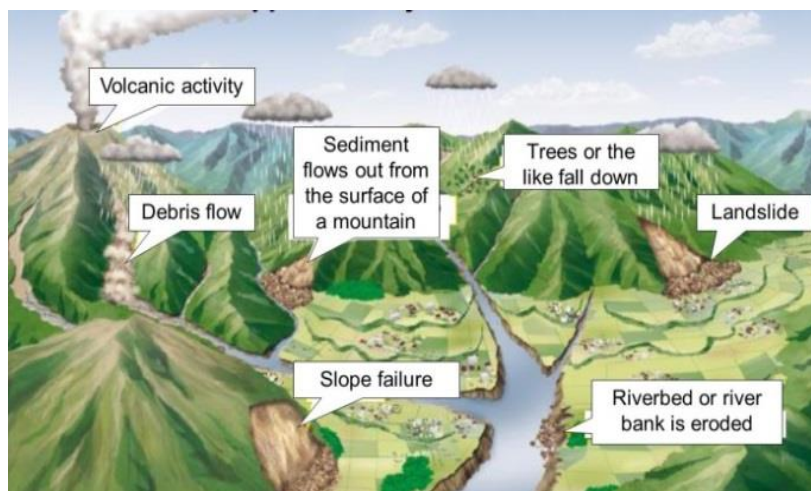


Figure 1.1 Sediment-related disasters(Photo source : DPWH, Japan)

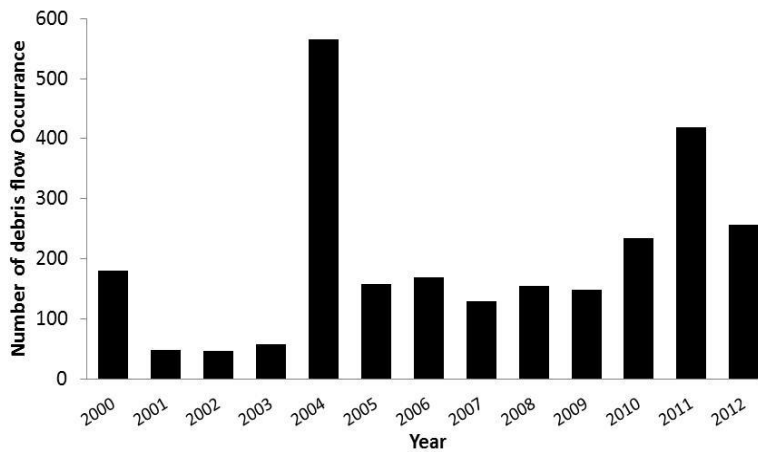


Figure 1.2 Number of debris flow occurrences in Japan(Data source : MLIT, Japan)

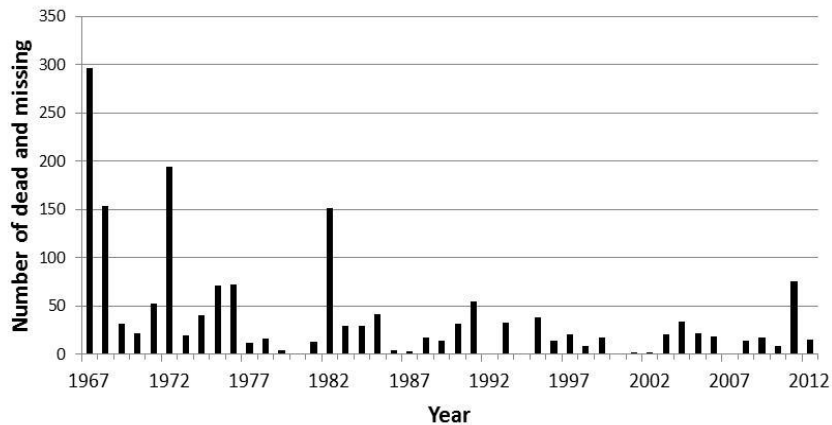


Figure 1.3 Number of dead and missing in Japan(Data source : MLIT, Japan)

There are various types of mass movement involving water and sediments: lahars, debris flows, debris avalanches, granular flows, hyperconcentrated flows, and mud flows. It may difficult to distinguish one phenomenon from another. The criteria for making such distinctions are different from researcher to researcher. Debris flow is mass movement involving water and air. Debris flows have been defined by many previous researchers. The generic term “debris flow” can be divided into “open-slope debris flow” and “channelized debris flow”(Evans. 1982). It is “a type of mass movement that involves water-charged, predominantly coarse-grained inorganic and organic material flowing rapidly down a steep confined, pre-existing channel”(VanDine 1985). “Debris flows occur when masses of poorly-sorted sediment, agitated and saturated with water surge down slopes in response to gravitational attraction.”(Iverson 1997). “Debris flow is a mixture of sediment and water flowing as if it was a continuous fluid driven by gravity, and it attains great mobility due to the enlarged void space saturated with water or slurry.”(Takahashi

2007). Therefore, a debris flow starts upstream of mountainous area and is a common type of mass movement.

Debris flows are found in mountainous environments, and they consist of fully saturated mixtures of water, sediment, and debris. Debris flows are widely recognized as one of the geomorphic processes in steep mountainous areas. Debris flows are initiated high on the slope of a hill when unconsolidated material becomes saturated and unstable or originate directly from landslides. They contain various particle sizes from fine material to large boulders from the channels and these large boulders accumulate at the front of the flow. It can flow down several kilometers and damage any residential areas at the foot of the mountain. Debris flows frequently cause extensive damage to property and loss of life. Because of their high density and speed, they have huge destruction power. In addition, debris flows can cause morphological changes, serious casualties, and damage to property.

Figure 1.2 shows the number of occurrences of debris flow in Japan. Figure 1.3 shows the number of dead and missing due to debris flow in Japan. Debris flows occur annually and almost every year, people are threatened with debris flow disasters. Therefore, to mitigate debris flow hazard, it is important to understand debris flow through past events. Figure 1.4 shows the debris flow disaster that occurred on July 20, 2003 at the city of Minamata in Kumamoto Prefecture, Japan. Figure 1.5 shows the debris flow disaster that occurred on July 18, 2004 at the city of Sabae in Fukui Prefecture, Japan.

Countermeasures designed to reduce debris flow disasters are classified into structural and non-structural measures. Structural measures include Sabo dams, guide levees, and training channels, while non-structural measures include warning systems, proper land use in subject areas, reinforcement of houses etc. Sabo dams are an effective structural countermeasure to control debris flow. They play an important role in the management and development of a river basin. Sabo dams can be distinguished into two types: the closed and the open dam (Di Silvio., 1990; Armanini et al., 1991). Closed-type Sabo dams intercept debris flow to downstream. In contrast, open-type Sabo dams are constructed with suitable openings in the body of the structure. Therefore, part of the sediment is allowed to pass through. These two types of Sabo dams are constructed in series along the channel.

The advance of science and technology has led to better countermeasures for mitigating debris flow damage. To increase the effectiveness of Sabo dams, the control functions of such dams have been reported. Such Sabo dam functions have been described in many laboratory experimental studies and numerical simulation studies (Honda et al., 1997; Imran, J. et al., 2001). Also, considerable theoretical and numerical works have been undertaken on the size, shape and structure of Sabo dams (Mizuyama et al., 1988; Johnson et al., 1989). These studies contribute to technical standard guidelines on debris flows.



Figure 1.4 Debris flow at Hougawachi, Kumamoto Prefecture, Japan
(Data source : Asia Air Survey Co., Ltd)



Figure 1.5 Debris flow at Kuratsukuri, Miyama Town, Asuwa Gun, Fukui Prefecture Japan
(Data source : SABO Dept. MLIT, Japan)

However, further studies are required in order to develop general guidelines on a series of Sabo dams. Few studies have reported the control functions of a series of Sabo dams. Therefore, the main objective of this study is to develop a reliable method to mitigate debris flow disasters with a series of Sabo dams through laboratory experiments and numerical simulations.

1.2 Literature review

1.2.1 Classification of Debris Flow

Various classifications of mass movement have been proposed. Varnes(1978) classified five kinematically distinct types of movement in the sequence: fall, topple, slide, spread, and flow.

Takahashi(2001) classified subaerial mass flows consisting of granular materials focusing attention on the essential mechanisms for controlling the phenomena(Figure 1.6).

Table1.1 Varnes' classification of slope movements

Type of Movement		Type of material		
		Bedrock	Engineering soils	
			Predominantly coarse	Predominantly fine
Falls		Rock fall	Debris fall	Earth fall
Topples		Rock topple	Debris topple	Earth topple
Slides	Rotational	Rock slump	Debris slump	Earth slump
	Translational	Rock block slide Rock slide	Debris block slide Debris slide	Earth Block slide Earth slide
Lateral Spread		Rock spread	Debris spread	Earth spread
Flows		Rock flow	Debris flow	Earth flow
		(deep creep)	Soil creep	
Complex		Combination of two or more principal types of movement		

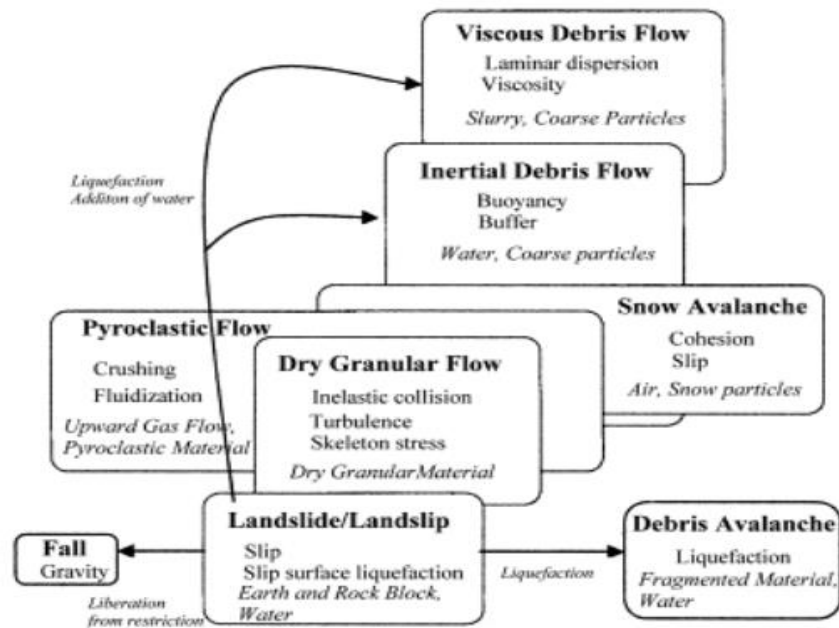


Figure 1.6 Takahashi's classification of slope movements

(Data source : Takahashi, T.: Debris flow: Mechanics, Prediction and Countermeasures)

1.2.2 Countermeasures

Countermeasures designed to reduce debris flow disasters are usually classified into structural and non-structural measures. Structural measures include Sabo dams, guide levees and training channels, while non-structural measures include warning systems, proper land use in subject areas, reinforcement of houses etc. Egashira(2007) classified measures into direct and indirect methods against landslides and debris flow(Figure 1.7). Structural countermeasures are designed to effectively control debris flow occurrence, runoff, discharge and so on. On the other hand, non-structural measures are designed to mitigate loss of property and life through systems like warning and evacuation.

Structural countermeasures

As mentioned above, there are several kinds of structural countermeasure against debris flow. One of them, the Sabo dam, is an effective structural countermeasure to control debris flow. The Sabo dam plays an important role in the management and development of a river basin. Sabo dams can be distinguished into two types: closed and open dams(Di Silvio., 1990; Armanini et

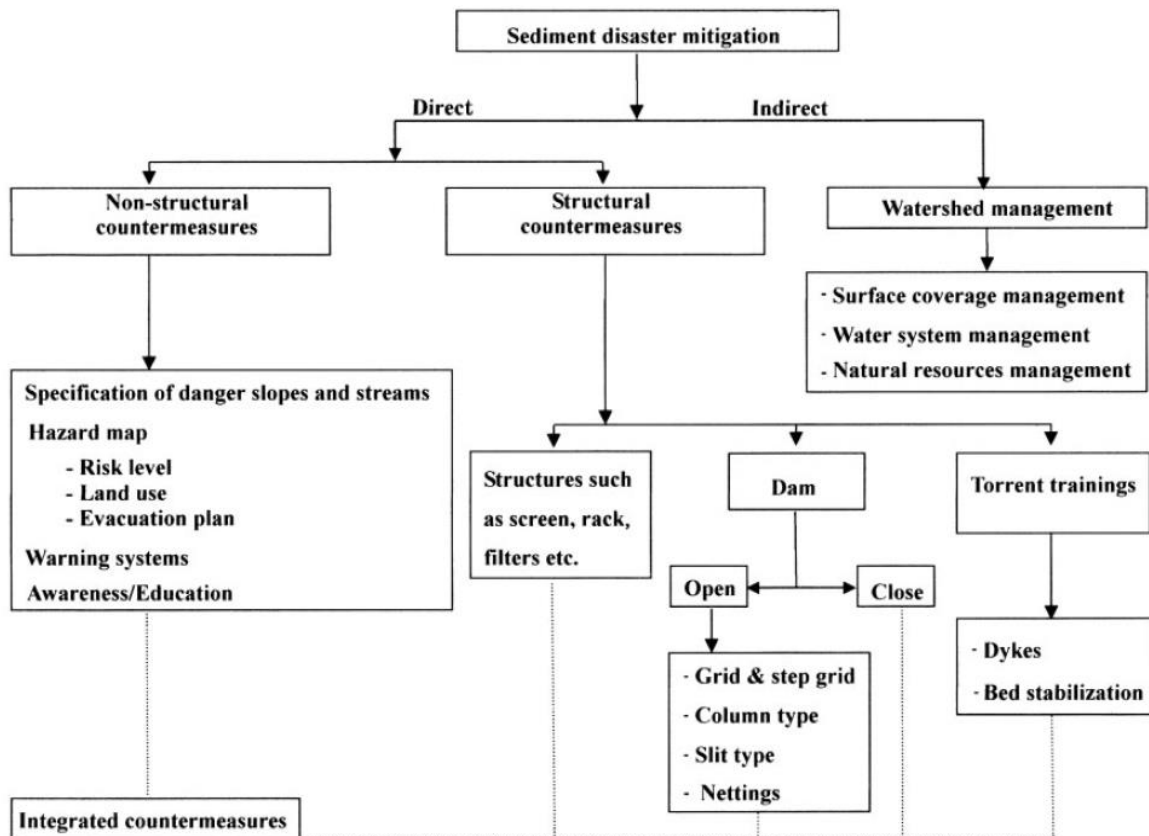


Figure 1.7 Classification countermeasures against sediment hazards(Egashira., 2007)
 (Data source : Egashira, S.: Review of Research Related to Sediment Disaster Mitigation)

al., 1991). Closed-type Sabo dams intercept debris flow to downstream. In contrast, open-type Sabo dams are constructed with suitable openings in the body of the structure. Therefore part of the sediment is allowed to pass through. These two types of Sabo dam are constructed in series along the channel.

Lateral walls(training channel)

Lateral walls are constructed parallel to the desired path of the debris flow. Figure 1.8 shows the design of lateral walls along the lower portion of the transportation zone of Alberta Creek, Canada.

Closed-type Sabo dam

The closed-type Sabo dam is designed to mitigate debris flow or to stop debris flow. However, the closed-type dam is soon filled by sediment in areas of active sediment yield, decreasing its sediment storage capacity, thus, it cannot control debris flows successfully if it loses its storage capacity. Figure 1.9 shows a closed-type Sabo dam before and after filled up sediment.

Open-type Sabo dam

The purpose of the open-type Sabo dam is that it is an eco-friendly structure that self-cleans debris deposition upstream of the dam. The main part of the dam is composed of a grid, silt or screen structure. With an open-type Sabo dam, the upstream part and downstream part are continuous. Therefore, sediment carried by usual flow can take the deposited sediment and transport it downstream. However, self-cleaning is rarely occurs because the usual flow is not large enough to erode the deposited sediment. Figure 1.10 shows an open-type Sabo dam.



Figure 1.8 Lateral walls(channel)
(Data source: British Columbia)



(a) Before filled with up debris flow



(b) After filled with up debris flow

Figure 1.9 Debris flow captured by a closed-type Sabo dam . Oita Prefecture, Japan, 12 July, 2012.

(Data source : MLIT)



(a) Grid Sabo dam in Gifu Prefecture, Japan
(Data source : Shresta et al., 2008)



(b) Silt Sabo dam at Kanagawa Prefecture, Japan in 2003 (Data source: Kanagawa Prefectural government)



(c) Ringnet (Data source : http://www.wsl.ch/fe/gebirgshydrologie/masse/bewegungen/projekte/KTI_Murgang/barrier_EN)

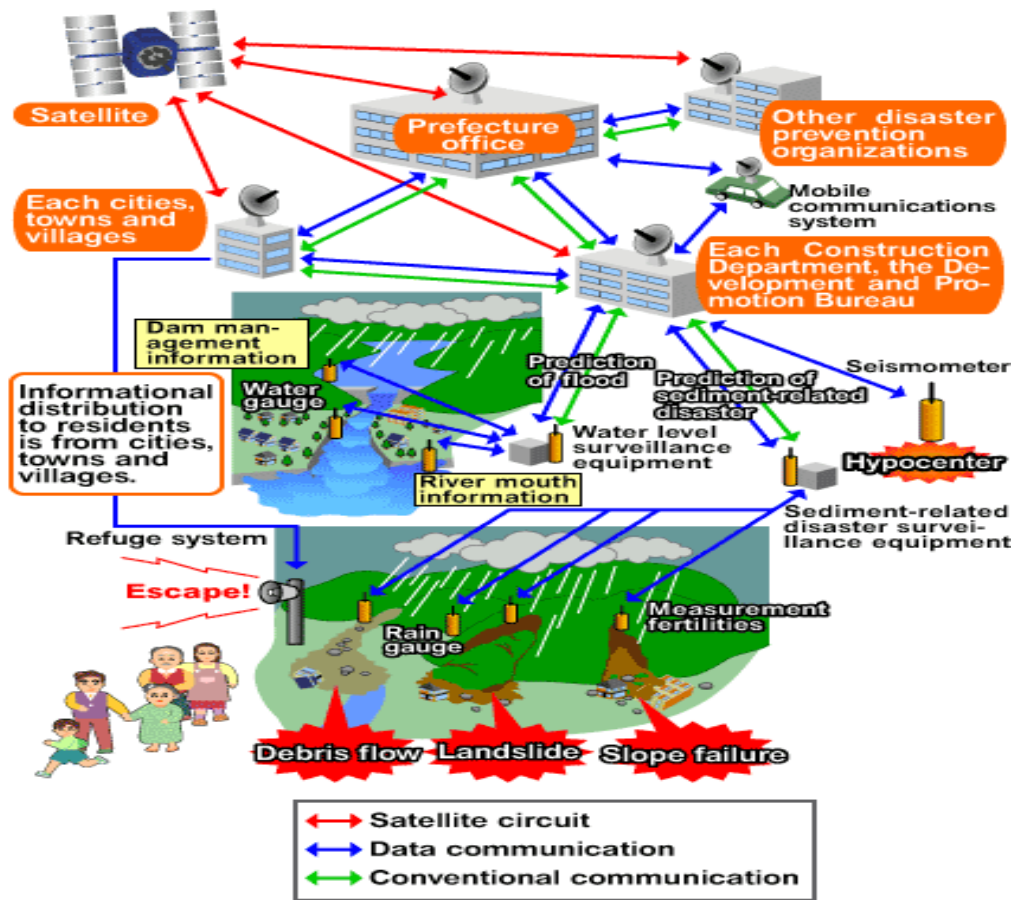


(d) Debris breaker in Hodaka, Japan 2014

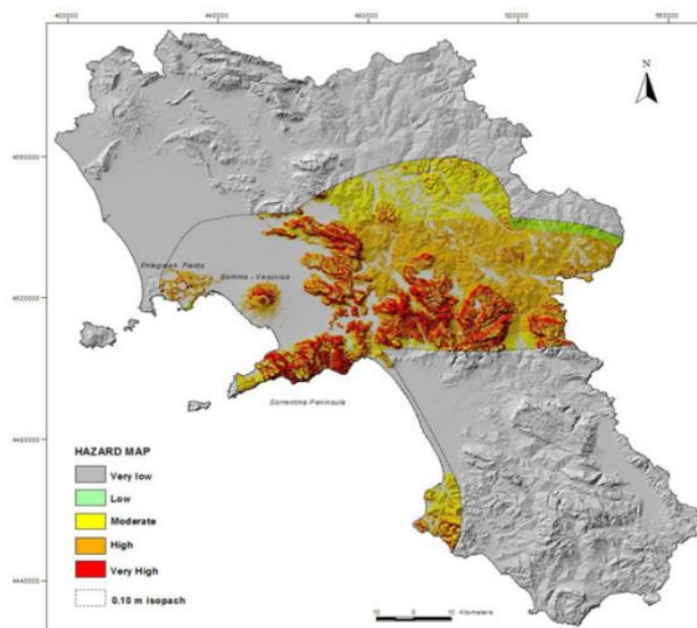
Figure 1.10 Open-type Sabo Dam

Non-Structural countermeasures

In order to provide maximum protection for people's lives, it is important to establish non-structural measures along with structural countermeasures because debris flows cannot be fully controlled by structural countermeasures. Non-structural countermeasures aim to mitigate damage by establishing disaster information communication systems. There are two main non-structural countermeasures. The first is the warning and evacuation system. The other is the hazard map. Figure 1.11 shows non-structural countermeasures.



(a) Warning and evacuation system (Data source : Wakayama Prefectural government)



(b) Example of a hazard map(Data source:INGV, Italy)

Figure 1.11 Non-structure countermeasure

1.2.3 Numerical Model of Debris Flow

Many researchers have developed various numerical models for the simulation of debris flow based on rheological models. The rheological properties depend on a variety of factors. Based on respective rheological models, dynamic approaches have been utilized. Respective rheological models can be classified into Bingham flow (Johnson, 1970; Hunt, 1994), dilatant flow (Bagnold, 1954; Takahashi, 1978), and turbulent flow (O'Brien and Julien, 1993). At the same time, empirical-statistical approaches have been utilized. Takahashi (1991) presented empirical formulas for the thickness and probable maximum length of debris-flow deposits to delineate debris-flow hazard areas. Based on experimental data, Shieh and Tsai (1997) built the relationships among the maximum length, width and thickness of debris-flow-affected areas. These many kinds of numerical models developed can analyze debris flow and evaluate the control function of Sabo dams. However, an essential remaining problem is how the constitutive equation is obtained between particles and the interstitial fluid. Thus, flow is considered using a one-phase constant-density fluid model (O'Brien et al., 1993) or a two-phase model (Takahashi and Nakagawa, 1994; Egashira et al., 1997). The one-phase model is usually used to analyze mud flow, whereas the two-phase model is used for simulation of granular flow. Lately, debris flow theories tend to utilize the two-phase model.

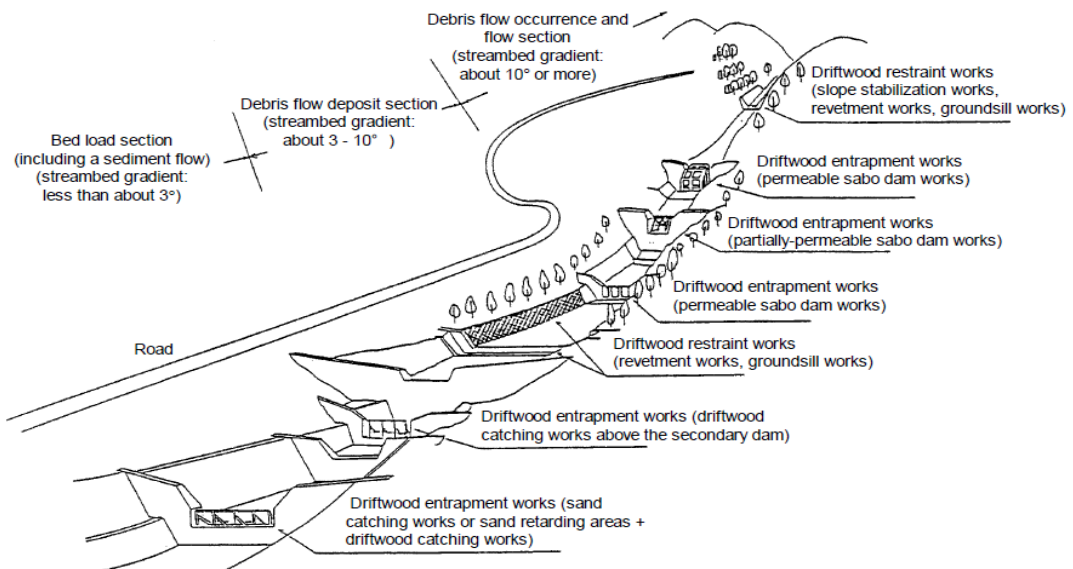
1.2.4 A series of Sabo Dams

The Sabo dam is one of the most effective countermeasures to mitigate debris flow. The advance of science and technology has led to better countermeasures for mitigating debris flow damage. To increase the effectiveness of a Sabo dam, the control functions of such dams have been reported. Such Sabo dam functions have been described in many laboratory experimental studies and numerical simulation studies (Honda et al., 1997; Imran, J. et al., 2001). In the real field, not just one Sabo dam but several Sabo dams are installed on the channel to control the debris flow. Figure 1.12 shows a series-type Sabo dam. These plans should consider the relationships between each Sabo dam. Fujita et al. (2001), Nakatani et al. (2009) studied the function of a series of Sabo dams in sediment runoff control using a numerical simulation. However, further studies are required so as to develop general guidelines on a series of Sabo dams. Few studies have reported the control functions of a series of Sabo dams.



(a) A series of Sabo dams in Nagano Prefecture

(Data source : http://www5.plala.or.jp/Y_YUKI/SABO/qa.html)



(b) Concept of layout of driftwood countermeasure facilities(MLIT)

Fig.1.12 A series of Sabo Dam

1.3 Objectives of the research

The main objective of this study is to study debris flow reduction effect by a series of Sabo dams through numerical simulations and laboratory experiments. Some of the objectives of this research are as follows.

1. To develop a one-dimensional numerical model of the debris flow reduction effect by a series of Sabo dams
2. To suggest a calculation method for estimating debris flow discharge at a series of Sabo dams.
3. To investigate the effectiveness of a series of Sabo dams in reducing the debris flow.
4. To suggest a discharge coefficient for a series of Sabo dams in the case of debris flow.

1.4 Outlines of the Dissertation

This research consisting of five chapters is organized as follows.

Chapter 1 presents a brief review of the previous literature, background to the work, and objectives of the study.

Chapter 2 presents laboratory experimental studies to calculate debris flow outflow discharge and sediment concentration at a Sabo dam, and to obtain data on debris flow deposition upstream of a series of Sabo dams.

Chapter 3 presents a numerical simulation model of debris flow with a series of closed-type Sabo dams. Overflow equations and free overfall equations are presented to evaluate debris flow discharge at the dam position.

Chapter 4 presents a discharge coefficient for debris flow. The discharge coefficient of the overflow equations and free overfall equations is estimated through regression analysis.

Chapter 5 summarizes the conclusions of the study and recommendations for the future researches.

CHAPTER 2

EXPERIMENTS ON

ARRANGEMENT OF

SABO DAMS

2.1 General

In mountain areas, Sabo dams are an effective structure for the control of the debris flow. Sabo dams are installed to reduce sediment runoff by storing sediment in the channels of steep gullies to mild channel beds. Sabo dams have three functions when installed on channels: 1) to reduce sediment runoff volume; 2) to reduce the channel gradient; 3) to protect against failure of the sidewall of the valley. When installed on debris slides, the volume of reduction shall be distributed over the design sediment storage capacity of the Sabo dam. The sediment storage capacity of the Sabo dam is determined by normal sediment gradient and planned sediment gradient. Figure 2.1 shows the sediment storage capacity of Sabo dam. When a Sabo dam is installed on the channel, sediment starts to accumulate upstream of the Sabo dam due to debris flow. After the Sabo dam is filled up to a stable state by sediment, debris flow flows to downstream of the Sabo dam. At this time, some sediment is deposited temporarily on the stable slope because the gradient is changed more gently from channel gradient to normal sediment gradient. This amount of sediment is the potential storage volume. This sediment is removed by flat flow and once again the potential storage part is empty. When debris flow occurs again, this potential storage part catches the sediment. Through this process debris flow is controlled by the Sabo dam. Figure 2 shows the debris-flow-capturing process.

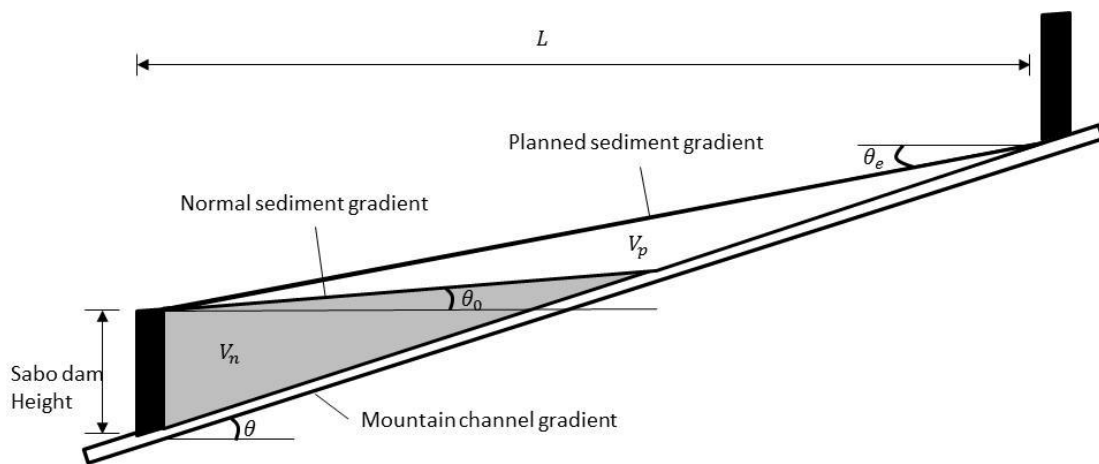


Figure 2.1 Sediment storage capacity of a Sabo dam.

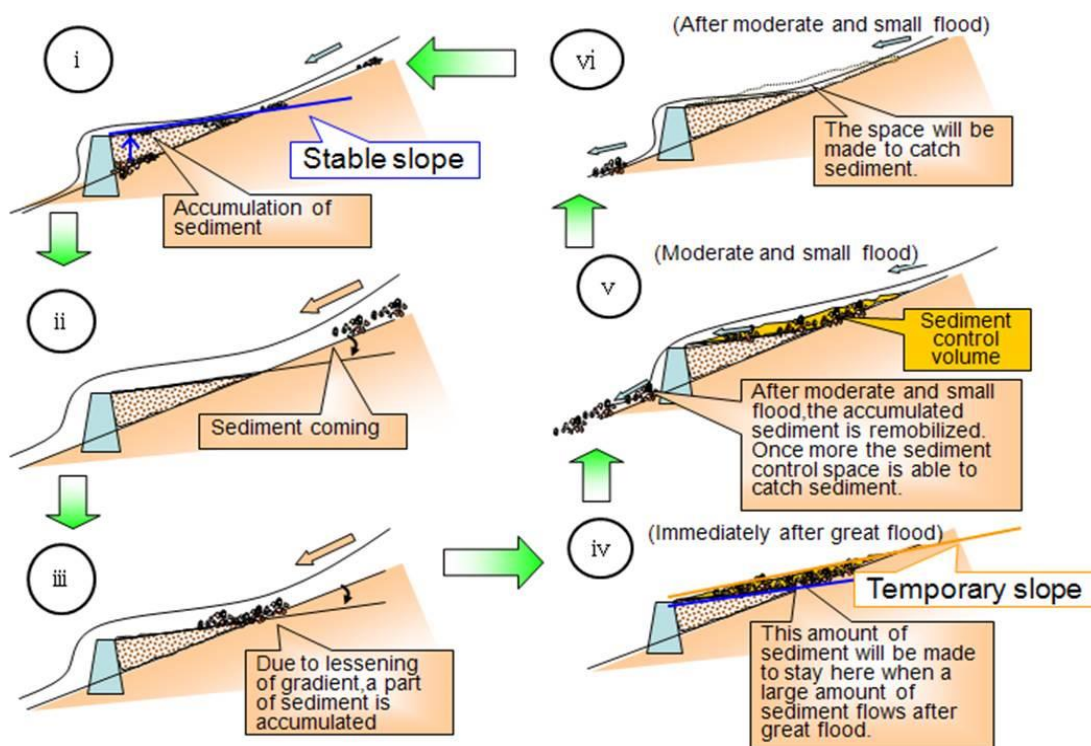


Figure. 2.2 Debris-flow-capturing process(MLIT)

As stated above, Sabo dams are installed not singly in one channel. When a series of Sabo dams is installed, the relationships among each of the Sabo dams are important for controlling the debris flow effectively.

As shown in Figure 2.2, the spacing between Sabo dams depends on the channel gradient, dam height, and angle of deposition of material behind the dam. Chatwin et al. (1994) provides a formula for the spacing of Sabo dams:

$$L > \frac{H_d}{\tan(\theta - \theta_e)} \quad (2.1)$$

where L is the minimum between Sabo dams, H_d is the height of dam, θ is original channel gradient, and θ_e is the equilibrium bed slope.

Minimum spacing between dams is determined by the capture volume of the Sabo dam. Since the evaluation of the control function of Sabo dams is based on the assumption that Sabo dams are initially filled with sediment up to the crest level, estimation of the sediment volume trapped by each Sabo dam is carried out based on the potential storage volume (V_p) of each dam, which can be defined by the equilibrium and initial bed deposition slopes. V_p is described as follows.

$$V_p = \frac{(H_d \cos\theta)^2 B}{2} \left\{ \frac{1}{\tan(\theta - \theta_e)} - \frac{1}{\tan(\theta - \theta_0)} \right\} \quad (2.2)$$

where H_d is height of the dam, B is the flow width, and θ_0 is the initial bed slope of the storage area before the occurrence debris flow.

Minimum spacing between Sabo dams is determined according to the potential storage volume. This potential storage volume is determined by the planned sediment gradient and normal sediment gradient. The slope of normal sediment gradient is half of the tangential value of the original bed slope. And the slope of the planned sediment gradient is two-thirds of the tangential value of the original bed slope. These values are derived from past disasters (Osansi 2010). Another way is where the storage volume of the Sabo dam can be changed according to the distance between two Sabo dams. In other words, the potential storage volume depends on the distance between two Sabo dams.

2.2 Laboratory Experiments

To understand the reduction effects of debris flow discharge and to clarify debris flow deposition upstream of Sabo dams, experiments were carried out in two flumes located at the Ujigawa Open Laboratory of the Disaster Prevention Research Institute, Kyoto University, Kyoto, Japan.

2.2.1 Experiments of Debris Flow Deposition by Arrangement of Sabo Dams

Experimental setup

Initially, a recirculating flume is used to study debris flow deposition upstream of Sabo dams. The flume length is 4.7 m, 20 cm high, 10 cm wide, slope 18° (Figure 2.3). This flume is divided into two parts by a 10 cm high sand stopper. The upper part of the flume is movable bed, and the lower part is fixed bed. In the movable bed, sediment deposition height is 10 cm.

Debris flow is generated upstream of the sand stopper and generated debris flow flows to downstream of the sand stopper. At the downstream part of the flume, the first Sabo dam is set 10 cm above the outlet of the flume and the second Sabo dam is set at 30 cm, 55 cm, 80 cm, respectively, above the first Sabo dam (Figure 2.4). The height of the Sabo dams is 6 cm high, the thickness is 1 cm, and they are the closed-type.

At the upstream part of the flume, a sediment bed of 1.5 m long and 10 cm deep is positioned 3 m to 4.5 m upstream measured from the outlet of the flume (Figure 2.5). The sediment consists of gravel sand (G1 and G2) and silica sand (S1, S2, S3, S4, S5 and S6). Table 2.1 shows the median value of diameters and mixing ratio of the sediments. Figure 2.6 shows the particle size distribution of mixed sediment. Mixed sediment materials are mean diameter $d_m = 2.86$ mm maximum diameter $d_{max} = 15$ mm and density $\sigma = 2.65$ g/cm³. The internal friction angle of a sediment is $\tan \phi = 0.7$.



Figure 2.3 Experimental flume

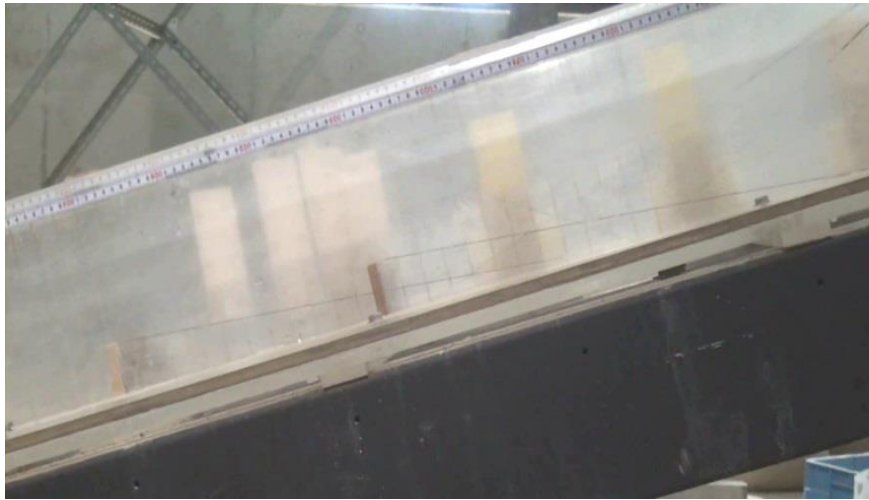


Figure 2.4 Experimental Sabo dam

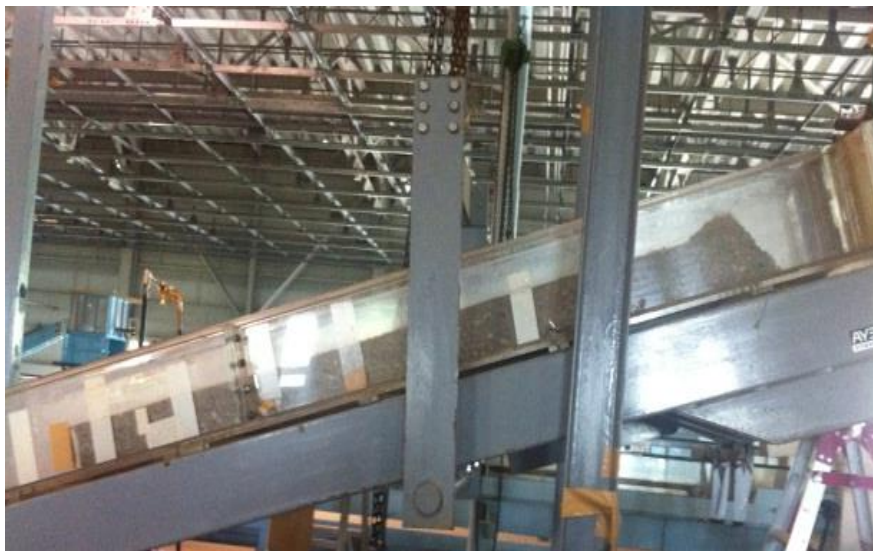


Figure 2.5 Upstream deposited sediment

Table 2.1 Sediment Material

Type	G1	G2	S1	S2	S3	S4	S5	S6
D ₅₀ (mm)	15	10	4.26	2.56	1.85	0.94	0.67	0.29
Ratio	1	2	1.5	1	1	1	1	0.5

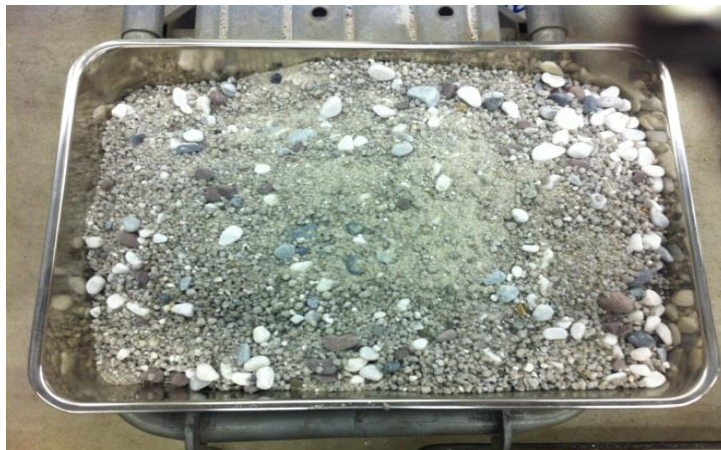
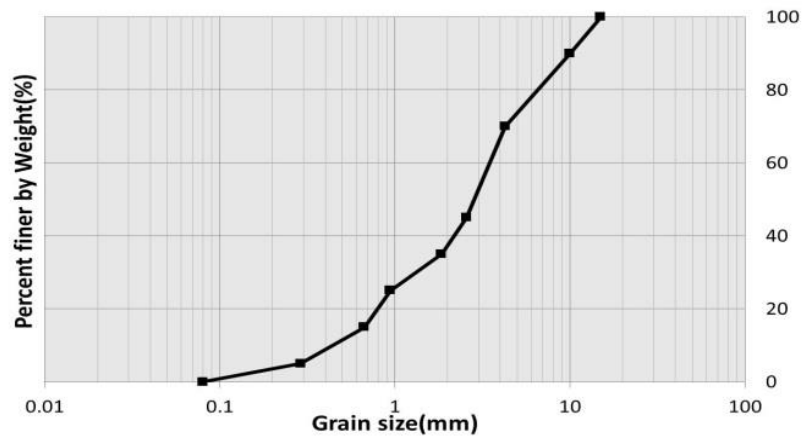


Figure 2.6 Particle size distribution of sediment materials

Experimental methods

To generate debris flow, water is supplied to the deposited sediment upstream of the flume. Under dry conditions, debris flow is not generated. Thus, before water is supplied, the deposited sediment bed should be saturated (Figure 2.7). There are two pumps. The main pump (a) supplies a constant water discharge to generate debris flow, and the other pump (b) supplies a little water discharge to saturate the sediment bed. While the bed is being saturated, the water level should be lower than the height of the sediment bed. If the water level is higher than the height of the sediment bed, the sediment bed will collapse. In order to prevent this situation, additional sediment is provided at the upstream end of the sediment bed. After fully saturating the sediment bed (a thin water layer is formed on the sediment bed), debris flow is generated by supplying the water using the main pump. The generated debris flow goes to the downstream part of the flume, and it is captured by the Sabo dams. This process is recorded by video cameras (Figure 2.8).



Figure. 2.7 Upstream part of the flume

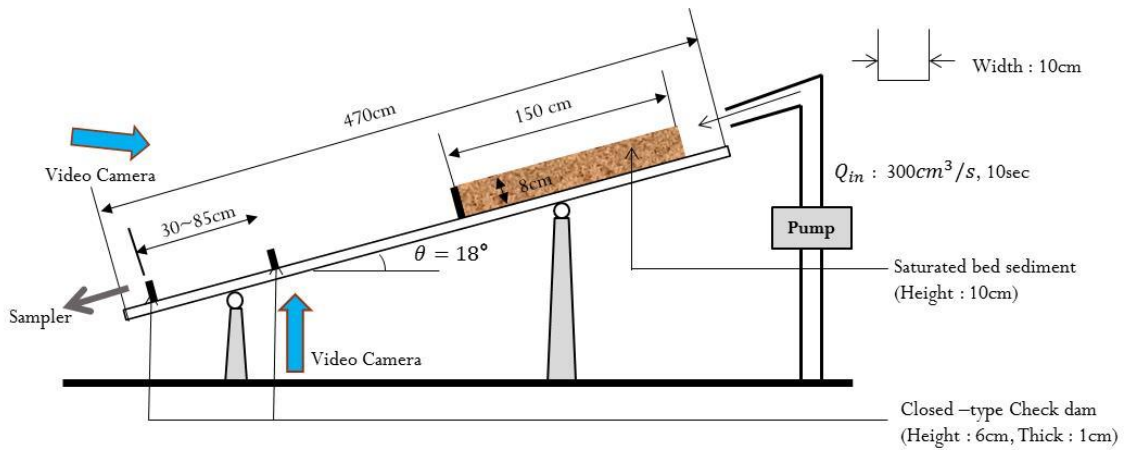


Figure. 2.8 Experimental method

Experimental conditions

Table 2.2 shows the experimental conditions. Experimental cases are divided by distance between two Sabo dams and supply water time. Case A and B mean that the durations of supply water are 10 and 20 seconds, respectively. Case 1, 2 and 3 mean that the distances between Sabo dams are 30cm, 55cm, and 80cm respectively. As the height of each Sabo dam is 6cm, the standard distance between two Sabo dams are around 55 cm through Equation (2.1). Therefore, the distance between the Sabo dams is set to be shorter and further, respectively, than the standard.

Table 2.2 Experimental conditions

Experiment no.	Supply water discharge (cm ³ /s)	Time (sec)	Distance between each dam (cm)	Movable bed height (cm)
Case.A-1	300	10	30	10
Case.A-2	300	10	55	
Case.A-3	300	10	80	
Case.B-1	300	20	30	
Case.B-2	300	20	55	
Case.B-3	300	20	80	

Table 2.3 Experimental conditions

Experiment No.	Supply water Discharge (cm ³ /s)	Time (sec)	Distance of each dam (cm)	Movable bed height (cm)
Case.C-1	300	20	30	8
Case.C-2	300	20	55	
Case.C-3	300	20	80	

2.2.2 Experiments of Debris flow Discharge by Arrangement of Sabo Dams

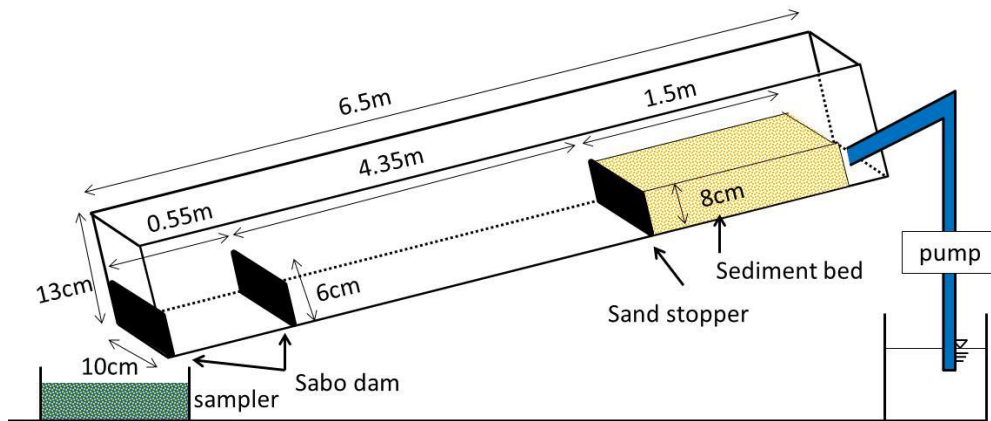
This experimental method is similar to the above experimental method. A recirculating flume of 6.5m long, 10cm wide, 13cm deep, and with a slope of 18° was used. Movable bed height is 8 cm. The first Sabo dam is set at the downstream end of the flume, and the second Sabo dam is set 30cm, 55cm and 80cm, respectively, far from the first Sabo dam. Table 2.3 shows the experimental conditions. This condition is the same as that of Case B except flume length. The reason for separating divide Case B and C even under the same conditions that Case B is for debris flow capture volume, and Case C is for debris flow discharge, and debris flow deposition upstream of Sabo dam.

To measure the debris flow discharge and sediment concentration, sampler boxes were used. Through the video camera, the residence time of debris flow in each sampler box was calculated. Figure 2.9 shows the sampler box under the flume mouth. This measurement was conducted

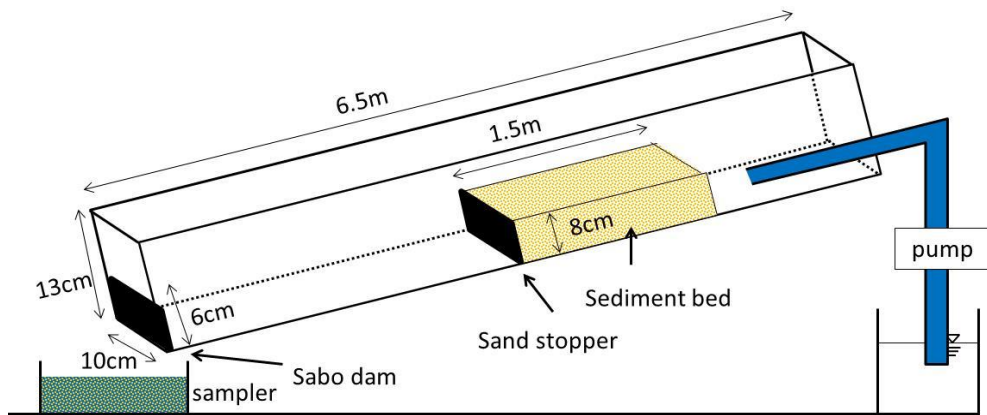
several times under same experimental conditions in order to obtain reliable data. However, it was difficult to measure the debris flow discharge and sediment at the second Sabo dam(upper Sabo dam) during the course of the experiment. Therefore, the positions of the Sabo dam and sediment bed were moved. Figure 2.10 shows the positions of Sabo dam and the sediment bed.



Figure 2.9 sampler boxes



(a) Measuring debris flow discharge at the first located Sabo dam (lower Sabo dam)



(b) Measuring debris flow discharge at the first Sabo dam (Upper Sabo dam)

Figure 2.10 Experimental setup

2.3 Results and Discussions

2.3.1 Deposition Process by Arrangement of Sabo Dams

Figure 2.11 shows the total debris flow capture volume at each Sabo dam. Case B-2 shows the biggest value of total debris flow capture volume at the lower Sabo dam. And debris flow captured volume is similar to each other. By the way, Case A-1, Case B-1, and Case B-2 the upper Sabo dam was buried (Figure 2.13). This means that the distance between Sabo dams was insufficient.

Figure 2.12 and Figure 2.13 show the final debris flow deposition by arrangement of Sabo dams. From the figure, the longer the water supply time, the higher the deposition height and the longer the deposition length. The reason is that, in Case A, the generated debris flow was almost completely captured by two Sabo dams. There was a small amount of debris flow discharge at the outlet of the flume

As mentioned above, Case A-1, Case B-1, and Case A-2 show that the upper Sabo dam was buried by debris flow. This means that the planned sediment gradient of the lower Sabo dam was changed due to the upper Sabo dam. As the planned sediment gradient changed, the potential storage volume is changed.

Figure 2.14 shows the debris flow deposition according to the change of duration in Case C-1, Case C-2, Case C-3. In this figure, Time 0 means that the debris flow's arrival time to the upper Sabo dam. Debris flow is deposited by the Sabo dams and the deposited sediment in the most upstream area of the deposition is eroded by the coming debris flow at the upper Sabo dam.

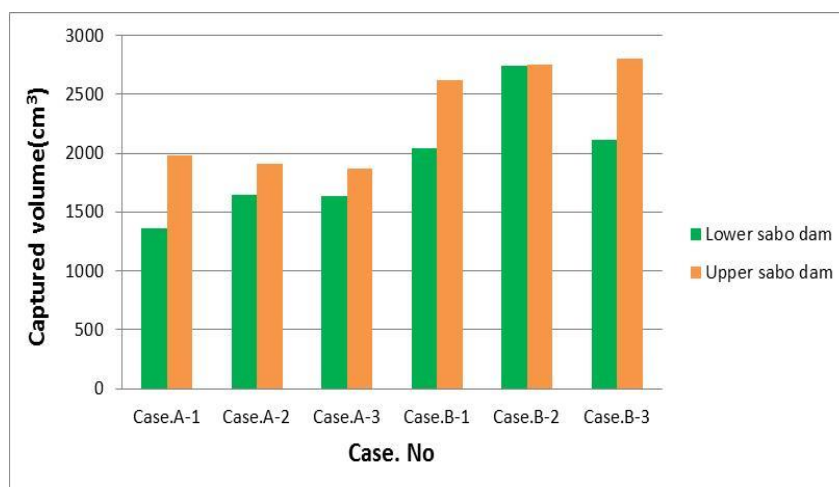
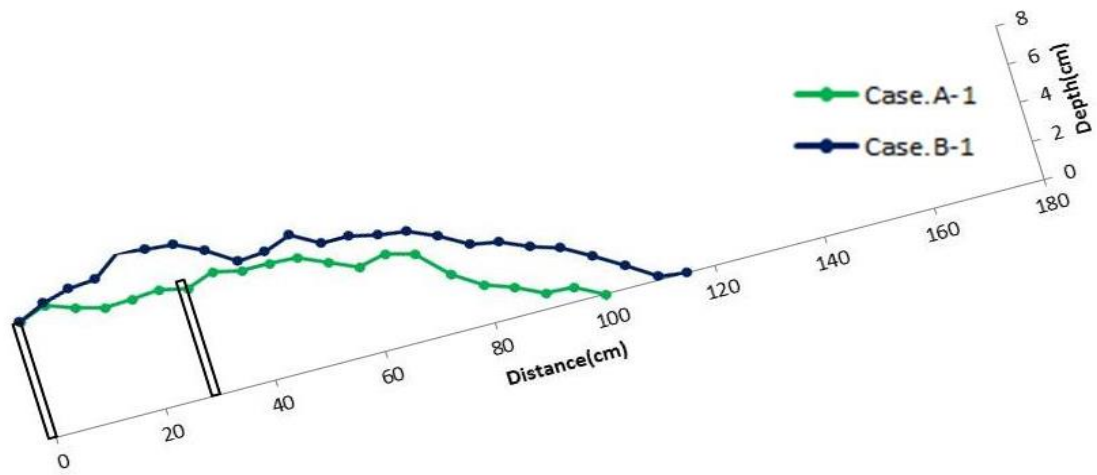
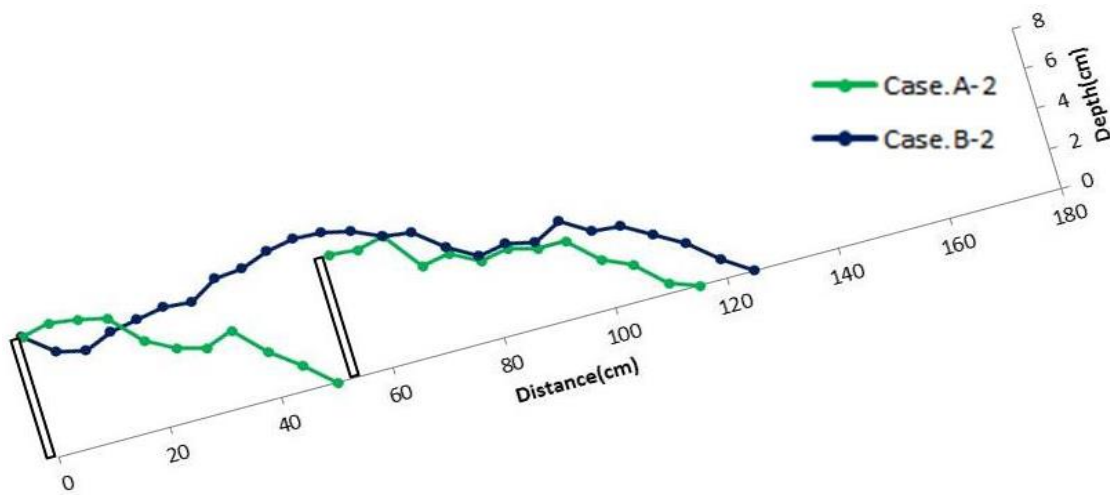


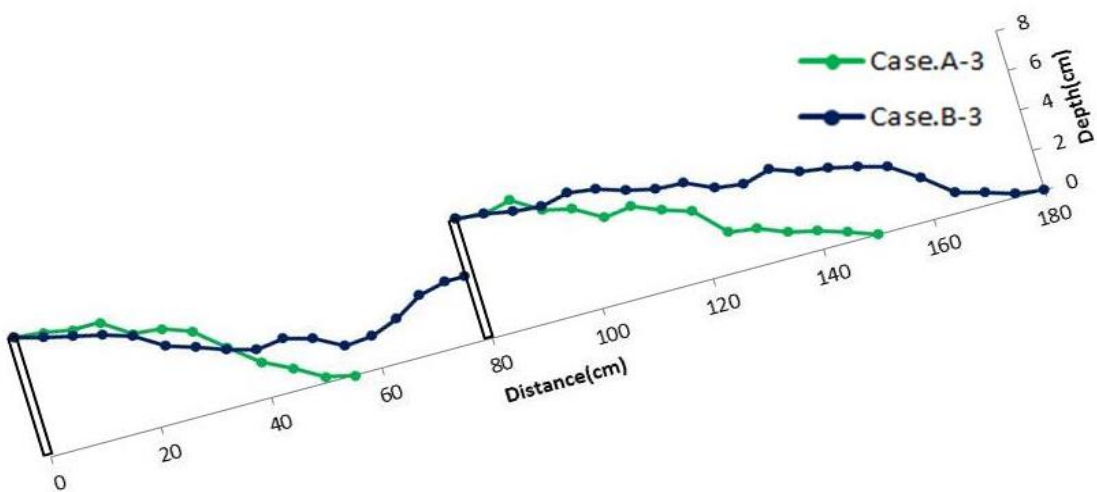
Fig.2.11 Debris flow captured volume



(a) Case.A-1, B-1



(b) Case.A-2, B-2



(c) Case.A-3, B-3

Figure 2.12 Final debris flow deposition upstream of the Sabo dams



Case A-1, B-1

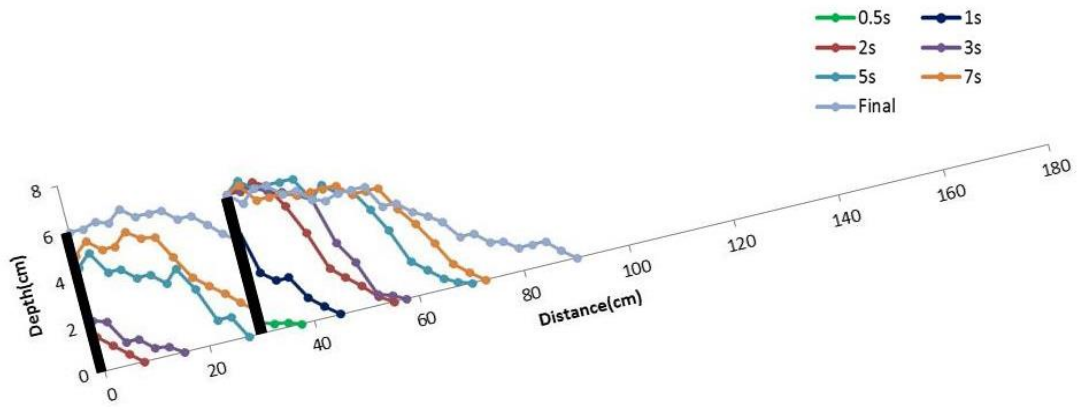


Case A-2, B-2

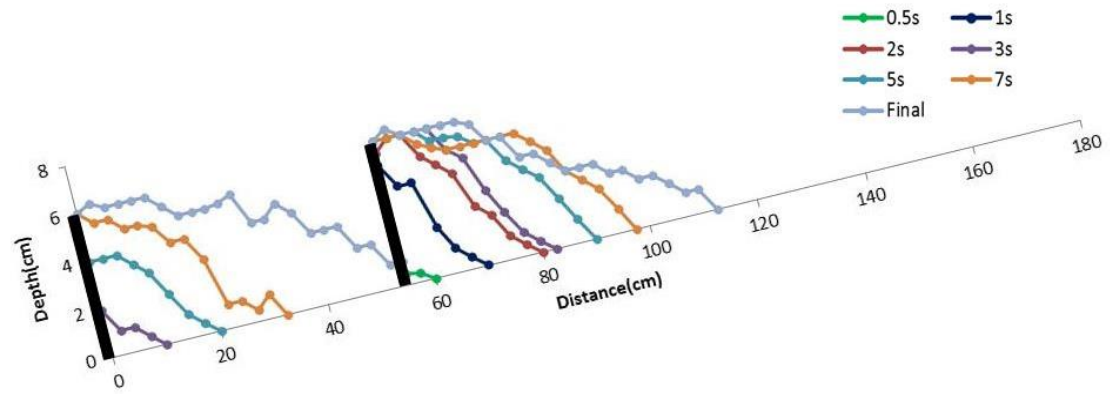


Case A-3, B-3

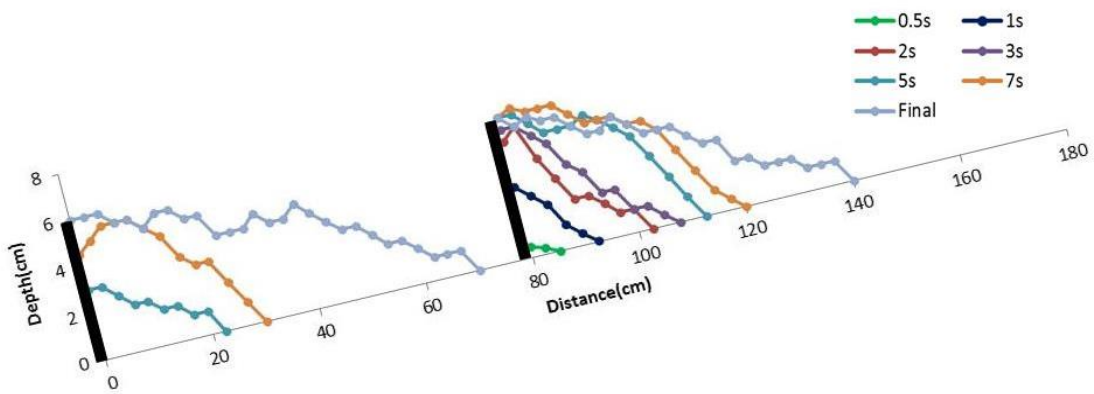
Figure 2.13 Final debris flow deposition upstream of the Sabo dams(picture)



(a) Case C-1,



(b) Case C-2,



(c) Case C-3,

Figure 2.14 Debris flow deposition process upstream of Sabo dams

2.3.2 Discharge and Sediment Concentration without a Sabo Dam

To calculate the discharge and sediment concentration, experimental data of Case C was used. Before measuring the debris flow discharge and sediment concentration at the Sabo dam, a preparatory experiment was conducted without Sabo dams. In the following figures, time 0 means that the debris flow's arrival time to the downstream end of the flume.

Figure 2.15 shows the clear water discharge at the outlet of the flume. There is no sediment bed in this case.

Figure 2.16 shows the debris flow discharge, sediment discharge, and sediment concentration at the outlet of the flume. In this case, there is sediment bed at the upstream of the flume. Debris flow peak discharge was $872 \text{ cm}^3/\text{s}$, and peak sediment discharge was $346.1 \text{ cm}^3/\text{s}$, sediment concentration indicated 35~40%.

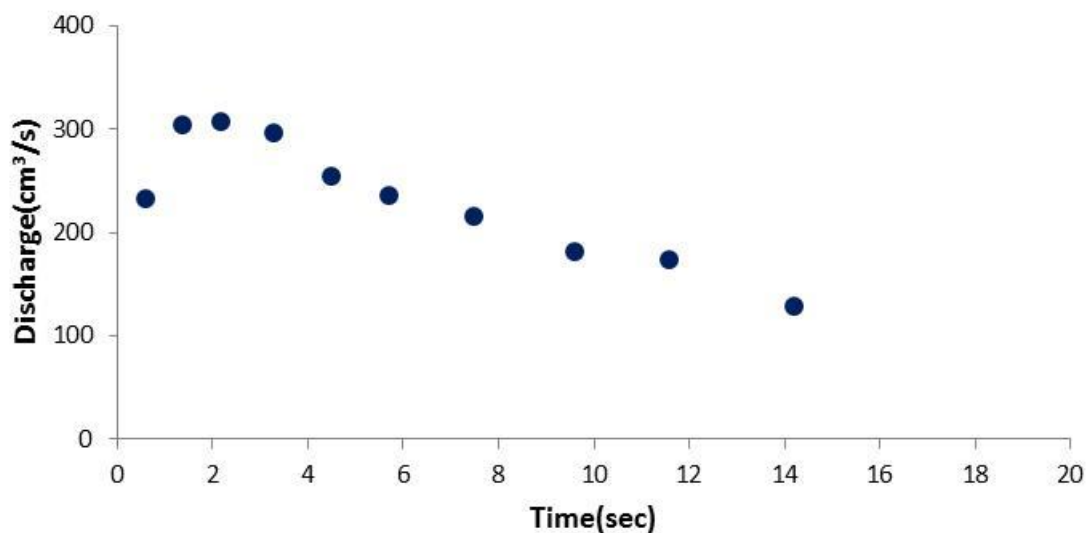
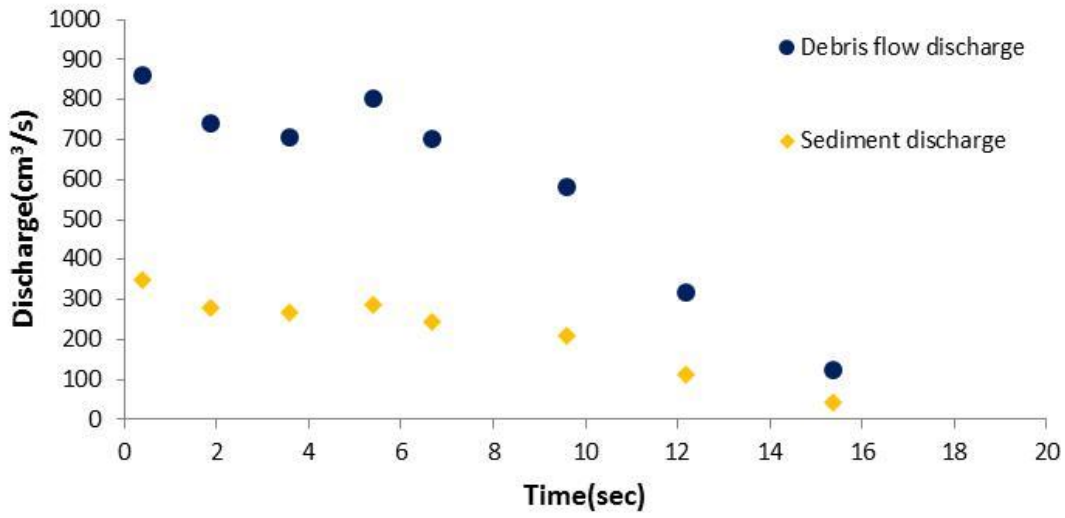
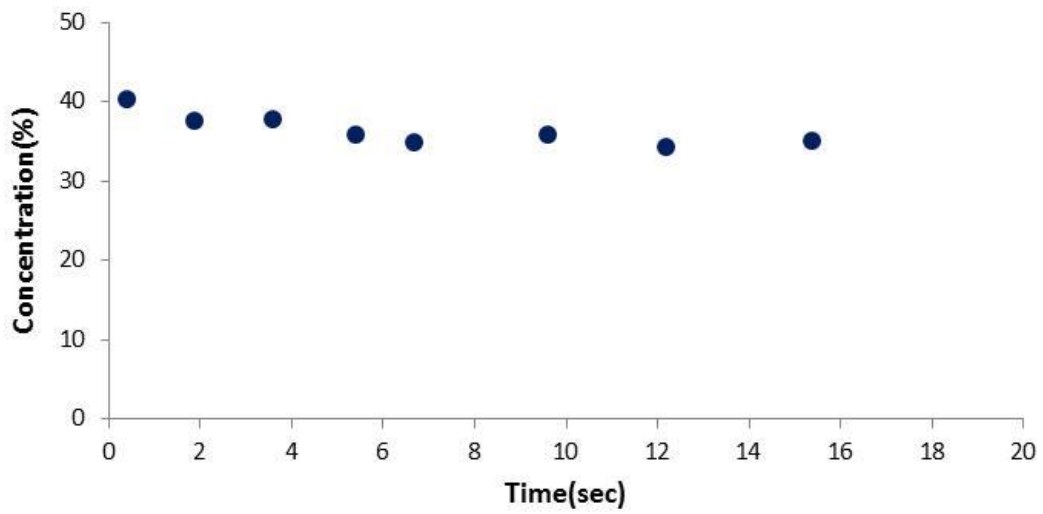


Figure 2.15 Clear water discharge at the outlet flume without Sabo dam



(a) Debris flow discharge and sediment discharge



Sediment concentration

Fig2.16 Debris flow discharge, sediment discharge, and sediment concentration without Sabo dam

2.3.3 Discharge and Sediment Concentration with a Sabo Dam

Figure 2.17 shows the debris flow discharge at the dam point. In this graph, Time 0 means the time of starting to supply clear water in the flume. The start time of the red color means the overflow time at upper Sabo dam. The start time of the green color means the overflow time at lower Sabo dam. The start time of the blue color has no meaning, because the value of blue color is calculated at outlet of Sabo dam. It is just moved to time 12sec to compare no Sabo dam case and with Sabo dam case easily. As the debris flow goes by the Sabo dam, discharge was decreased. Also, sediment discharge was decreased. In the case of no Sabo dam, debris flow peak discharge was 872 cm³/s and peak sediment discharge was 346.1 cm³/s. Peak debris flow discharge in Case C-1 was decreased to 619 cm³/s at the upper Sabo dam and to 490.5 cm³/s at the lower Sabo dam. Sediment peak discharge was decreased to 206.7 cm³/s at the upper Sabo dam and 134.1 cm³/s at the lower Sabo dam. Peak debris flow discharge in Case C-2 was decreased to 629.9 cm³/s at the upper Sabo dam and to 447.3 cm³/s at the lower Sabo dam. Sediment peak discharge was decreased to 219.2 cm³/s at the upper Sabo dam and to 125.5 cm³/s at the lower Sabo dam. Peak debris flow discharge in Case C-3 was decreased to 588.2 cm³/s at the upper Sabo dam and to 413.6 cm³/s at the lower Sabo dam. Sediment peak discharge was decreased to 198.2 cm³/s at the upper Sabo dam and to 116.9 cm³/s at the lower Sabo dam. Table 2.4 shows the decrease rate of debris flow and sediment. Decrease rate is calculated as follows:

Decrease rate at the upper Sabo dam

$$\begin{aligned} & \text{Decrease rate}(\%) \\ & = 1 - \left(\frac{\text{Peak discharge at the upper Sabo dam}}{\text{Peak discharge in case of No Sabo dam}} \right) \times 100 \end{aligned} \quad (2.1)$$

Decrease rate at the lower Sabo dam

$$\text{Decrease rate}(\%) = 1 - \left(\frac{\text{Peak discharge at the lower Sabo dam}}{\text{Peak discharge at upper Sabo dam}} \right) \times 100 \quad (2.2)$$

Total decrease rate

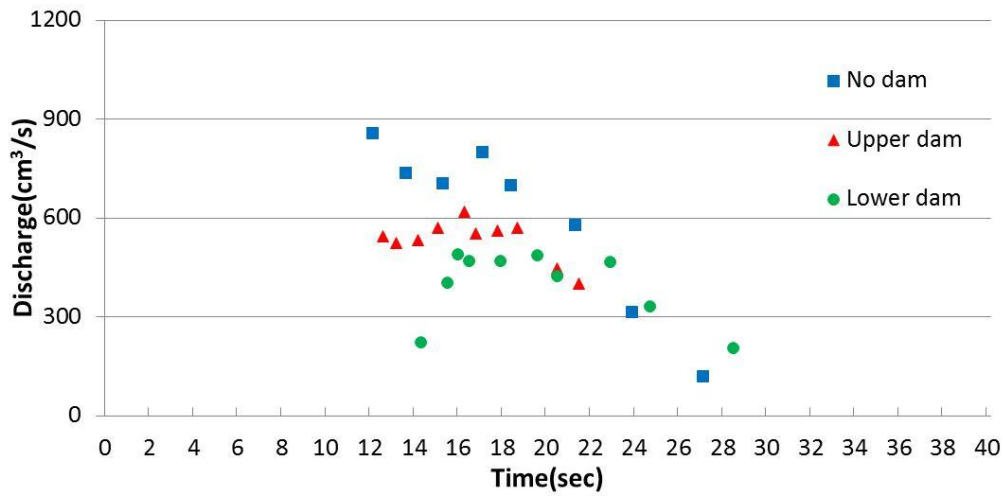
$$\begin{aligned} & \text{Total decrease rate}(\%) \\ & = 1 - \left(\frac{\text{Peak discharge at the lower Sabo dam}}{\text{Peak discharge in case of No Sabo dam}} \right) \times 100 \end{aligned} \quad (2.3)$$

From the table, the greater the distance between two Sabo dams, the higher decrease rate of debris flow and sediment discharge.

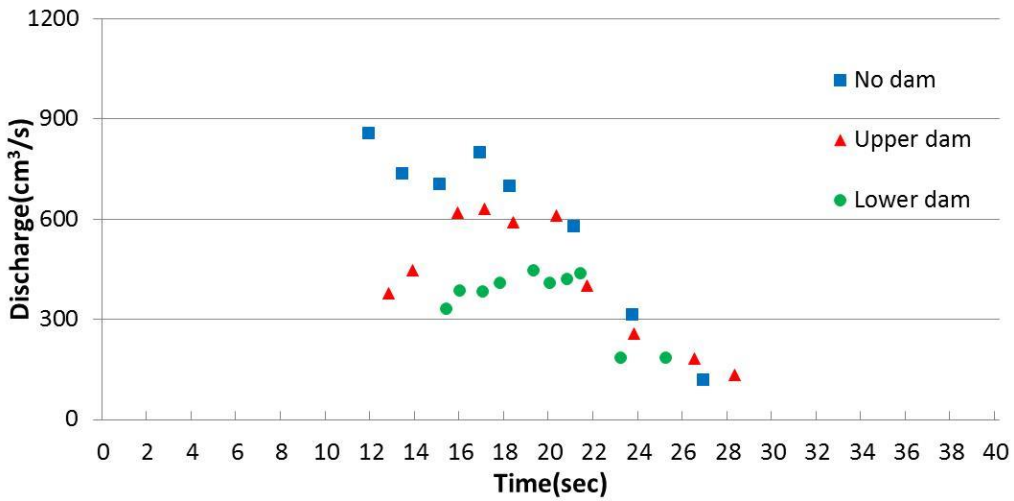
Figure 2.18 shows the sediment concentration. In the case of no Sabo dam, sediment concentration is consistent at around 35%. As the debris flows past the upper Sabo dam, sediment concentration decreased to around 30% and when passing the lower Sabo dam, sediment concentration further decreased. However, overflowed debris flow at the lower Sabo dam does not have a consistent sediment concentration. The initial sediment concentration is lower than 5%. This means that debris flow is not fully developed reaches at the lower Sabo dam. As debris flow overflows the Sabo dam, sediment is captured by the Sabo dam. Therefore, the forefront of the debris flow has a low sediment concentration.

Table 2.4 Debris flow and sediment peak discharge

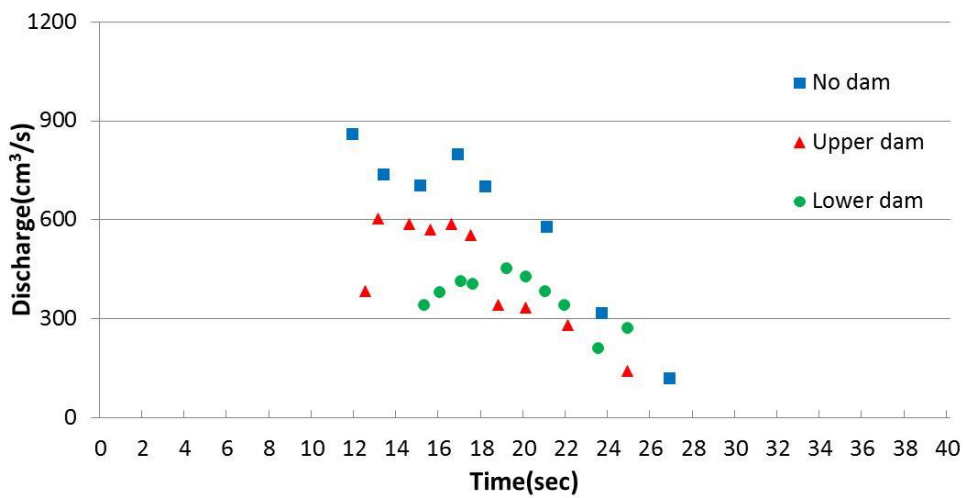
	No dam		Case C-1				Case C-2				Case C-3			
	Debris flow	Sediment	Debris flow		Sediment		Debris flow		Sediment		Debris flow		Sediment	
			upper	lower	upper	lower	upper	lower	upper	lower	upper	lower	upper	lower
Peak discharge (cm ³ /s)	872	346.1	619.0	490.5	206.7	134.1	629.9	447.3	219.2	125.5	588.2	413.6	198.2	116.9
Decrease Rate (%)	-	-	29.1	20.8	40.2	35.1	27.9	28.9	36.6	42.7	32.6	29.6	42.7	41.0
Total decrease Rate (%)	-	-	43.8		61.2		48.8		63.7		52.6		66.2	



(a) Case.C-1

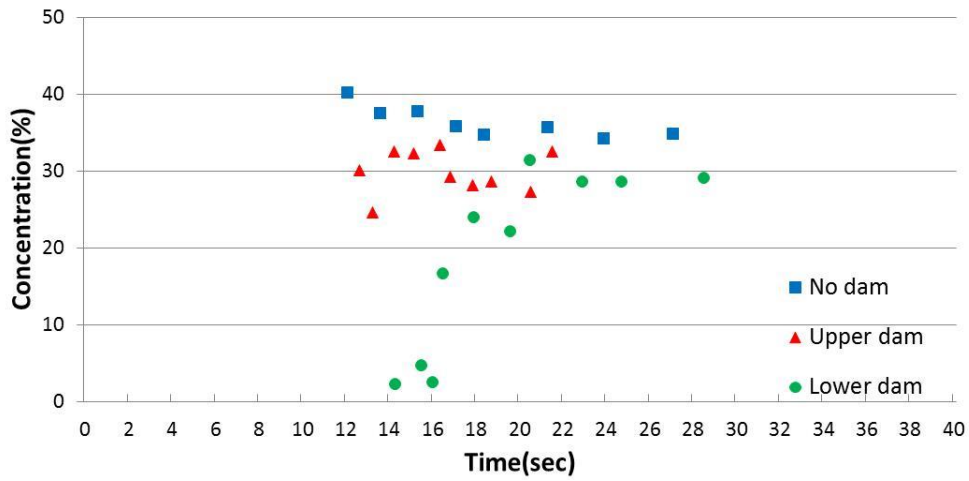


(b) CaseC-2

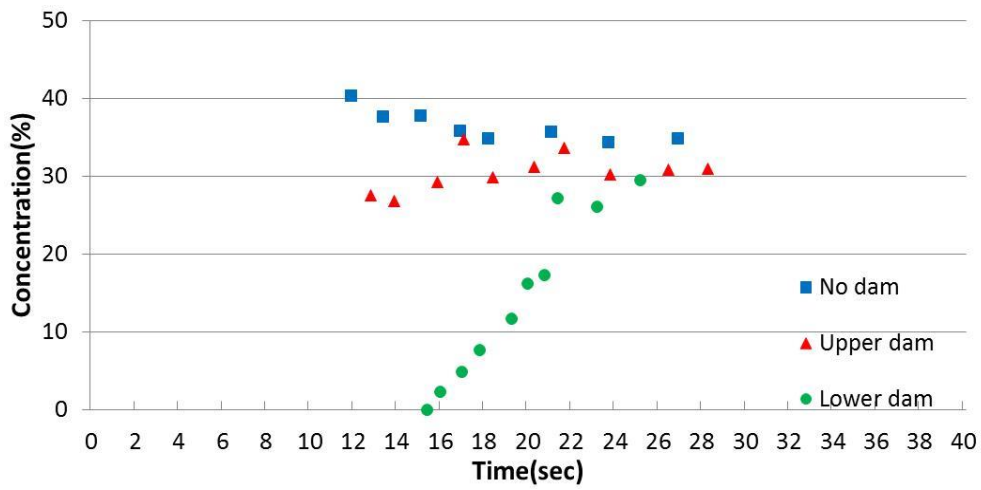


(c) CaseC-3

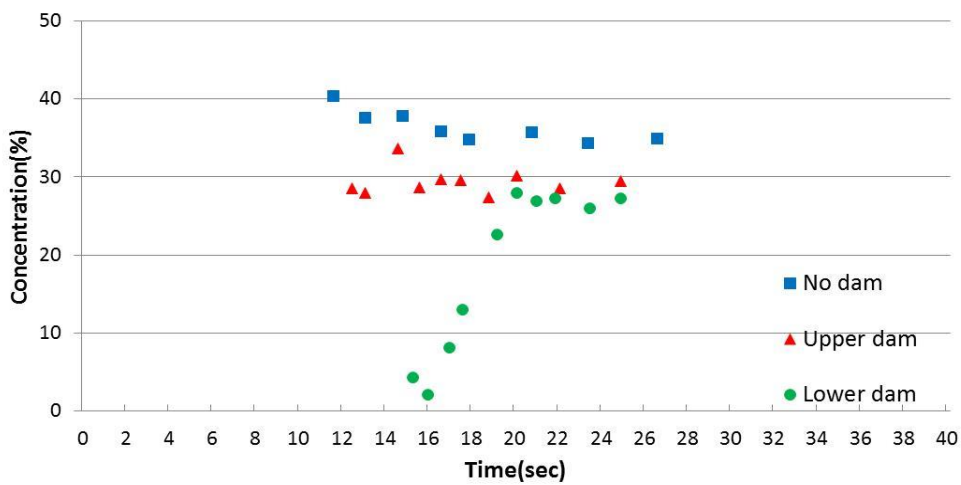
Figure 2.17 Debris flow discharge at each Sabo dams



(a) Case.C-1



(b) CaseC-2



(c) CaseC-3

Figure 2.18 Sediment concentration at each Sabo dams

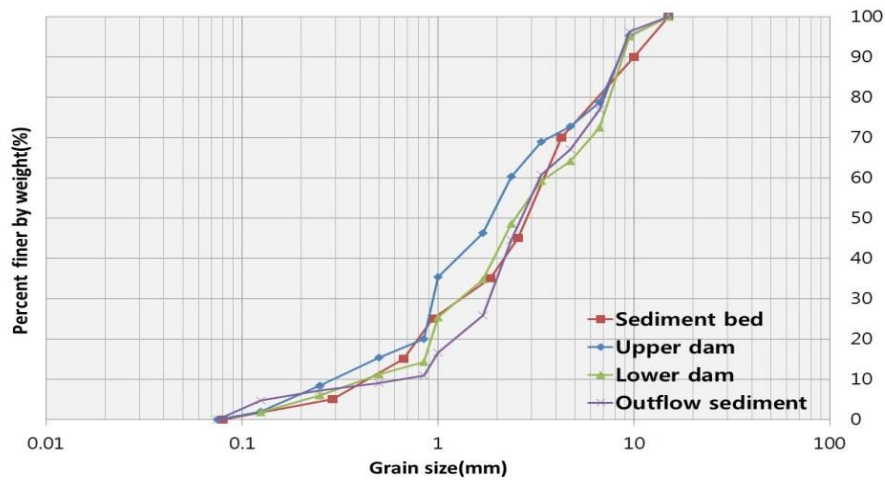
2.3.4 Sediment Distributions

Debris flow transports sediment of various sizes from fine particles to large boulders. According to grain size, the debris flow properties change. Grain size distribution analyses were performed to find the median grain diameter and how the grain size changes as debris flow is captured by the Sabo dam. Figure 2.19 shows the grain size distribution. All of cases show the same aspects. The median value of the sediment captured by the upper Sabo dam was smaller than sediment captured by the lower Sabo dam. And the median value of the sediment that captured by the lower Sabo dam was smaller than the sediment captured by sampler boxes. Sediment in the sampler boxes means that outflowed debris flow at the outlet of the flume.

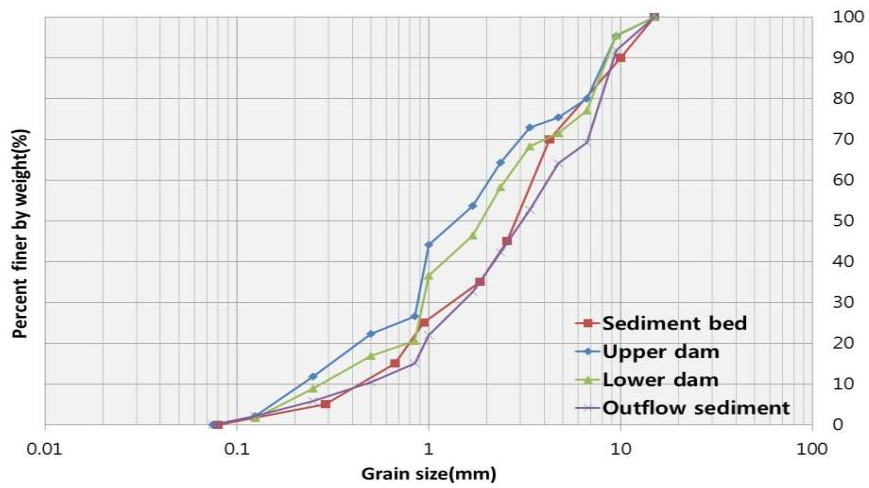
In reality, the forefront part of debris flow have big boulders. Therefore it is expected that the median value of the sediment captured by the upper Sabo dam is larger than that of sediment captured by the lower Sabo dam. However, the experimental results represent against the real situation. This is because the flume length is not enough to make a fully developed debris flow. In other words, if flume length is enough long to make that big boulders move in front part of debris flow in the equilibrium bed gradient, the median value of the sediment captured by upper Sabo dam will bigger than that of sediment captured by lower Sabo dam.

Table 2.5 Sediment size distribution (unit : mm)

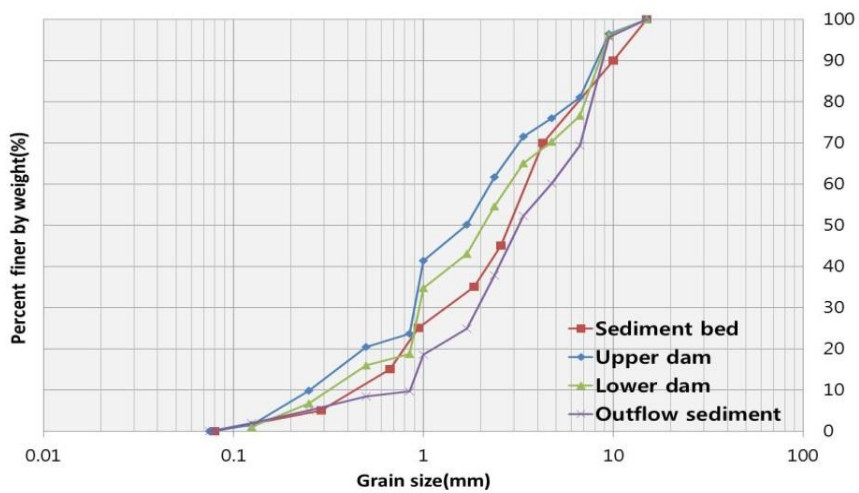
	Sediment bed	CaseC-1			CaseC-2			CaseC-3		
		upper	lower	outer	upper	lower	outer	upper	lower	outer
Median diameter	2.86	1.86	2.48	2.73	1.44	1.91	2.12	1.75	2.09	3.18



(a) Case C-1



(b) Case C-2



(c) Case C-3

Figure 2.19 Sediment Distributions

2.4 Summary

This chapter describes the experimental setup and method in order to measure the debris flow discharge and debris flow deposition by arrangement of Sabo dams. Debris flow deposition at each Sabo dams could be measured during the course of the experiment. However measuring the debris flow discharge at the each Sabo dams are difficult during the course of the experiment. Therefore, to obtain the debris flow discharge at each Sabo dams, experiments were carried out two times in same conditions. First time, debris flow discharge is measured at the lower Sabo dam. Second time, debris flow discharge is measured at the upper Sabo dam through change the position of Sabo dam and sediment bed.

From the debris flow deposition results, lower Sabo dam was buried in Case A-1, Case B-1 and Case A-2. This means that the planned sediment gradient of the lower Sabo dam was changed by upper Sabo dam. Because of upper Sabo dam, debris-flow-capturing capacity of lower Sabo dam was changed. Therefore, the distance between Sabo dams should be determined considering upper Sabo dam's affects to debris-flow-capturing capacity of lower Sabo dam.

From the debris flow discharge results, debris flow discharge, and sediment concentration were decreased as debris flowed past the Sabo dam. However, the sediment concentration at lower Sabo dam was lower than 5% in the beginning, and rise up to around 30%.

These experimental results are compared with the simulation results in chapter 3.

CHAPTER 3

NUMERICAL SIMULATION OF DEBRIS FLOW WITH ARRANGEMENT OF SABO DAMS

3.1 General

A number of countries have been affected by debris flows. Recently, the risk of debris flow has increased owing to global climatic change. This has led to an understanding of the physical mechanisms that govern the triggering of debris flow, their mobilization along the channel, deposition in the fan areas and so on. Many researchers of a variety of countries' studies have been conducted in Japan, Korea, China, US, Canada, France, Switzerland, Italy and so on. Many numerical models of debris flow as a mixture of sediment and water have been developed.

Bagnold(1954) presented his dilatant fluid model, and a large number of other constitutive laws have been put forward. Takahashi(1991) gives a critical account of the mechanisms of debris flow. He used the model equations of the two-phase model, which were simplified to a one-phase model. Similarly, Chen(1987) presents a detailed analysis of rheological models. Scheiwiller & Hutter (1982) study the formulation of the constitutive relations for granular materials under rapid shearing. Campbell(1990) reviews the interaction rules for collision. And Straub(1995) demonstrates in a voluminous dissertation its use in pyroclastic flows. Table 3.1 shows the hierarchy of debris flow models.

In this study, a two-phase model was chosen. An important concept is the mechanism of solid-liquid phase flow. Respective rheological models can be classified as Bingham flow, dilatant flow, and turbulent flow of high-concentration flow. Bingham flows have been studied with fine

Table 3.1 Varnes' classification of slope movements

	Single-phase model	Two-phase model	Diffusive model
Balance relations	<ul style="list-style-type: none"> ■ Mixture mass ■ Mixture momentum 	<ul style="list-style-type: none"> ■ Solid mass ■ Fluid mass ■ Solid momentum ■ Fluid momentum 	<ul style="list-style-type: none"> ■ Solid mass ■ Fluid mass ■ Mixture momentum
Constitutive relations	<ul style="list-style-type: none"> ■ Mixture stress 	<ul style="list-style-type: none"> ■ Solid stress ■ Fluid stress ■ Interaction force 	<ul style="list-style-type: none"> ■ Diffusive mass flux ■ Mixture stress
Remarks	<ul style="list-style-type: none"> ■ Mixture meaning : solids + fluids ■ Deposition and erosion processes allow no spate treatment of water and sediments 	<ul style="list-style-type: none"> ■ Deposition and erosion can be incorporated. ■ The model appropriate when density variations over depth are significant. 	<ul style="list-style-type: none"> ■ Thermodynamics implies that the model is appropriate only in a hydraulic-type formulation
Possible extensions	<ul style="list-style-type: none"> ■ Incorporation of fluctuation energy balance relations for mixtures. 	<ul style="list-style-type: none"> ■ Incorporation of fluctuation energy balance relations for fluids and solids 	<ul style="list-style-type: none"> ■ Incorporation of fluctuation energy balance relations for mixtures.

particles, yield shear stress and apparent coefficient of viscosity. Study of dilatant flows requires two kinds of methodology for the flow mechanism. One is where the shear stress of flow can be evaluated from energy loss due to the non-elastic properties of particles during the collision of particles. The other is where the shear stress of flow can be evaluated as a component of the repulsive force in the flow direction due to the elastic properties of particles during the collision of particles. The turbulent flow analysis method is not being utilized systematically. Only few experimental studies have been reported.

The advance of science and technology has led to better countermeasures for mitigating debris flow damage. To increase the effectiveness of Sabo dams, the control functions of such dams have been reported. Such Sabo dam functions have been described in many theoretical and numerical simulation studies (Honda et al., 1997; Imran, J. et al., 2001). Also, considerable theoretical and numerical works have been conducted on the size, shape and structure of Sabo

dams (Mizuyama et al., 1988; Johnson et al., 1989; Deymier et al., 1994). These studies contribute to technical standard guidelines on debris flows. Thus, there are studies on methods of evaluating the control function of a series of Sabo dams (Osti et al., 2008). However, further studies are required so as to develop general guidelines on a series of Sabo dams. Few studies have reported the control functions of a series of Sabo dams.

This paper describes a methodological approach for estimating debris flow discharge at a series of Sabo dams, and proposes equations for evaluating the effectiveness of a series of closed-type Sabo dams. A one-dimensional numerical model of debris flow is presented. Numerical simulations were conducted including debris flow overflow at the dam point and analyzed with boundary conditions.

3.2 Analysis of Debris Flow

3.2.1 Basic Equations

Debris flows are fluid mixtures that consist of granular materials and water. The equations used are the depth-averaged one-dimensional momentum and continuity equations. The equations for the mass conservation of sediment-water mixture and mass conservation of sediment are as follows.

Momentum equation of sediment and water flow mixture:

$$\frac{\partial M}{\partial t} + \beta \frac{\partial(uM)}{\partial x} = gh \sin \theta_b - gh \cos \theta_b \frac{\partial h}{\partial x} - \frac{\tau_b}{\rho_T} \quad (3.1)$$

Continuity equation of flow mixture:

$$\frac{\partial h}{\partial t} + \frac{\partial M}{\partial x} = i\{C_* + (1 - C_*)s_b\} \quad (3.2)$$

Continuity equation of sediment particles:

$$\frac{\partial(Ch)}{\partial t} + \frac{\partial(CM)}{\partial x} = iC_* \quad (3.3)$$

where, $M (= uh)$ is the x components of the flow flux, x is the flow direction coordinate, t is time, β is the momentum correction factor equal to 1.25 for a stony debris flow (Takahashi et al., 1992), u is the components of mean velocity, g is the acceleration of gravity, h is flow depth, θ_b is the bed slope, τ_b is components of the resistance to flow, ρ_T is mixture density ($\rho_T = \sigma C + (1 - C)\rho$), σ is density of the sediment particles, ρ is density of the water, i is erosion (> 0) or deposition (≤ 0) velocity, C is the sediment concentration in the flow, C_* is maximum sediment concentration in the bed, and s_b is the degree of saturation in the sediment bed equal to 1 for a fully saturated sediment bed.

The equation of bed variation due to erosion or deposition is given as follows:

$$\frac{\partial z_b}{\partial t} = -i \quad (3.4)$$

where, z_b is the erosion or deposition thickness of the bed measured from the original bed surface elevation. In a fixed bed, z_b equals 0. In fact, the sediment in a fixed bed should be contained in the flow parts when erosion occurs. However there is no sediment in a fixed bed.

3.2.2 Erosion and Deposition Velocity Equations

Erosion and deposition velocity i are source terms. These equations to analyze the process of debris flow development and decline by erosion and deposition on the sediment bed have been given by Takahashi et al.(1992) and Egashira et al.(1993a)

Takahashi et al.'s equations

Erosion velocity, if $C < C_\infty$:

$$i = \delta \frac{C_\infty - C}{C_* - C_\infty} \frac{M}{d_m} \quad (3.5)$$

Deposition velocity, if $C \geq C_\infty$:

$$i = \delta \frac{C - C_\infty}{C_* - C_\infty} \frac{M}{d_m} \quad (3.6)$$

where, δ is the erosion coefficient, δ' is the deposition coefficient, d_m is the mean diameter of the sediment, and C_∞ is the equilibrium sediment concentration described as follows (Nakagawa et al., 2003).

If $\tan\theta_w > 0.138$, a stony type debris flow occurs, and

$$C_\infty = \frac{\rho_m \tan \theta_w}{(\sigma - \rho_m)(\tan \phi - \tan \theta_w)} \quad (3.7)$$

If $0.03 < \tan\theta_w \leq 0.138$, an immature type of debris flow occurs, and

$$C_\infty = 6.7 \left\{ \frac{\rho_m \tan \theta_w}{(\sigma - \rho_m)(\tan \phi - \tan \theta_w)} \right\}^2 \quad (3.8)$$

If $\tan\theta_w \leq 0.03$, a turbulent water flow with bed load transport occurs, and

$$C_\infty = \frac{(1 + 5 \tan \theta_w) \tan \theta_w}{\frac{\sigma}{\rho_m} - 1} \left(1 - \alpha_0^2 \frac{\tau_{*c}}{\tau_*} \right) \left(1 - \alpha_0^2 \sqrt{\frac{\tau_{*c}}{\tau_*}} \right) \quad (3.9)$$

$$\alpha_0^2 = \frac{2\{0.425 - (\sigma/\rho_T) \tan \theta_w / (\sigma/\rho_T - 1)\}}{1 - (\sigma/\rho_T) \tan \theta_w / (\sigma/\rho_T - 1)} \quad (3.10)$$

$$\tau_{*c} = 0.04 \times 10^{1.72 \tan \theta_w} \quad (3.11)$$

where, θ_w is the water surface gradient, ρ_m is the density of the interstitial muddy fluid, ϕ is the internal friction angle of the sediment τ_{*c} is the non-dimensional critical shear stress and τ_* is the non-dimensional shear stress.

Egashira et al.'s equations

Egashira (1993a) proposed an erosion rate formula assuming that the bed slope is always adjusted to its equilibrium value in case of debris flows over erodible bed. The erosion and deposition equations are as follows:

$$i = -\frac{u}{C_*} \tan(\theta_e - \theta_b) \quad (3.12)$$

where, u is the depth-averaged velocity of the debris flow body, θ_e is the equilibrium bed slope

corresponding to the sediment concentration of the debris flow body as follows.

$$\theta_e = \tan^{-1} \left\{ \frac{\left(\frac{\sigma}{\rho} - 1\right)C}{\left(\frac{\sigma}{\rho} - 1\right)C + 1} \tan \phi \right\} \quad (3.13)$$

Sediment erosion takes place when the bed slope is steeper than the equilibrium bed slope resulting in a negative value of deposition occurring.

3.2.3 Bottom Shear Stress

Takahashi et al.'s constitutive equations and bottom shear stress

The constitutive equations of Takahashi et al. (1997) are described as follows:

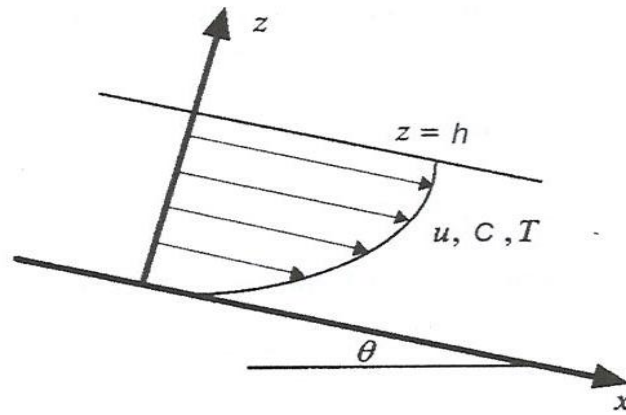


Figure 3.1 Coordinates of uniform debris flow

$$\tau = \tau_y + a_i \sin \alpha_i \left\{ \left(\frac{C^*}{C} \right)^{1/3} - 1 \right\}^2 \sigma d_m^2 \left(\frac{\partial u}{\partial z} \right)^2 \quad (3.14)$$

$$\tau_y = p_s \tan \phi \quad (3.15)$$

where, a_i is the experiment constant, α_i is the collision angle of the particle ($a_i \sin \alpha_i = 0.02$)(Takahashi et al., 1992), z is the coordinate perpendicular to the bed and positive upward

in the normal direction of flow (figure 3.1), and p_s is static pressure which can be expressed as follows.

$$p_s = \alpha_e(\sigma - \rho)Cg(h - z) \cos \theta \quad (3.16)$$

in which α_e is the mean grain concentration above height z , and α_e is the ratio of the quasi-static skeletal pressure to the total pressure. This is given as

$$\alpha_e = \begin{cases} 0 & ; C \leq C_3 \\ \left(\frac{C - C_3}{C_* - C_3}\right)^m & ; C_3 < C \leq C_* \\ 1 & ; C_* \leq C \end{cases} \quad (3.17)$$

where, C_3 is the particle concentration in a volume larger than that particles move with enduring contact with each other ($C_3 = 0.48$). Exponent m is unknown at present. So $m = 1$ is used.

The bottom shear stress for debris flow is derived by substituting the constitutive equations into the momentum conservation equation under steady and uniform flow conditions. The momentum conservation equation is given as follows:

$$\tau(z) = \rho_T g(h - z) \sin \theta \quad (3.18)$$

where, $\tau(z)$ is the shear stress at any distance from the bed along the z -axis. By substituting the constitutive equations of Takahashi et al. (1997) in the momentum equation, the following equation is obtained.

$$\frac{\partial u}{\partial z} = \frac{du}{dz} = \left[\frac{\rho_T g(h - z) \sin \theta - \alpha_e(\sigma - \rho)Cg(h - z) \cos \theta \tan \phi}{a_i \sin \alpha_i \left\{ \left(\frac{C_*}{C} \right)^{1/3} - 1 \right\}^{-2} \sigma d_m^2} \right]^2 \quad (3.19)$$

By introducing dimensionless quantities as $\tilde{u} = u/\sqrt{gh}$ and $\tilde{z} = z/h$, the above equation is modified as follows:

$$\frac{\partial \tilde{u}}{\partial \tilde{z}} = K_T \sqrt{\sin \theta} \frac{h}{d_m} (1 - \tilde{z})^2 \quad (3.20)$$

$$\frac{u(\bar{z})}{u_*} = \frac{2}{3} K_T \frac{h}{d_m} \{1 - (1 - \bar{z})^2\} \quad (3.21)$$

$$\frac{u}{u_*} = \frac{2}{5} K_T \frac{h}{d_m} \quad (3.22)$$

$$u_* = \sqrt{gh \sin \theta} \quad (3.23)$$

$$K_T = \left\{ \frac{\rho_T - \alpha_e(\sigma - \rho)C \frac{\tan \phi}{\tan \theta}}{a_i \sin \alpha_i \left\{ \left(\frac{C_*}{C} \right)^{1/3} - 1 \right\}^{-2}} \right\}^2 \quad (3.24)$$

where, u_* is the friction velocity. The yield stress is given as follows:

$$\tau_y = p_s \tan \phi = f(C)(\sigma - \rho)Cgh \cos \theta \tan \phi \quad (3.25)$$

The coefficient of resistance f_b is calculated by assuming the equilibrium state to be

$$\rho_T gh \sin \theta = f(C)(\sigma - \rho)Cgh \cos \theta \tan \phi + \rho f_b |u|u \quad (3.26)$$

The following equation is obtained by solving the above equation

$$f_b = \frac{gh \sin \theta \left(\rho_T - f(C)(\sigma - \rho)C \frac{\tan \phi}{\tan \theta} \right)}{\rho u^2} \quad (3.27)$$

By using Equations (3.22) and (3.23), Equation (3.27) can be given as

$$f_b = \frac{1}{8} \frac{(\sigma/\rho)}{\{(C_*/C)^{1/3} - 1\}^2} \left(\frac{d_m}{h} \right)^2 \quad (3.28)$$

The bottom shear stress for debris flow is derived as follows.

For a fully developed stony debris flow ($C > 0.4C_*$)

$$\tau_b = \frac{\rho_T}{8} \left(\frac{d_m}{h} \right)^2 \frac{u|u|}{\{C + (1 - C)\rho/\sigma\} \{(C_*/C)^{1/3} - 1\}^2} \quad (3.29)$$

For an immature debris flow ($0.02 \leq C \leq 0.4C_*$)

$$\tau_b = \frac{\rho_T}{0.49} \left(\frac{d_m}{h} \right)^2 u|u| \quad (3.30)$$

For a turbulent flow ($C < 0.02$)

$$\tau_b = \frac{\rho g n^2 u|u|}{h^{1/3}} \quad (3.31)$$

Egashira et al.'s constitutive equations and bottom shear stress

The constitutive equations of Egashira et al.(1997) are given as follows:

$$\tau = \tau_y + \sigma k_d (1 - e^2) C^{1/3} d_m^2 \left(\frac{\partial u}{\partial z} \right)^2 + \rho k_f \frac{(1 - C)^{5/3}}{C^{2/3}} d_m^2 \left(\frac{\partial u}{\partial z} \right)^2 \quad (3.32)$$

$$\tau_y = p_s \tan \phi \quad (3.33)$$

where, e is the restitution of sediment particles, and $k_d = 0.0828$ and $k_f = 0.16$ are empirical constants. The static pressure is described as follows:

$$p_s = \alpha_e (\sigma - \rho) C g (h - z) \cos \theta \quad (3.34)$$

in which α_e is described as

$$\alpha_e = \left(\frac{C}{C_*} \right)^{1/5} \quad (3.35)$$

By substituting the constitutive equations of Egashira et al. (1997) in the momentum equation, the following equations are obtained.

$$\frac{\partial \tilde{u}}{\partial \tilde{z}} = K_H \sqrt{\sin \theta} \frac{h}{d_m} (1 - \tilde{z})^2 \quad (3.36)$$

$$\frac{u(\tilde{z})}{u_*} = \frac{2}{3} K_E \frac{h}{d_m} \{1 - (1 - \tilde{z})^{3/2}\} \quad (3.37)$$

$$\frac{u}{u_*} = \frac{2}{5} K_E \frac{h}{d_m} \quad (3.38)$$

$$K_E = \left\{ \frac{\left(\frac{\sigma}{\rho} - 1\right) C + 1 - \left(\frac{\sigma}{\rho} - 1\right) C f(C) \frac{\tan \phi}{\tan \theta}}{k_f \frac{(1 - C)^{5/3}}{C^{2/3}} d_m^2 \left(\frac{\partial u}{\partial z}\right)^2 + k_g (\sigma/\rho) (1 - e^2) C^{1/3}} \right\}^2 \quad (3.39)$$

Yield stress is described as

$$\tau_y = p_s \tan \phi = f(C) (\sigma - \rho) C g h \cos \theta \tan \phi \quad (3.40)$$

The coefficient of resistance f_b is calculated as follows:

$$f_b = \frac{25}{4} \left\{ k_f \frac{(1 - C)^{5/3}}{C^{2/3}} + k_g (\sigma/\rho) (1 - e^2) C^{1/3} \right\} \left(\frac{d_m}{h} \right)^2 \quad (3.41)$$

The bottom shear stress is derived as

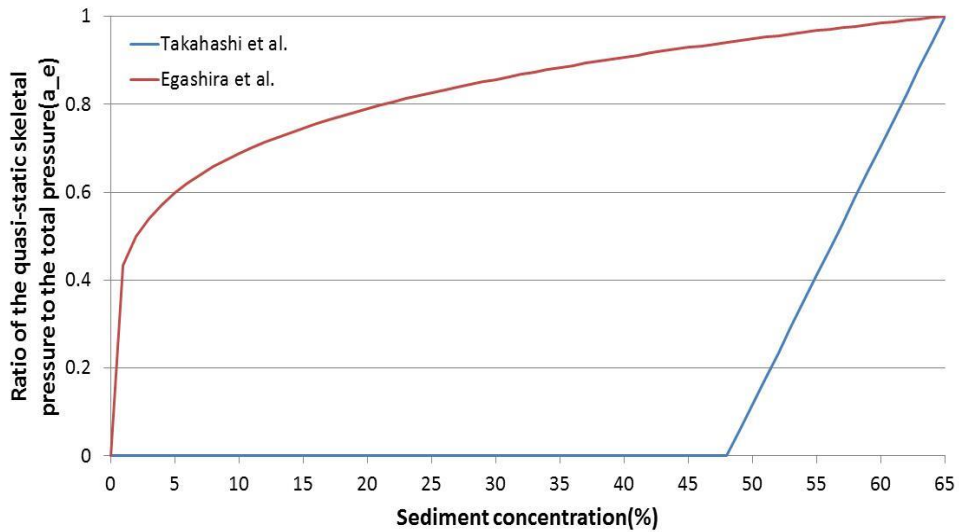


Figure 3.2 Ratio of the quasi-static skeletal pressure to the total pressure according to Takahashi et al. (1997) and Egashira et al. (1997)

$$\tau_b = \tau_y + \rho \frac{25}{4} f \left\{ k_f \frac{(1-C)^{5/3}}{C^{2/3}} + k_g (\sigma/\rho) (1-e^2) C^{1/3} \right\} \left(\frac{d_m}{h} \right)^2 |u|u \quad (3.42)$$

Figure 3.2 shows the ratio of the quasi-static skeletal pressure to the total pressure

3.3 Analysis of Arrangement of Sabo Dams

3.3.1 Boundary conditions of Sabo dam

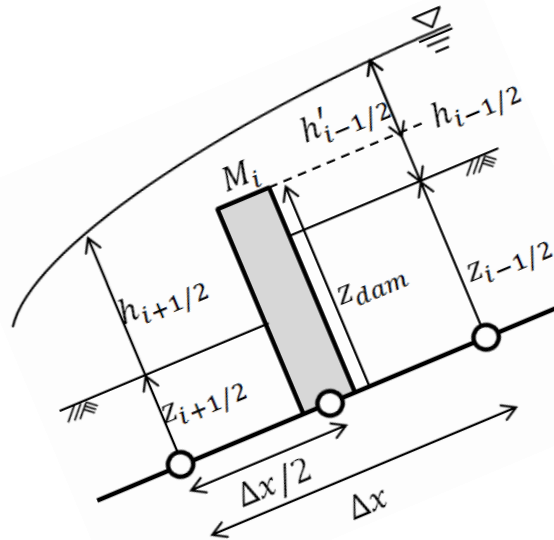


Figure 3.3 Definition of the variables

The closed-type Sabo dam is set at the grid line where discharge is calculated (Figure 3.3). The grid size is 5 cm. The flow surface gradient, $\theta_{w,i}$, and bed gradient, $\theta_{b,i}$, are calculated at the center of the cell. Flow surface gradient $\theta_{w,i}$ and bed gradient $\theta_{b,i}$ are calculated by the average of each value of $\theta_{w,i+1}$, $\theta_{b,i+1}$ and $\theta_{w,i-1}$, $\theta_{b,i-1}$. However, if there is a Sabo dam, the calculation method is changed as follows:

Gradient at the dam point ($z_{i-1/2} < z_{dam}$):

$$\theta_b = \tan^{-1} \frac{z_{i-3/2} - z_{i-1/2}}{\Delta x} \quad (3.43)$$

$$\theta_w = \tan^{-1} \frac{z_{i-3/2} - z_{i-1/2} + h_{i-3/2} - h_{i-1/2}}{\Delta x} \quad (3.44)$$

Gradient at the dam point ($z_{i-1/2} \geq z_{dam}$);

$$\theta_b = \tan^{-1} \frac{z_{i-3/2} - z_{i+1/2}}{2\Delta x} \quad (3.45)$$

$$\theta_w = \tan^{-1} \frac{z_{i-3/2} - z_{i+1/2} + h_{i-3/2} - h_{i+1/2}}{2\Delta x} \quad (3.46)$$

3.3.2 Overflow Equations for Debris Flow Discharge

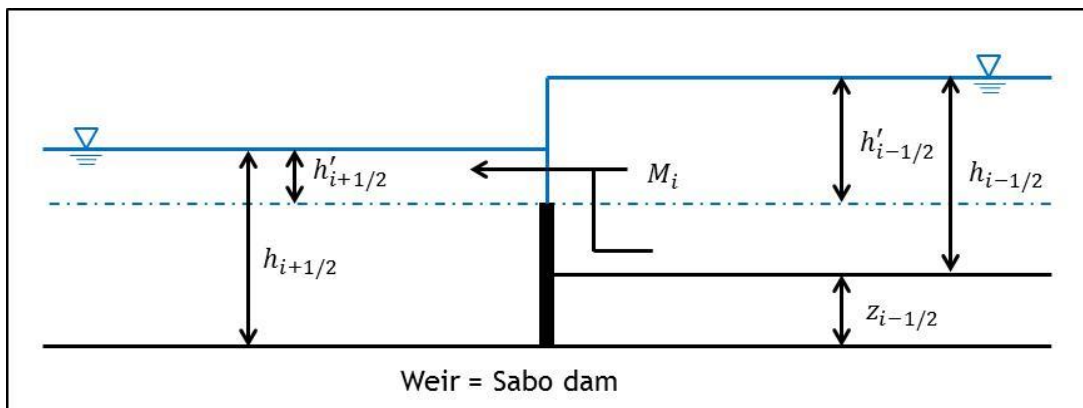


Figure 3.4 Overflow situation

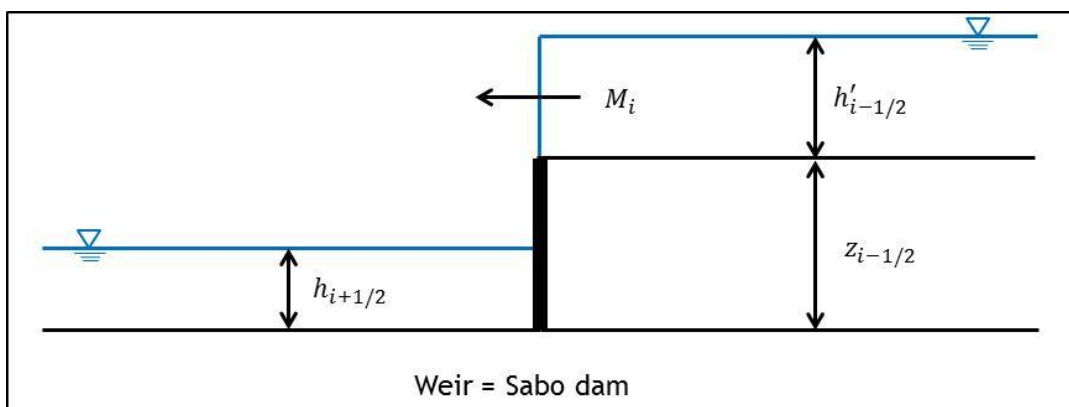


Figure 3.5 Free overfall situation

Sabo dams involve obstructing the path of flow. This is a vertical obstruction over which the debris must flow such as a weir. At that time, outflow discharge at the dam point can be calculated using certain equations. To calculate debris flow discharge at the dam point, the overflow equation and free overfall equation are applied. Figure 3.4 and 3.5 shows the overflow equation and free overfall equation by debris flow deposition upstream of Sabo dam.

Overflow equation (complete overflow):

$$\left(\frac{h'_{i+1/2}}{h'_{i-1/2}} \leq \frac{2}{3}\right) \quad M_i = c_1 h'_{i-1/2} \sqrt{2gh'_{i-1/2}} \quad (3.47)$$

Overflow equation (incomplete overflow):

$$\left(\frac{h'_{i+1/2}}{h'_{i-1/2}} > \frac{2}{3}\right) \quad M_i = c_2 h'_{i+1/2} \sqrt{2g(h'_{i-1/2} - h'_{i+1/2})} \quad (3.48)$$

Free overfall equation:

$$(Z_{i-1/2} > Z_{dam}) \quad M_i = c_3 h'_{i-1/2} \sqrt{gh'_{i-1/2}} \quad (3.49)$$

Table 3.2 Flow conditions at Sabo dam

	Condition	Calculated M_i
Flow 1	$z_{i-1/2} + h_{i-1/2} \leq z_{dam}$	0
Flow 2	$z_{i-1/2} + h_{i-1/2} > z_{dam}$ $z_{i-1/2} < z_{dam}$ $z_{i+1/2} + h_{i+1/2} \leq z_{dam}$	Overflow equation (Complete flow) (Equation. 3.47)
Flow 3	$z_{i-1/2} + h_{i-1/2} > z_{dam}$ $z_{i-1/2} < z_{dam}$ $z_{i+1/2} + h_{i+1/2} > z_{dam}$	Overflow equation (Complete flow, Incomplete flow) (Equation. 3.47,3.48)
Flow 4	$z_{i-1/2} + h_{i-1/2} > z_{dam}$ $z_{i-1/2} \geq z_{dam}$ $z_{i+1/2} + h_{i+1/2} \leq z_{dam}$	Free overfall equation (Equation. 3.48)
Flow 5	$z_{i-1/2} + h_{i-1/2} > z_{dam}$ $z_{i-1/2} \geq z_{dam}$ $z_{i+1/2} + h_{i+1/2} > z_{dam}$	Momentum equation (Equation. 3.1)

where, M_i is the debris flow discharge per unit width at the dam point, c is the overflow coefficient, and h'_i is the overflow depth. As the overflow equation and free overfall equation are adjusted at the dam point, flow conditions are changed by the bed elevation (Table 3.2). In flow Condition 1, the deposition height plus flow depth is less than the height of the Sabo dam. In this condition, debris flow does not overflow the Sabo dam. Therefore, the flow discharge is equal to zero. In flow Condition 2, the deposition height plus flow depth is higher than the height of the Sabo dam. And the deposition height does not reach the dam crown. In this condition, the overflow(complete overflow) equation is applied. Flow Condition 3 is the same as Flow condition 2, but there is deposition in front of the Sabo dam. So the flow height in front of the Sabo dam is sometimes higher than that behind the Sabo dam. Therefore, the incomplete flow equation is applied. In flow condition 4, the debris flow deposition height is higher than the dam height. In this case, the free overfall equation is applied. Flow Condition 5 is the same to flow condition 4, but debris flow is also deposited in front of the Sabo dam due to the lower Sabo dam. At that time, the deposition height in front of the Sabo dam is higher than the Sabo dam, and the momentum equation is applied because this case is same as the no Sabo dam case.

3.4 Solution Methods

3.4.1 Calculation Method of Conservation of Momentum

The leap-frog scheme is one of the most ordinary methods of finite differential. This scheme is used for the governing equations in the coordinate system of Figure 3.6. When the values of scalar

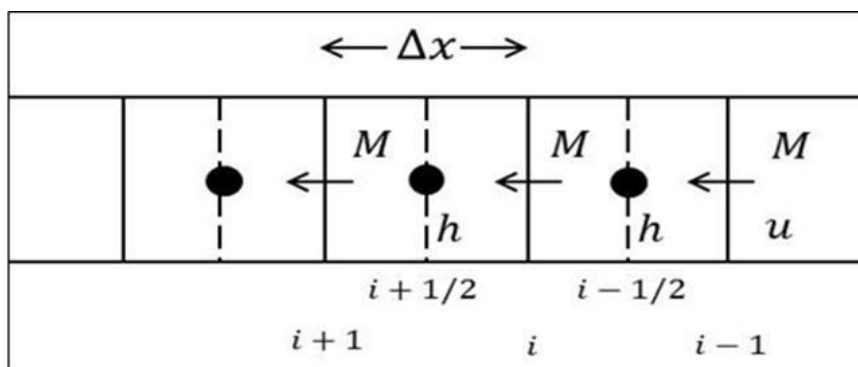


Figure 3.6 Definition of arrangement of variables on meshes

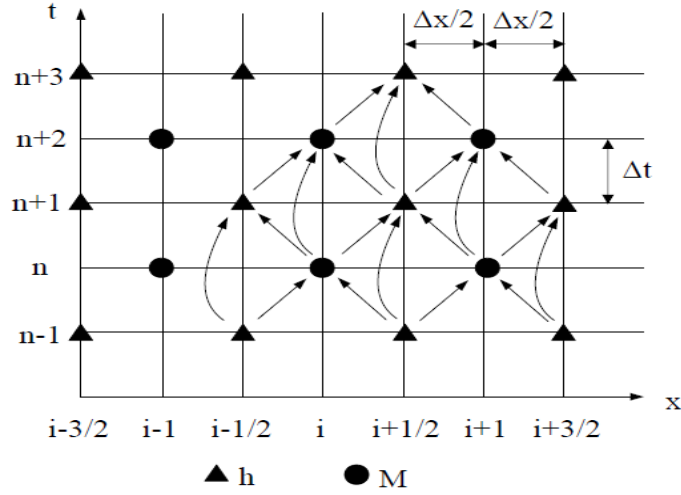


Figure 3.7 Method of advancing the calculation

quantities such as h, c and z_b are given or obtained from the beginning to step $n+1$ ($t = (n + 1)\Delta t$), and the values of vector quantities M are given or obtained to step n , the value of vector M_i^{n+2} in Figure 3.7 can be obtained from following finite differential equation:

$$\begin{aligned}
 \frac{M_i^{n+2} - M_i^n}{2\Delta t} + \beta(XDX) &= g \frac{h_{i+1/2}^{n+1} + h_{i-1/2}^{n+1}}{2} \sin \theta_m^{n+1} \\
 -g \frac{h_{i+1/2}^{n+1} + h_{i-1/2}^{n+1}}{2} \cos \theta_m^{n+1} &\frac{h_{i+1/2}^{n+1} - h_{i-1/2}^{n+1}}{\Delta x} - \frac{1}{\rho_T} \left(\tau_y + \rho f \frac{M_i^{n+2} + M_i^n}{2\bar{h}} \left| \frac{M_i^n}{\bar{h}} \right| \right)
 \end{aligned} \tag{3.50}$$

in which XDX is a convection term. This term is calculated with following condition on $\overline{u_{i+1/2}}$ and $\overline{u_{i-1/2}}$.

$$XDX = \begin{cases} \frac{u_i^n M_i^n - u_{i-1}^n M_{i-1}^n}{\Delta x} & : u_i^n \geq 0, u_{i-1}^n \geq 0 \\ \frac{u_i^n M_i^n - 0}{\Delta x} & : u_i^n \geq 0, u_{i-1}^n < 0 \\ \frac{u_{i+1}^n M_{i+1}^n - u_i^n M_i^n}{\Delta x} & : u_i^n < 0, u_{i-1}^n < 0 \\ \frac{0 - u_{i-1}^n M_{i-1}^n}{\Delta x} & : u_i^n < 0, u_{i-1}^n \geq 0 \end{cases} \tag{3.51}$$

$$u_i^n = \frac{2M_i^n}{h_{i+\frac{1}{2}}^{n+1} + h_{i-\frac{1}{2}}^{n+1}} \quad (3.52)$$

The calculation of the above gives M_i^{n+2} in the following equation.

$$M_i^{n+2} = \frac{g\bar{h} \sin \theta_m^{n+1} - g\bar{h} \cos \theta_m^{n+1} \frac{h_{i+1/2}^{n+1} - h_{i-1/2}^{n+1}}{\Delta x} - \beta(XDX) - \frac{\tau_y}{\bar{\rho}_T} + \left(\frac{1}{2\Delta t} - \frac{\rho}{\bar{\rho}_T} f \frac{1}{2\bar{h}} \left| \frac{M_i^n}{\bar{h}} \right| \right) M_i^n}{\left(\frac{1}{2\Delta t} + \frac{\rho}{\bar{\rho}_T} f \frac{1}{2\bar{h}} \left| \frac{M_i^n}{\bar{h}} \right| \right)} \quad (3.53)$$

in which,

$$\bar{h} = \frac{h_{i+1/2}^{n+1} + h_{i-1/2}^{n+1}}{2} \quad (3.54)$$

$$\bar{\rho}_T = (\sigma - \rho)\bar{C} + \rho \quad (3.55)$$

$$\bar{C} = \frac{C_{i+1/2}^{n+1} + C_{i-1/2}^{n+1}}{2} \quad (3.56)$$

$$\sin \theta_m^{n+1} = \frac{\sin \theta_{i+1/2}^{n+1} + \sin \theta_{i-1/2}^{n+1}}{2} \quad (3.57)$$

$$\cos \theta_m^{n+1} = \frac{\cos \theta_{i+1/2}^{n+1} + \cos \theta_{i-1/2}^{n+1}}{2} \quad (3.58)$$

$$\theta_{i+1/2}^{n+1} = -\tan^{-1} \left(\frac{z_{i+1/2}^{n+1} - z_{i-1/2}^{n+1}}{\Delta x} \right) \quad (3.59)$$

$$\tau_y = f(\bar{C})(\sigma - \rho)\bar{C} \cos \theta_m^{n+1} \tan \phi \quad (3.60)$$

3.4.2 Calculation Method of Conservation of Mass and Bed

When the values of vector properties M are given or obtained from the beginning to step $n+2(t = (n + 2)\Delta t)$, and the values of scalar quantities such as h, c and z_b are given or obtained to step $n+1$, the value of scalar $z_{b_{i+1/2}}^{n+3}$, $h_{i+1/2}^{n+3}$, and $C_{i+1/2}^{n+3}$ in Figure 3.7 can be obtained from following finite differential equations.

$$\frac{h_{i+1/2}^{n+3} - h_{i+1/2}^{n+1}}{2\Delta t} + \frac{M_{i+1}^{n+2} - M_i^{n+2}}{\Delta x} = i_{i+1/2}^{n+1} \quad (3.61)$$

$$\frac{(Ch)_{i+1/2}^{n+3} - (Ch)_{i+1/2}^{n+1}}{2\Delta t} + CXDX = i_{i+1/2}^{n+1} C_* \quad (3.62)$$

$$CXDX = \begin{cases} \frac{C_{i+1/2}^{n+1} M_{i+1}^{n+2} - C_{i-1/2}^{n+1} M_i^{n+2}}{\Delta x} & : M_i^{n+2} \geq 0, M_{i+1}^{n+2} \geq 0 \\ \frac{C_{i+1/2}^{n+1} M_{i+1}^{n+2} - C_{i+1/2}^{n+1} M_i^{n+2}}{\Delta x} & : M_i^{n+2} \geq 0, M_{i+1}^{n+2} < 0 \\ \frac{C_{i+3/2}^{n+1} M_{i+1}^{n+2} - C_{i-1/2}^{n+1} M_i^{n+2}}{\Delta x} & : M_i^{n+2} < 0, M_{i+1}^{n+2} < 0 \\ \frac{C_{i+3/2}^{n+1} M_{i+1}^{n+2} - C_{i-1/2}^{n+1} M_i^{n+2}}{\Delta x} & : M_i^{n+2} < 0, M_{i+1}^{n+2} \geq 0 \end{cases} \quad (3.63)$$

$$\frac{z_{i+1/2}^{n+3} - z_{i+1/2}^{n+1}}{2\Delta t} = -i_{i+1/2}^{n+1} \quad (3.64)$$

3.5 Results and Discussions Compared with the Experimental

Results

According to overflow equations and free overfall equations, debris flow discharge, sediment concentration, and debris flow deposition upstream of Sabo dam are calculated by arrangement of Sabo dams. Here, all of discharge coefficients, c_1 , c_2 , and c_3 , are used as 1.0. And, the other parameters of the numerical simulation are shown in Table 3.3.

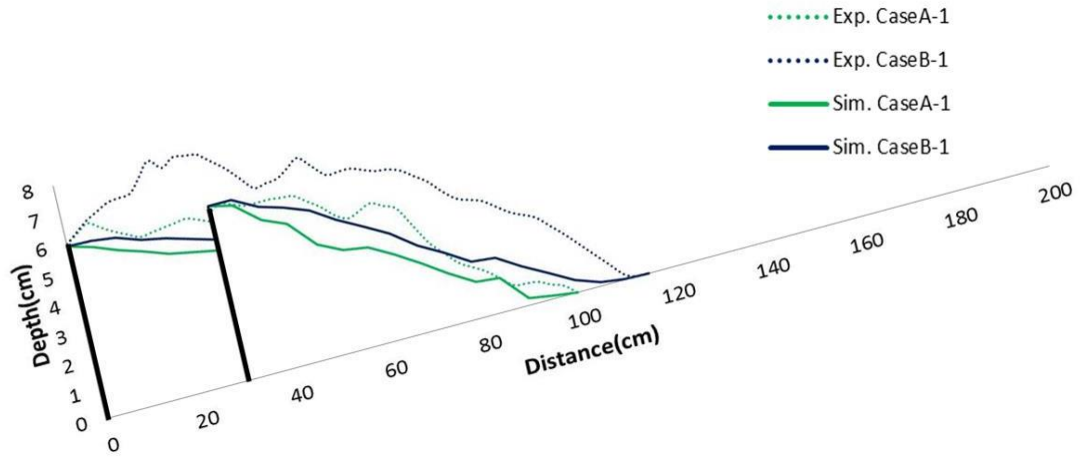
Table 3.3 Parameters for numerical simulation

<i>Parameter</i>	<i>Unit</i>	<i>Value</i>
Grid size (Δx)	cm	5
Time interval (Δt)	sec	0.001
Calculation time (Q_{time})	sec	60
Density of a sediment particle (σ)	g/cm ³	2.65
Density of a water (ρ)	g/cm ³	1
Interstitial muddy fluid	g/cm ³	1.15
Tangent of the internal friction angle of sediment ($\tan\phi$)	-	0.7
Volumetric concentration of the solids in the bed (C_*)	-	0.65
Limitative sediment concentration (C_3)	-	0.48
Erosion coefficient (δ_e)	-	0.01
Deposition coefficient (δ_d)	-	0.004

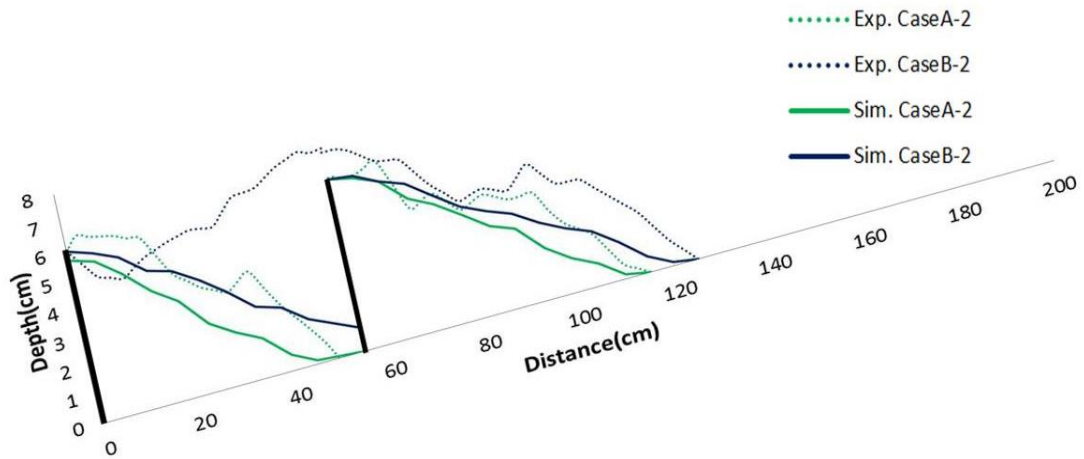
3.5.1 Debris Flow Deposition

Figure 3.8 and figure 3.9 show the simulated results and experimental results of final debris flow deposition upstream of a series of Sabo dams in case A, and Case B. And, Figure 3.10 and figure 3.11 show the simulated results and experimental results of debris flow deposition process upstream of a series of Sabo dams in Case C. In this graph, Time 0 means the debris flow's arrival time to the upper Sabo dam. The dotted line is the experimental results and the solid line is the simulation results. From the figure, the simulation results are in fair agreement with the experimental results. This is because a decrease in distance of between dams is able to increase the equilibrium bed slope by the upper Sabo dam. However, some discrepancies are found in the shape of the deposition between the simulated results and the experimental results. The height of deposition in the experimental results is higher than simulation results which use Takahashi et al.'s(1992) equations. The simulation results are underestimated. In contrast, simulation results which use Egashira et al.'s(1993a) equations are overestimated. This simulation results of debris flow deposition length is longer than experimental results.

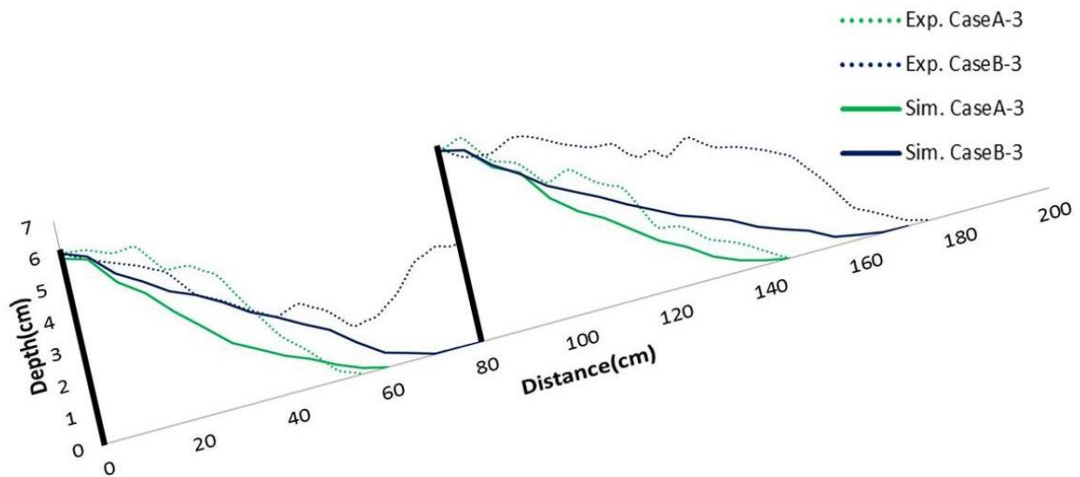
Therefore, when the Takahashi et al.'s(1992) equations are used, more feasible coefficient of erosion velocity and coefficient of deposition velocity are required. And when Egashira et al.'s(1993a) equations are used, experimental method should be changed because this equation is more applicable to the movable bed.



(a) Case A-1, Case B-1

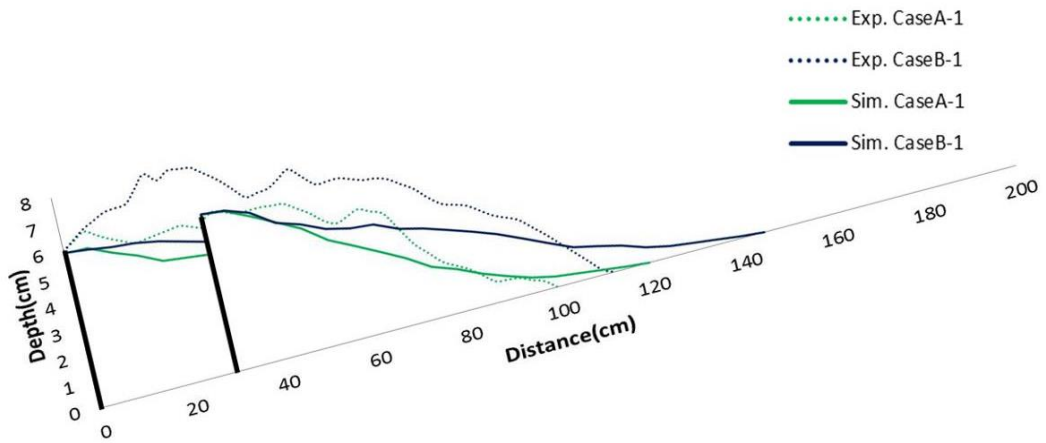


(b) Case A-2, Case B-2

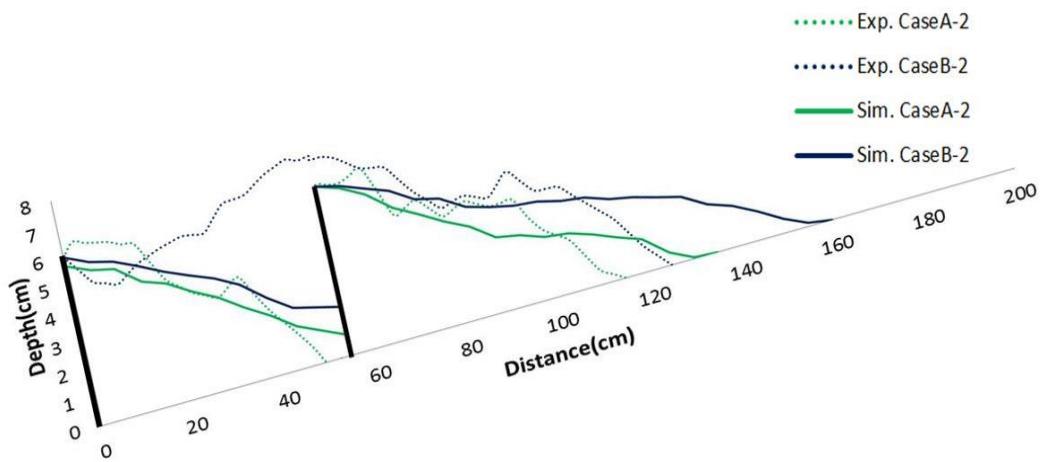


(c) Case A-3, Case B-3

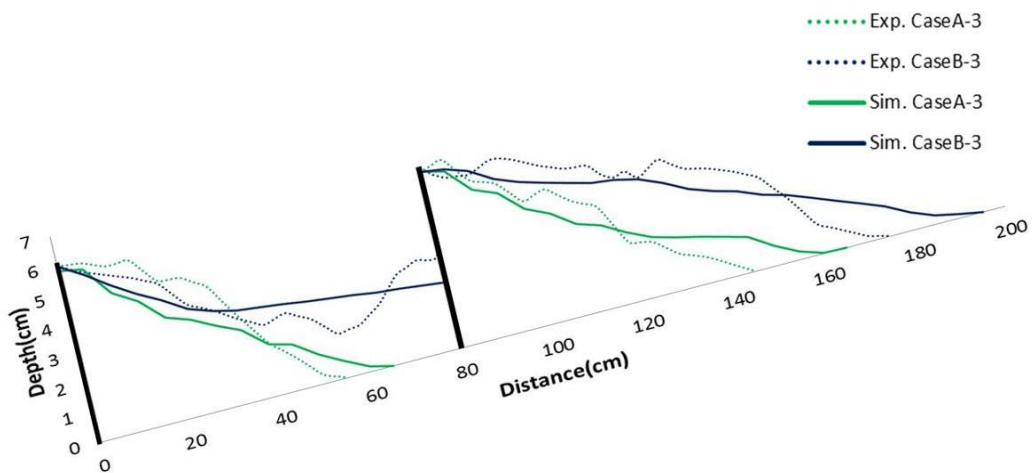
Figure 3.8 Final debris flow deposition upstream of the Sabo dam (equations of Takahashi et al.)



(a) Case A-1, Case B-1

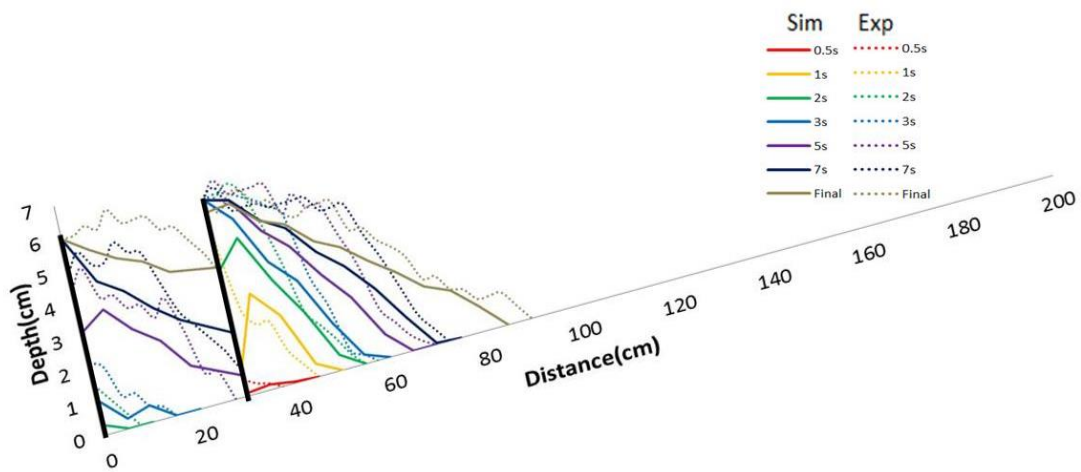


(b) Case A-2, Case B-2

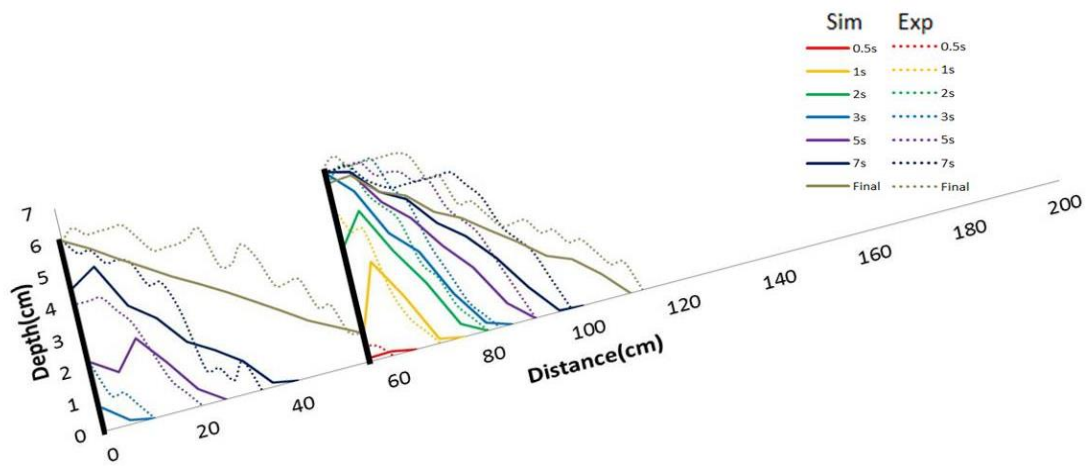


(c) Case A-3, Case B-3

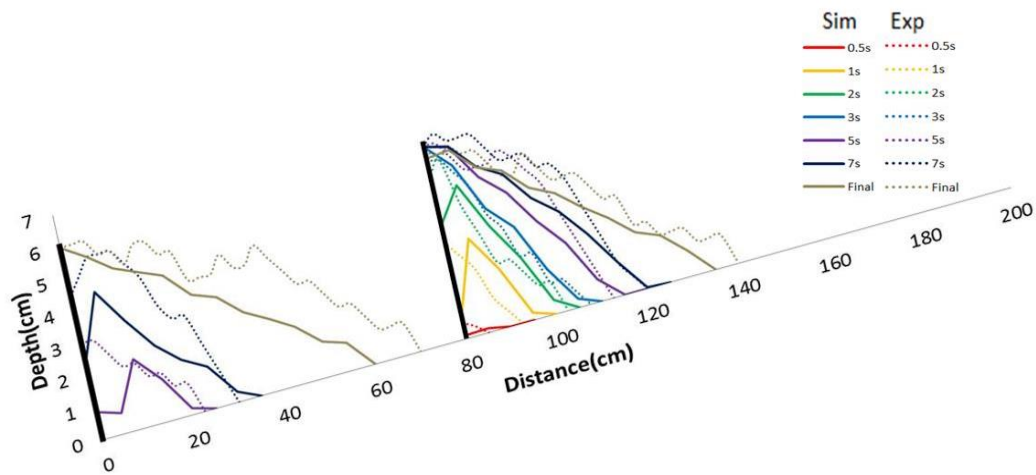
Figure 3.9 Final debris flow deposition upstream of the Sabo dam
(equations of Egashirea et al.)



(a) Case C-1

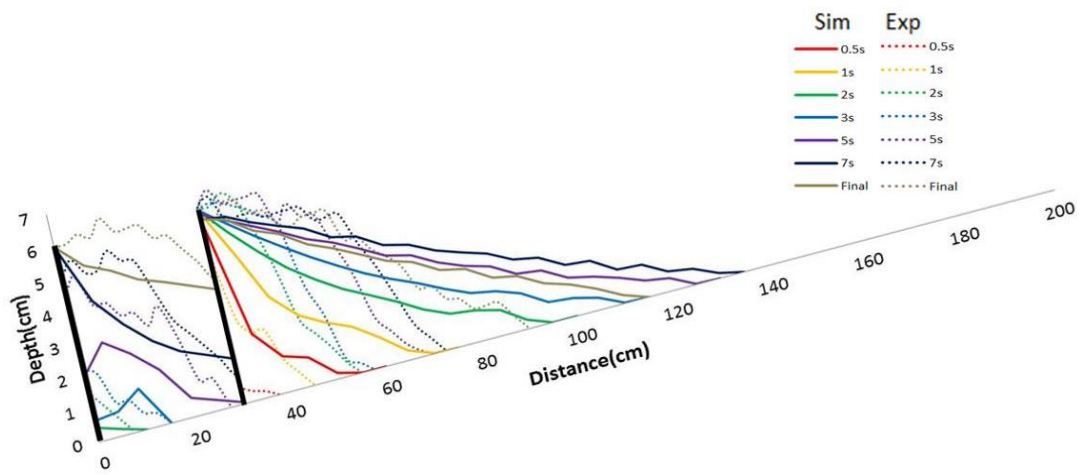


(b) Case C-2

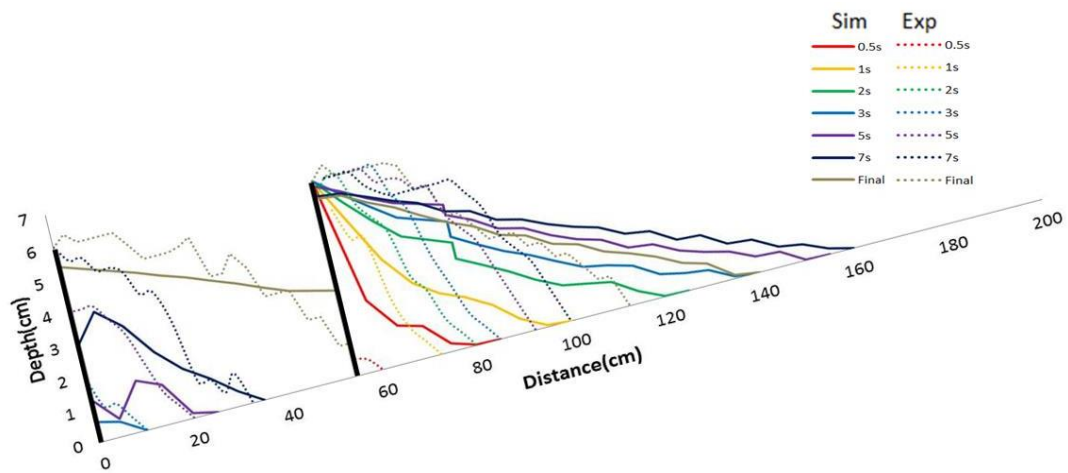


(c) Case C-3

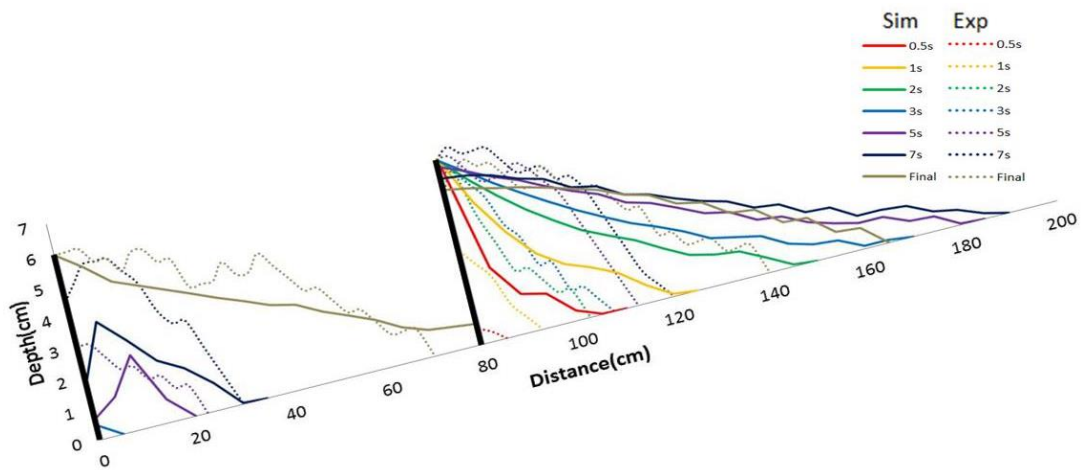
Figure 3.10 Debris flow deposition process upstream of the Sabo dam (equations of Takahashi et al.)



(a) Case C-1



(b) Case C-2



(c) Case C-3

Figure 3.11 Debris flow deposition process upstream of the Sabo dam (equations of Egashira et al.)

3.5.2 Debris Flow Discharge and Sediment Concentration

Figure 3.12 shows the experimental result and simulation result of clear water discharge at the outlet flume without Sabo dam. There is no sediment bed in this case. The simulation result matches with the experimental result. Figure 3.13 shows the debris flow discharge, sediment discharge and sediment concentration at the outlet of flume compared with the experimental results. In this graph, Time 0 means the debris flow's arrival time to outlet flume. The simulated results using Takahashi et al.'s(1992) equations, debris flow peak discharge was 949.68 cm³/s, peak sediment discharge was 332.38 cm³/s. Sediment concentration indicated 35~40%. The simulated results using Egashira et al.'s(1993a) equations, debris flow peak discharge was 1048.56 cm³/s, peak sediment discharge was 406.81 cm³/s. Sediment concentration indicated 35~40%.

Figure 3.14 and Figure 3.15 show the simulated results and experimental results of debris flow discharge and sediment concentration using Takahashi et al.'s(1992) equations. Figure 3.16 and Figure 3.17 show the simulated results and experimental results of debris flow discharge and sediment concentration using Egashira et al.'s(1993a) equations. In these graph, Time 0 means the start time of supplying clear water in the flume. The start time of the red color means the overflow time at upper Sabo dam. The start time of the green color means the overflow time at lower Sabo dam. The start time of the blue color has no meaning, because the value of blue color is calculated at outlet of Sabo dam. It is just moved to time 12sec to compare no Sabo dam case and with Sabo dam case easily.

Table 3.4 shows the debris flow peak discharge. In the experimental results, debris flow discharge is calculated at the downstream end of the flume under the no Sabo Dam case. The simulated results of debris flow discharge are consistent with the experimental results. Through

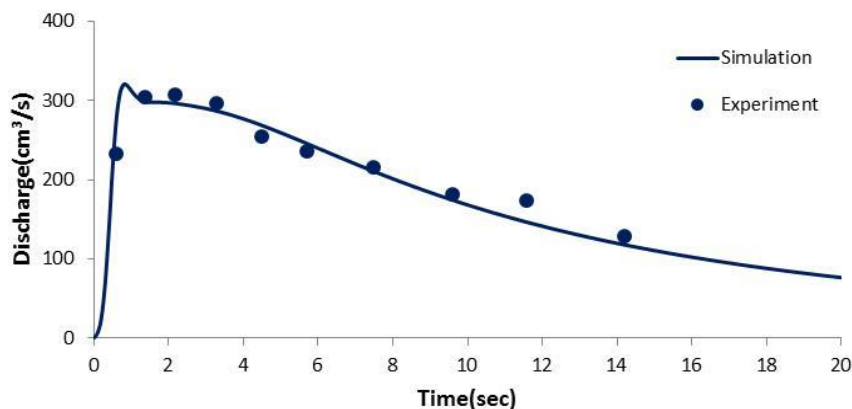
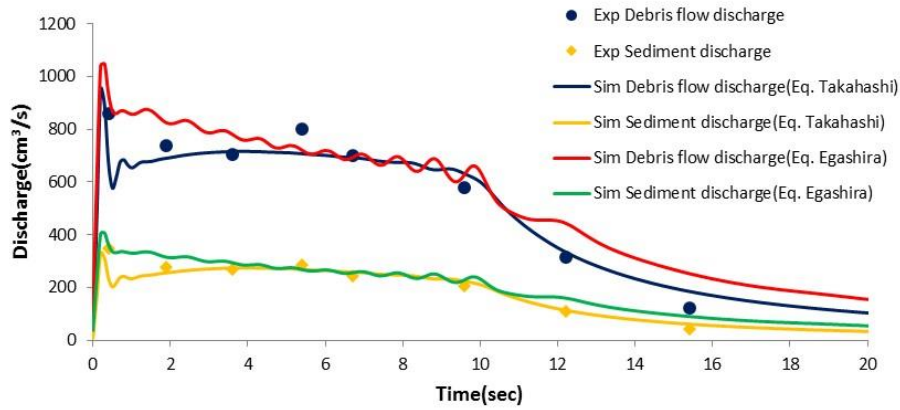
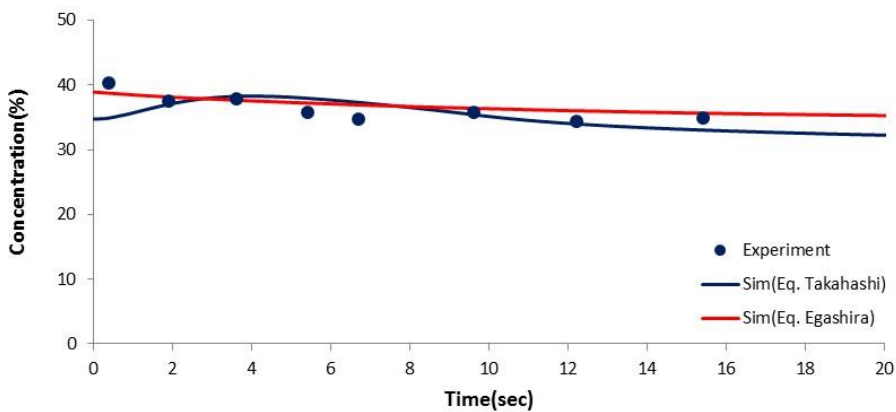


Figure 3.12 Clear water discharge at the outlet flume without Sabo Dam

the series of Sabo dams, the total discharge of debris flow and peak discharge is decreased. The total average peak discharge rate is 48.4% in the experimental results, 45.3% in the simulation results using Takahashi et al.(1992)'s equation, 49.4% in the simulation results using Egashira et al.'(1993a)s equation. However, the greater the distance between two Sabo dams, the higher the rate of total discharge decrease. In the experimental results, total debris flow decrease rate is 43.8% in Case C-1, 48.8% in Case C-2, and 52.6% in Case C-3. In the simulation results using Takahashi et al.(1992)'s equation, total debris flow decrease rate is 44.1% in Case C-1, 45.8% in Case C-2, and 46.1% in Case C-3. In the simulation results using Egashira et al.(1993a)'s equation, total debris flow decrease rate is 44.2% in Case C-1, 50.8% in Case C-2, and 53.3% in Case C-3.



(a) Debris flow and sediment discharge

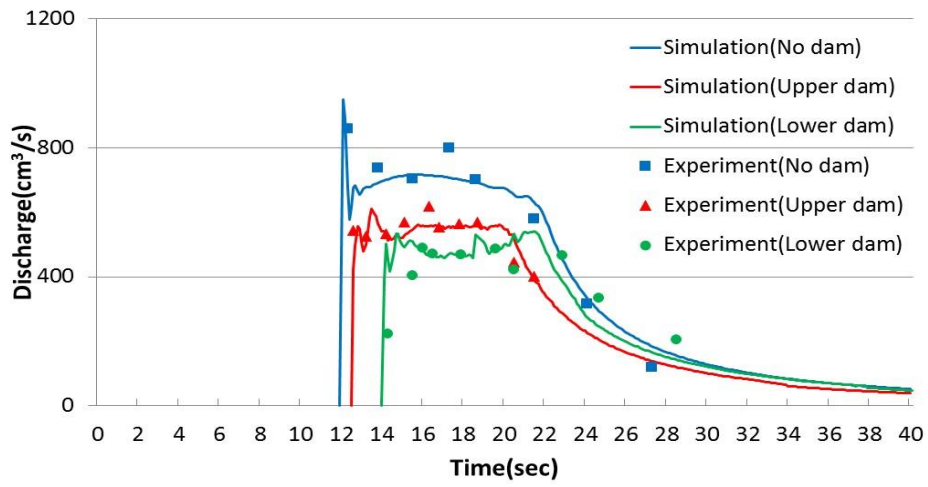


(b) Sediment concentration

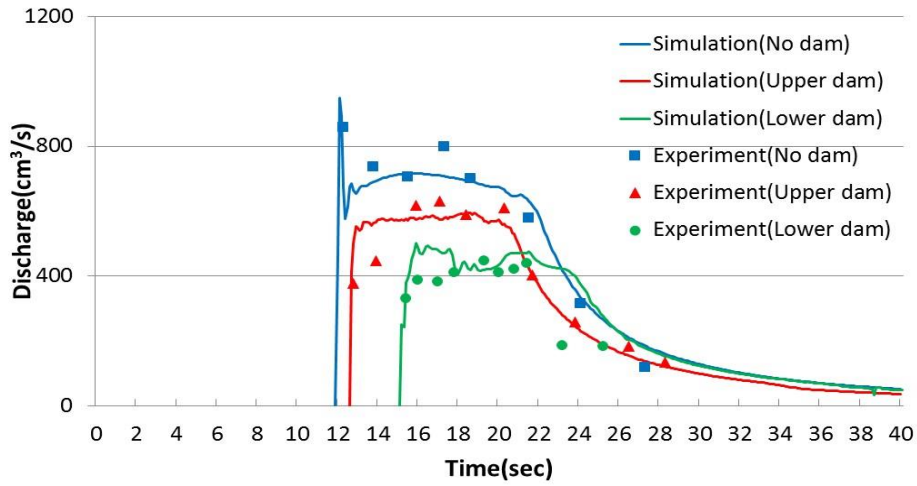
Figure 3.13 Debris flow discharge and sediment concentration at the outlet flume without Sabo Dam

The greater the distance between two Sabo dams, the easier it is to form a fully developed debris flow. The average decrease rate of the upper Sabo dam is 29.8% in the experimental results, 37.9% in the simulation results using Takahashi et al.(1992)'s equation and 33.3% in the simulation results using Egashira et al.(1993a)'s equation. However, the average decrease rate of the lower Sabo dam is 26.4% in the experimental results, 11.8% in the simulation results using Takahashi et al.(1992)'s equation and 21.2% in the simulation results using Egashira et al.(1993a)'s equation. The efficiency of the decrease rate of debris flow peak discharge at the lower Sabo dam is less than that of the upper Sabo dam.

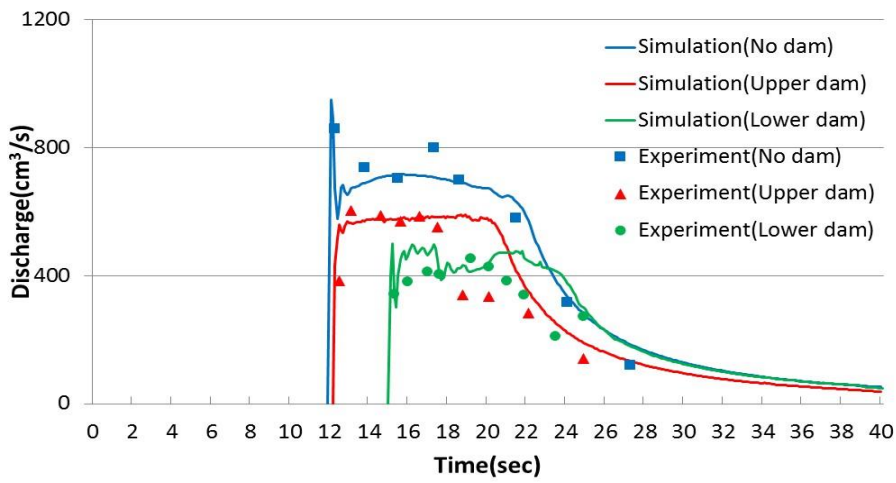
The simulated results of reduction of debris flow discharge using Takahashi et al.(1992)'s equation were in good agreement with the experimental results. The simulated results of reduction of debris flow discharge using Egashira et al.(1992)'s were overestimated compared with the simulated results of reduction of debris flow discharge using Takahashi et al.(1992)'s equation. Nevertheless, the simulated results of reduction of debris flow discharge using Egashira et al.(1992)'s were suited with experimental results. Therefore, the simulation results of debris flow discharge and sediment concentration using both equations were agreeable with the experimental results.



Case. C-1

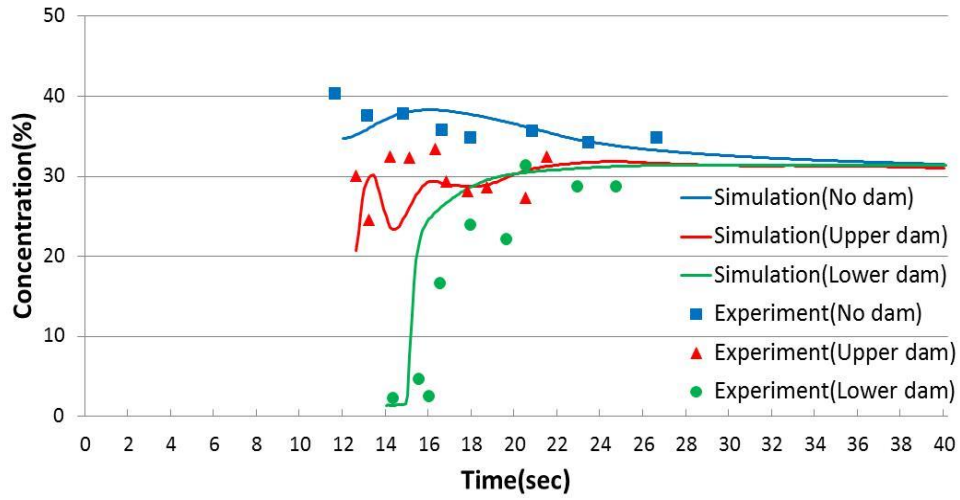


Case. C-2

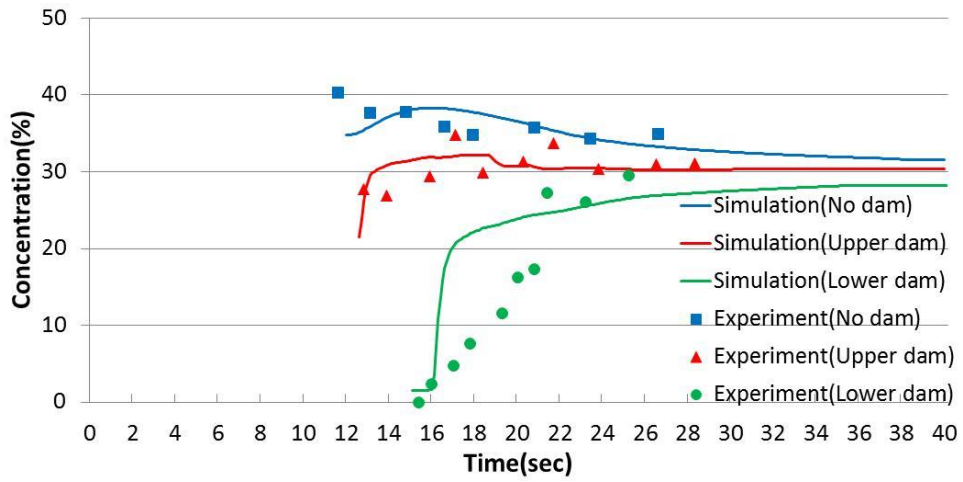


Case.C-3

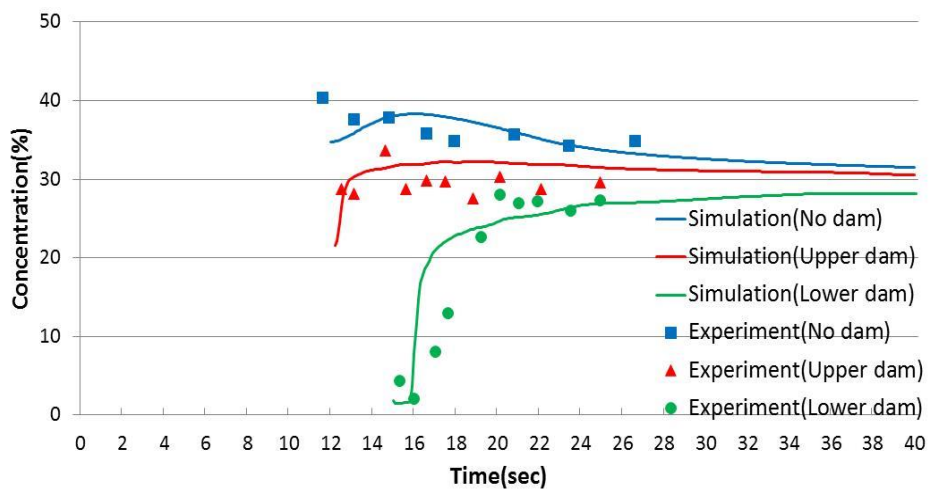
Figure 3.14 Debris flow discharge of the Sabo dams (equation of Takahashi et al.)



Case. C-1

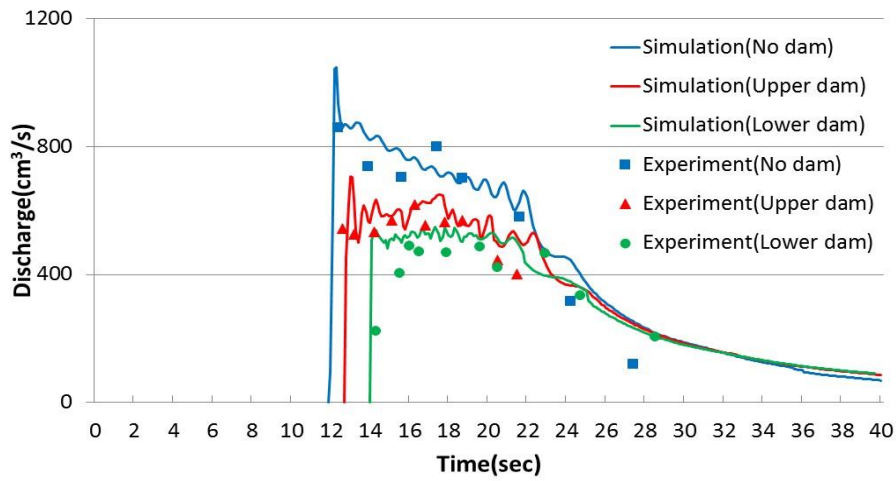


Case. C-2

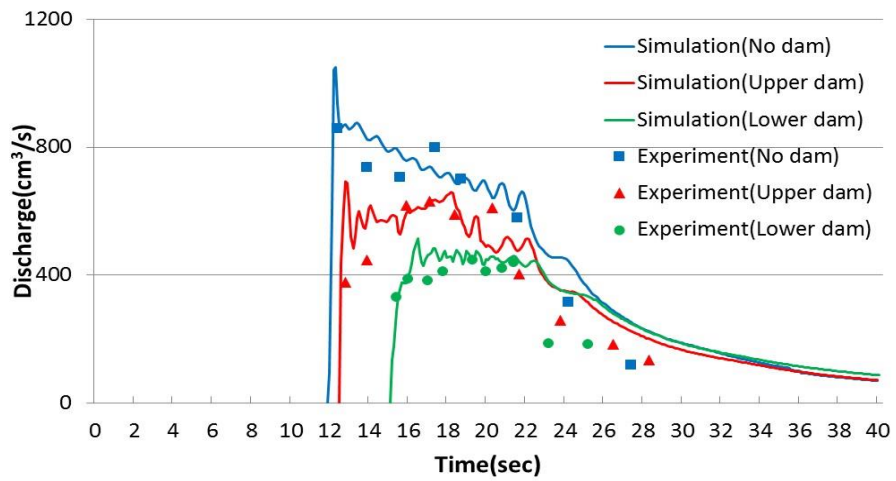


Case.C-3

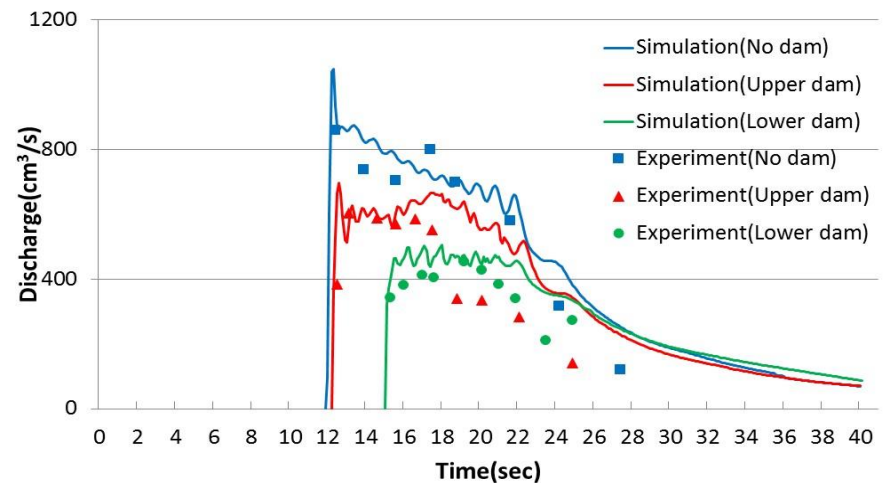
Figure 3.15 Sediment concentration(equation of Takahashi et al.)



Case. C-1

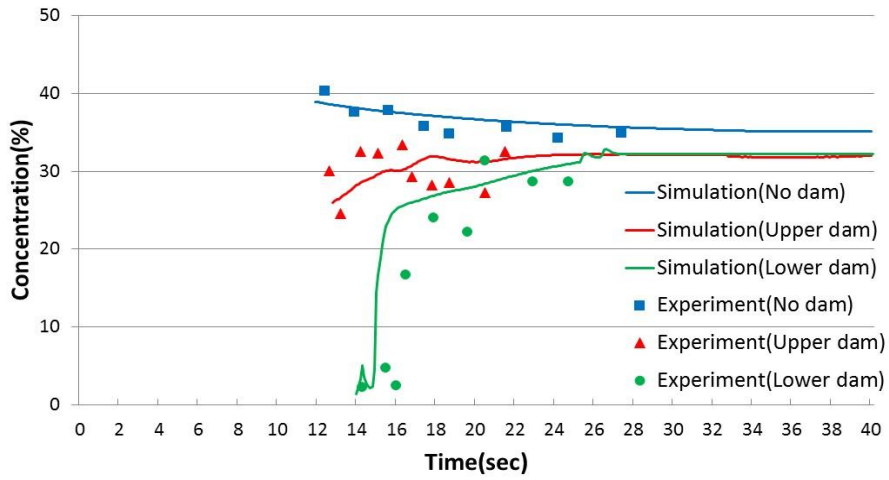


Case. C-2

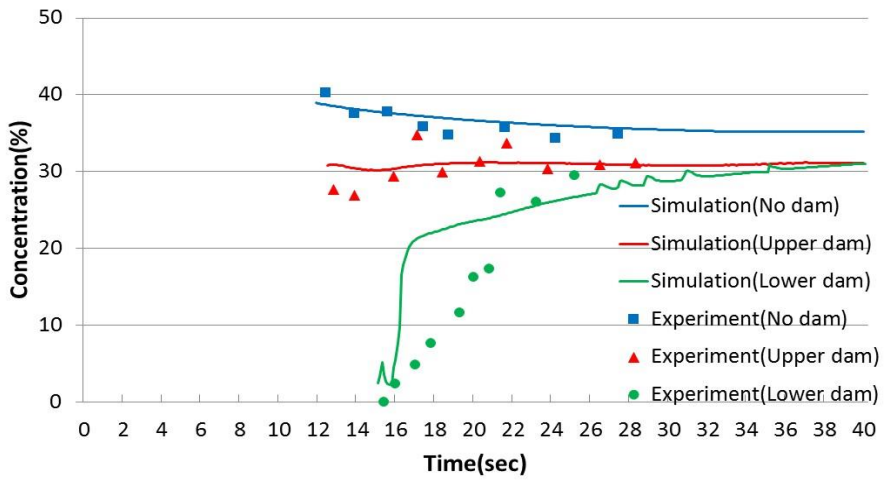


Case.C-3

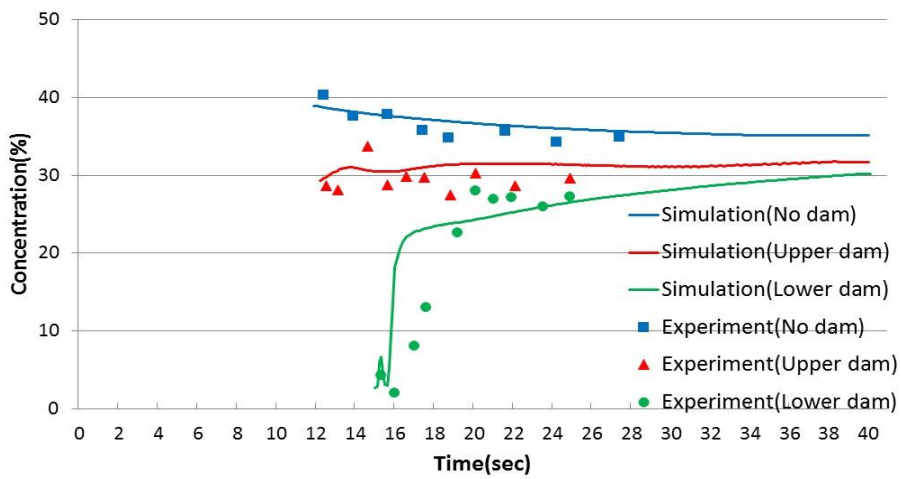
Figure 3.16 Debris flow discharge of the Sabo dams(equation of Egashira et al.)



Case. C-1



Case. C-2



Case.C-3

Figure 3.17 Sediment concentration(equation of Egashira et al.)

Table 3.4 Debris flow peak discharge

			Peak Discharge(cm ³ /s)	Decrease Rate (%)	Total decrease Rate(%)
Experiment	No Dam		872.00	-	-
	Case C-1	Upper	619.0	29.1	43.8
		Lower	490.5	20.8	
	Case C-2	Upper	629.9	27.9	48.8
		Lower	447.3	28.9	
	Case C-3	Upper	588.2	32.6	52.6
		Lower	413.6	29.6	
Simulation (equation of Takahashi et al.)	No Dam		949.68	-	-
	Case C-1	Upper	611.6	35.5	44.1
		Lower	530.6	13.2	
	Case C-2	Upper	577.7	39.2	45.8
		Lower	514.3	10.8	
	Case C-3	Upper	578.4	39.1	46.1
		Lower	512.1	11.4	
Simulation (equation of Egashira et al.)	No Dam		1048.56	-	-
	Case C-1	Upper	706.9	32.5	44.2
		Lower	585.1	17.2	
	Case C-2	Upper	691.9	34.0	50.8
		Lower	515.1	16.9	
	Case C-3	Upper	696.0	33.6	53.3
		Lower	488.8	29.7	

3.6 Summary

This chapter describes the developed numerical model to simulate the debris flow discharge at the dam point and presents the debris flow deposition process according to arrangement of Sabo dams. First, in the debris flow deposition results, the simulated results using Takahashi et al.'s(1992) equations were underestimated compared with the experimental results. In contrast,

the simulated results using Egashira et al.'s(1993a) equations were overestimated compared with the experimental results. However, the simulated results using both equations were agreeable with the experimental results. Second, Debris flow discharge is calculated by the overflow equations and the free overfall equations. The standard to divide the overflow situation and free overfall situation is debris flow deposition height upstream of Sabo dam. When the debris flow deposition is higher than Sabo dam elevation, a free overfall equations are applied, and when debris flow deposition is lower than Sabo dam elevation, an overflow equations are applied. Only in Case C-1, a complete overflow situation, an incomplete overflow situation and free overfall situation appeared. In case Case C-2 and C-3 does a complete flow situation, and free overfall situation appeared. The simulated results of reduction of debris flow discharge were in good agreement with the experimental results. Also the simulated results of debris flow concentration at the dam point were in agreement with the experimental results.

CHAPTER 4

ESTIMATION OF THE DISCHARGE COEFFICIENT FOR DEBRIS FLOW

4.1 General

Weirs are barriers vertically located to the main direction of water movement. They are widely used for measuring the flow of liquids in flumes and open channels. The most common types of weir are the broad-crested weir, the sharp-crested weir and the circular-crested weir. They are frequently used to measure the flow of water in laboratories and in small natural streams. A properly designed and operated weir of a given geometry has a unique discharge. So a large number of empirical discharge formulas have been proposed for weirs according to the relationship between flow depth and discharge. Many kinds of weirs and discharge formulas have been extensively studied using classical physics and experimental analyses to understand the characteristics of flow and to determine the coefficient of discharge. This coefficient represents effects not considered in the derivation of the equations used to estimate discharge from the flow depth. Such effects include viscosity, capillarity, surface tension, velocity distribution and streamline curvature attributable to weir contraction (Aydin et al., 2011).

The coefficients of discharge of full-width rectangular weirs and contracted rectangular notches are reported to be a function of the head-weir height ratio and width-contraction ratio (Kindsvater and Carter 1957). Harrison (1967) presented a new coefficient of discharge for a streamlined broad-crested weir based on critical flow theory. Farhoudi and Shahalami (2005) proposed the flow pattern governing the hydraulic principles of rectangular broad and short-crested weirs.

Gonzalez & Chanson (2007) conducted experiments in near-full-scale broad-crested weir.

Based on their investigations, theoretical equations have been presented for ideal flow from which approximate ratings can be obtained to within reasonable accuracy with an empirical discharge coefficient. The ratings for a wide variety of shapes and sizes of these weirs were computed with the model and fit to an empirical equation. However, these equations are for clear water; there are few works on debris flow.

In this study, experiments were conducted in an open channel, i.e., a rectangular flume. Measuring the flow rate of debris flow involves some type of obstruction in the path of the flow. In the experiment, a Sabo dam of 6 cm in height, 10 cm width, and 1 cm in thickness was used like a weir. A weir is a vertical obstruction that the debris flow must flow over. The measured flow depth, volume, and weight of debris flow were used to calculate the debris flow overflow discharge coefficient in an overflow equation. In the numerical model, a complete flow equation, and free overfall equation were used. To determine the discharge coefficient for each equation, regression analysis was conducted.

4.2 Experiment for Debris Flow Discharge Coefficient

The experimental method is almost the same as the above experimental method (Figure 4.1). For a rectangular flume, the experimental condition is the same. However the sediment distribution and material of at the bottom of the flume is changed. This is because debris flow deposition upstream of Sabo dams is very rapid and it is difficult to find the deposition height by a video camera due to gravel sand (Figure 4.2). For this reason, in this condition, the overflow situation is very short (figure 4.3). Therefore, to clear the debris flow deposition upstream of Sabo dams and to slow the debris flow velocity, some conditions are changed. Table 4.1 shows the experimental conditions.

The sediment used is silica sand(S1, S2, S3, S4, S5, and S6). The mixed sediment materials have a mean diameter of $d_m = 2.45$ mm, and a maximum diameter $d_{max} = 4.26$ mm. Table 4.1 shows the sediment material and Figure 4.4 shows the particle size distribution of sediment

Table 4.1 Experimental conditions

Experiment no.	Supply water discharge (cm ³ /s)	Time (sec)	Mean diameter (mm)
Case.D-1	400	15	2.45

materials. The material of the flume bottom is changed to make slow the debris flow velocity (Figure 4.5). Therefore, a test experiment was conducted to change the roughness coefficient using Manning's equation. Through the text experiment, roughness coefficient n is equal to $0.02 \text{ s/m}^{1/3}$.

$$Q = \frac{1}{n} R^{2/3} I^{1/2} w H \quad (4.1)$$

where Q is the discharge, R is the hydraulic radius, I is the slope of the hydraulic grade line, w is the width of flume, and H is the flow depth.

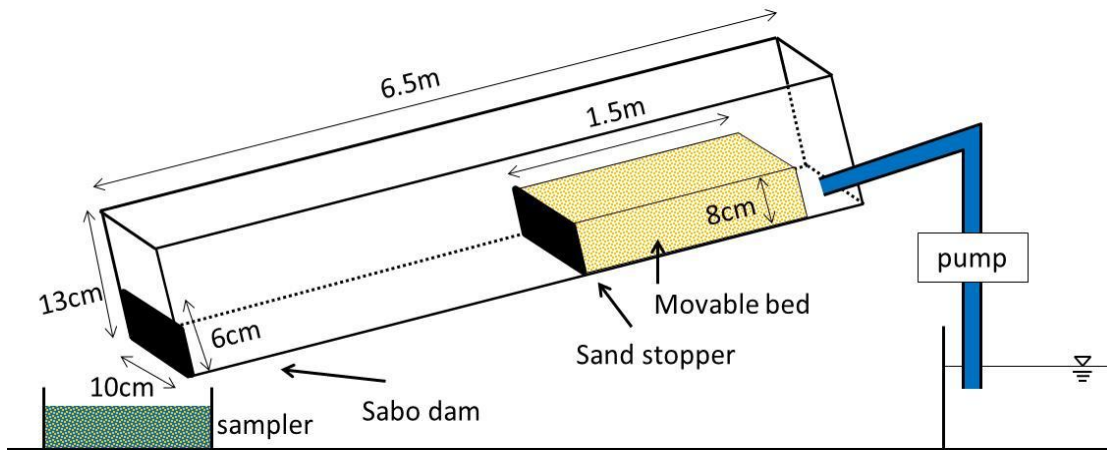


Figure 4.1 Experimental setup

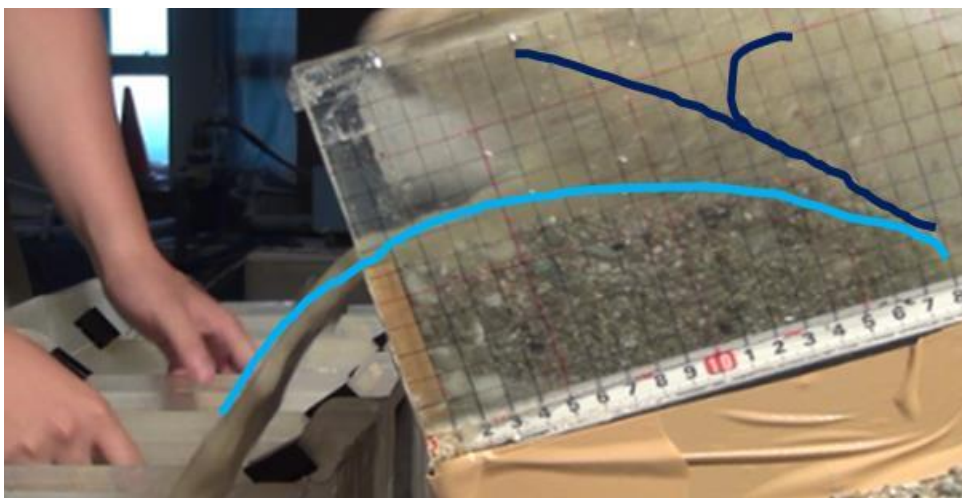


Figure. 4.2 Debris flow hit the deposited sediment

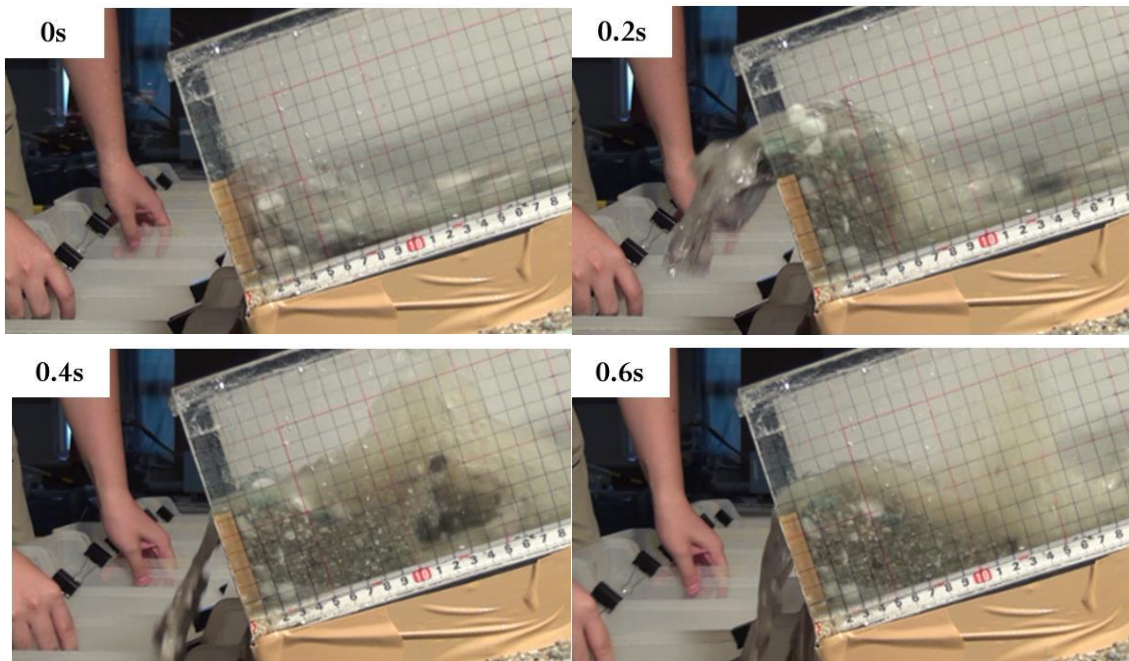


Figure 4.3 Time changeable to debris flow deposition

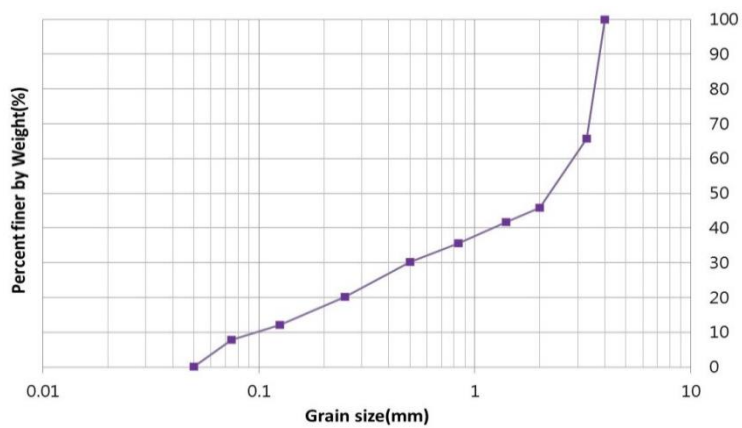
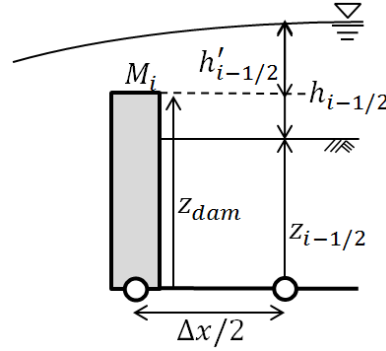


Figure 4.4 Particle size distribution of sediment materials



Figure 4.5 Bottom of the flume



4.3 Theoretical Analysis

As mentioned above, the overflow equation and free overfall equation were used to calculate the debris flow outflow discharge. To calculate the debris flow overflow discharge, the equation is determined according to the debris flow deposition height (Figure 4.6). When the debris flow deposition height is higher than Sabo dam, the complete overflow equation is applied. When the debris flow deposition height is lower than Sabo dam, the free overfall equation is applied. Therefore, while debris flow is being deposited upstream of the Sabo dam, debris flow discharge is calculated by the complete overflow equation. And, then, after deposition is finished, debris flow discharge is calculated by the free overfall equation. However, after the debris flow deposition height is equal to the dam crown, very small-size erosion and deposition is repeated in the numerical simulation. That erosion height is 0.001cm. In Figure 4.7, the red line and red point mean that overflow equation is applied. The blue line and blue point means that free overfall equation is applied. When the bed elevation at the upstream Sabo dams equal to height of Sabo dam, it looks as if it is 6 cm. However it is not 6cm. In reality, it is 5.999 cm. So, in case of a debris flow deposition height that is equal to 5.999 cm, discharge is calculated by the overflow equation. However, it is nonsense to apply the overflow equation due to the very small-size erosion. Therefore, in this case, the free overfall equation is applied. The new condition is as follows:

If $z_{i-1/2} < z_{dam} - \varepsilon$;

$$\left(\frac{h'_{i+1/2}}{h'_{i-1/2}} \leq \frac{2}{3} \right) \quad M_0 = c_1 h'_{i-1/2} \sqrt{2gh'_{i-1/2}} \quad (4.2)$$

If $z_{i-1/2} \geq z_{dam} - \varepsilon$;

$$(h'_{i-1/2} > z_{dam}) \quad M_0 = c_3 h'_{i-1/2} \sqrt{gh'_{i-1/2}} \quad (4.3)$$

where, ε is 0.001 cm. According to the discharge coefficient, the debris flow discharge is different from the experimental results. To determine the discharge coefficient for each equation, the root-mean-square deviation method is used. RMSD represents the sample standard deviation of the differences between predicted values and observed values. When measuring the average difference between two time series $x_{1,t}$ and $x_{2,t}$, the formula becomes:

$$RMSD = \sqrt{\frac{\sum_{t=1}^n (x_{1,t} - x_{2,t})^2}{n}} \quad (4.4)$$

where, $x_{1,t}$ is experimental results value of debris flow discharge, $x_{2,t}$ is simulation results value of debris flow discharge. n is observed number in experimental result that is 9.

4.4 Results and Discussion

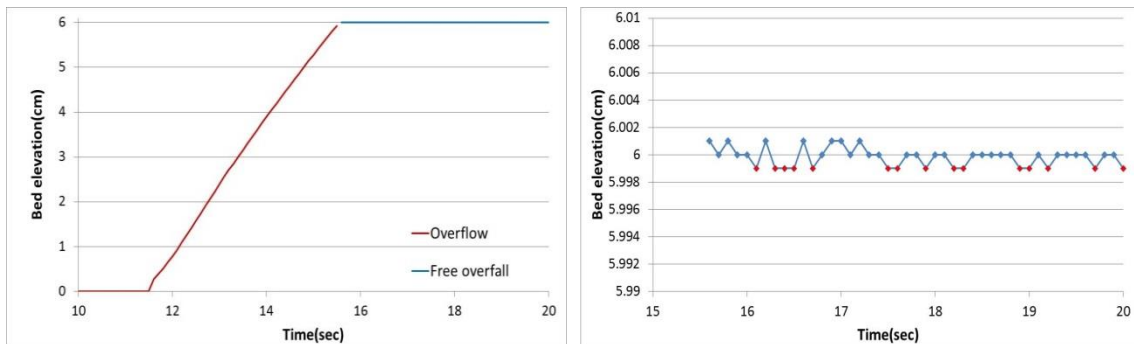


Figure 4.7 Bed elevation($z_{i-1/2}$)

4.4.1 Discharge coefficient by Arrangement of Sabo Dam

Numerical simulations and experiments were performed to calculate the debris flow outflow discharge. Discharge coefficient for Case C-1, Case C-2, and Case C-3 were determined by RMSD analysis. Smallest RMSD value were determined comparing the debris flow discharge. Sediment concentration was not considered to determine the smallest RMSD value. Discharge coefficient for Case D-1 was determined by regression analysis.

When the distance between two Sabo dams is far enough, incomplete overflow situation does not occur. In Case C-2 and Case C-3, therefore, an incomplete overflow situation does not occur. Only in Case C-1, an incomplete flow situation occurs. Therefore, in case C-2 and Case C-3, discharge coefficient c_2 is equal to 1.0.

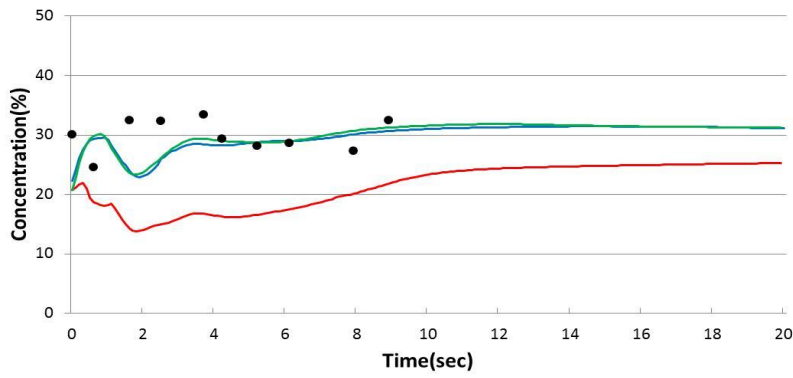
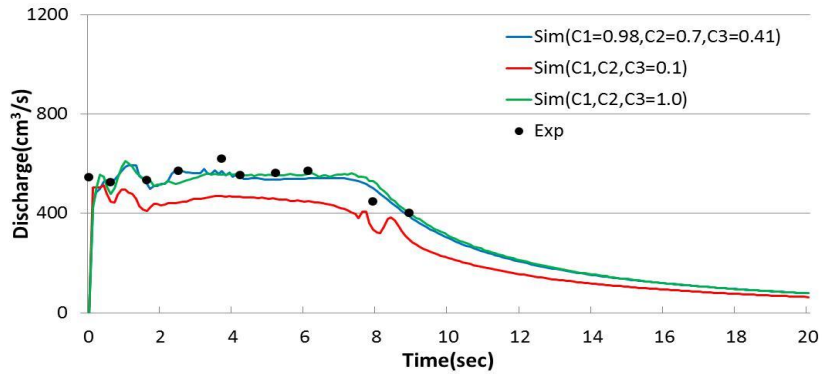
Figure 4.8, Figure 4.9, and Figure 4.10 show the debris flow discharge and sediment concentration at each of the Sabo dam points. In this graph, Time 0 means the start time of debris flow overflow at each sabo dam. The green line means that c_1 , c_2 , and c_3 are 1. The red line means that c_1 , c_2 , and c_3 are 0.1. The blue line means that the discharge coefficients are determined by the RMSD value. In other words, discharge coefficients where the RMSD value is the smallest are selected. Only in Case C-1 the incomplete flow situation occurs, so c_2 is determined at the upper dam. Except the Case C-1, incomplete flow situation does not occur So, c_2 value is not determined. Its value is used as 1.0.

Table 4.2 shows the suggested discharge coefficient. The discharge coefficient differs according to the distance between Sabo dams and the position of the Sabo dams. In Case C-1, $c_1 = 0.98$, $c_2 = 0.7$, and $c_3 = 0.41$ is determined at the upper Sabo dam and $c_1 = 0.86$, and $c_3 = 0.64$ is determined at the lower Sabo dam. In Case C-2, $c_1 = 0.86$, and $c_3 = 0.43$ is determined at the upper Sabo dam and $c_1 = 0.34$, and $c_3 = 0.47$ is determined at the upper Sabo dam. In Case C-3, $c_1 = 0.67$, and $c_3 = 0.52$ is determined at the upper Sabo dam and $c_1 = 0.53$, and $c_3 = 0.76$ is determined at the lower Sabo dam.

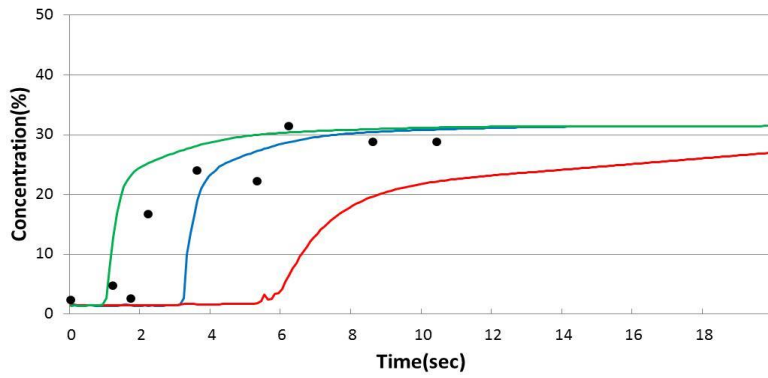
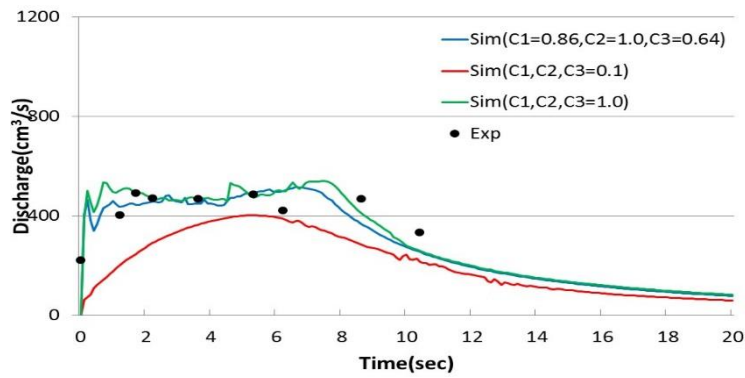
Through the suggested discharge coefficient, simulation results are in good agreement with experimental results. But suggested discharge coefficient are very different each other even if the same situation. These discharge coefficients are just used for matching the simulation results with experimental results. These discharge coefficients are difficult to be applied in reality. Therefore, it is necessary to find proper discharge coefficient to be applied in reality. In other words, consistent discharge coefficient is needed to calculate overflow debris flow discharge at the Sabo dam.

Table 4.2 Discharge coefficient by RMSD value

	Upper dam			RMSD	Lower dam			RMSD
	c_1	c_2	c_3		c_1	c_2	c_3	
Case C-1	0.1	0.1	0.1	307.86	0.1	0.1	0.1	324.05
	1	1	1	133.09	1	1	1	248.92
	0.98	0.7	0.41	112.33	0.86	-	0.64	229.75
Case C-2	0.1	0.1	0.1	397.77	0.1	0.1	0.1	406.26
	1	1	1	245.04	1	1	1	283.47
	0.86	-	0.43	241.37	0.34	-	0.47	185.32
Case C-3	0.1	0.1	0.1	307.33	0.1	0.1	0.1	414.69
	1	1	1	374.85	1	1	1	335.71
	0.67	-	0.52	239.01	0.53	-	0.76	232.17

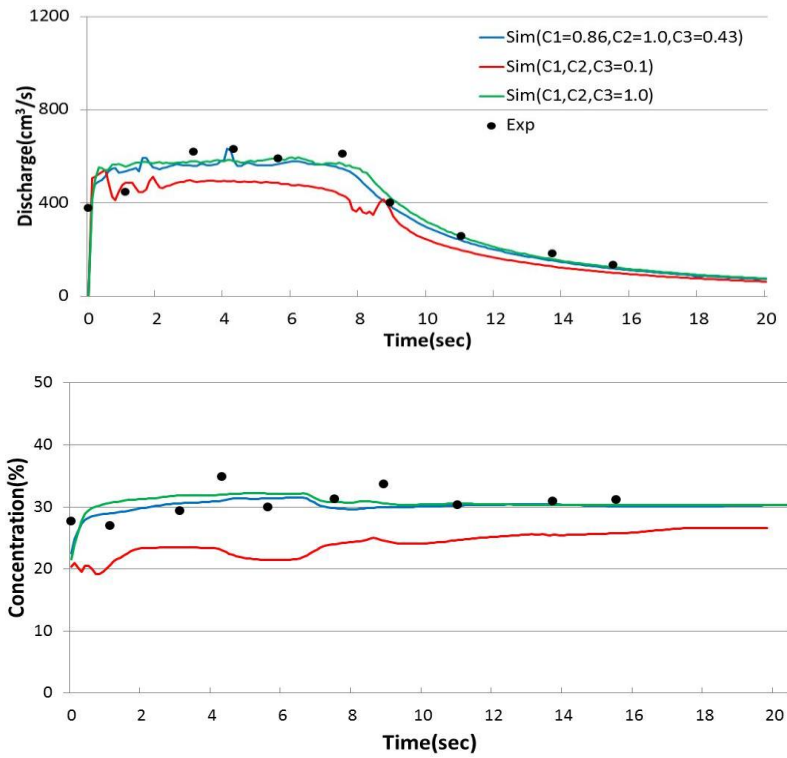


(a) Upper Sabo Dam

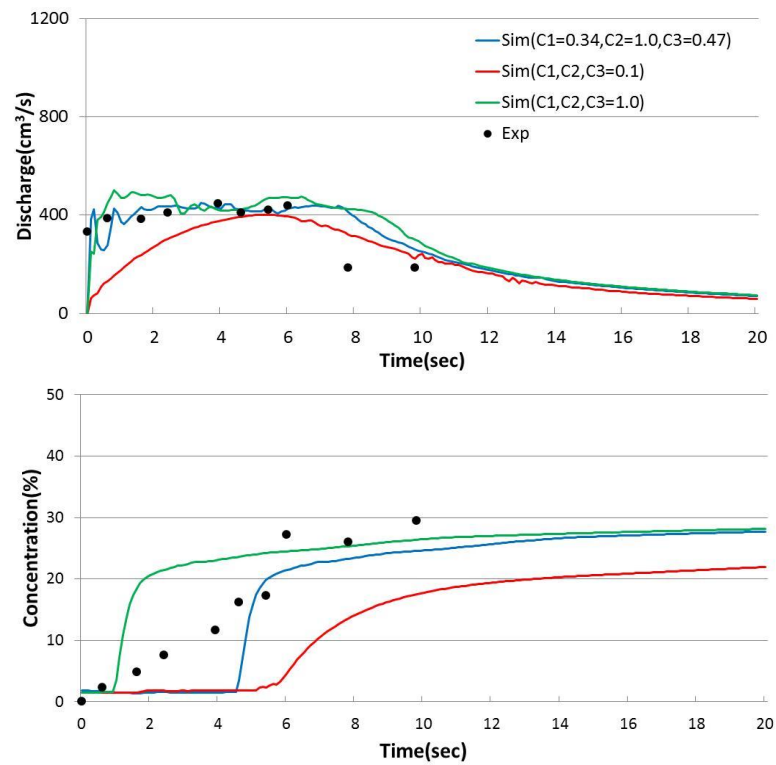


(b) Lower Sabo Dam

Figure 4.8 Debris flow discharge and sediment concentration (Case C-1)

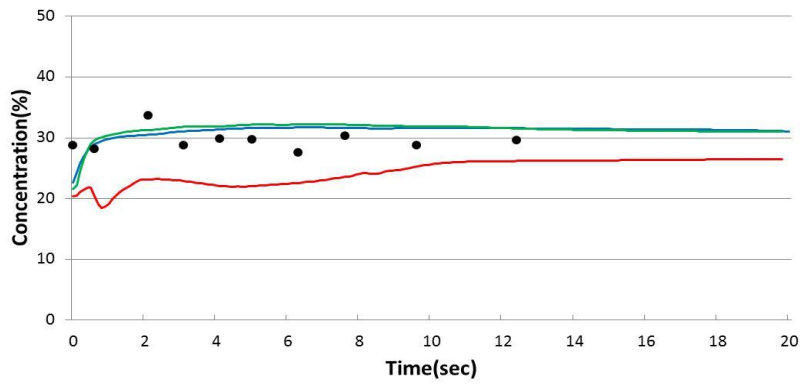
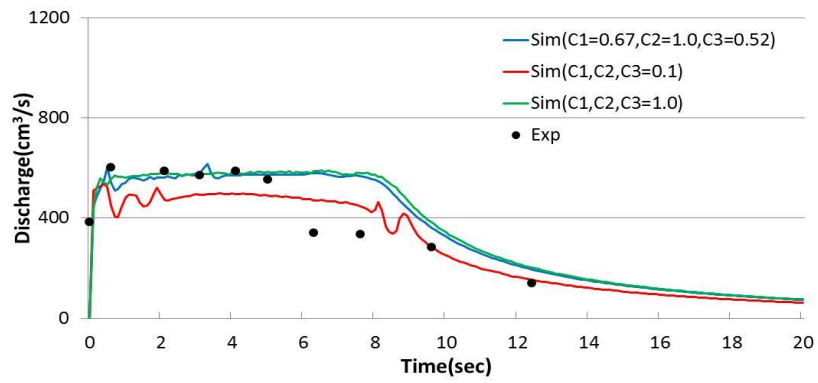


(a) Upper located Sabo Dam

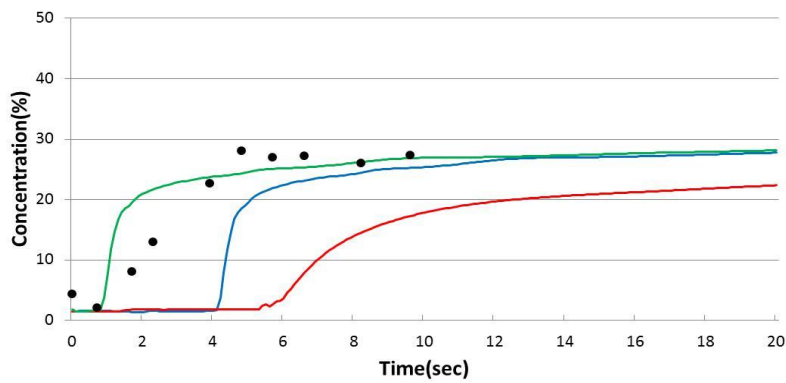
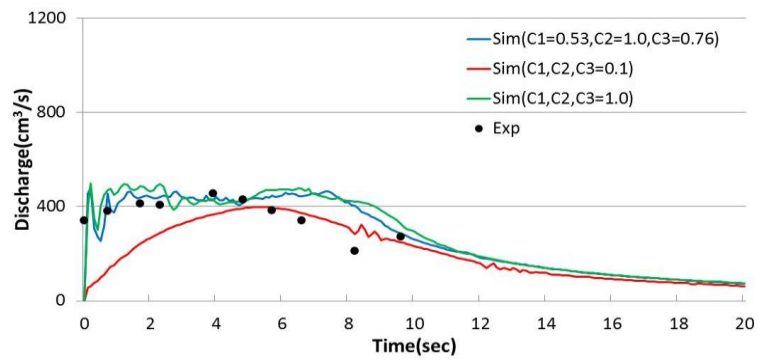


(b) Lower Sabo Dam

Figure 4.9 Debris flow discharge and sediment concentration (Case C-2)



(a) Upper Sabo Dam



(b) Lower Sabo Dam

Figure 4.10 Debris flow discharge and sediment concentration (Case C-3)

4.4.2 Discharge Coefficient by Regression Analysis

To determine the consistent discharge coefficient in overflow equations and free overfall equations, regression analyses are conducted. Figure 4.11, and Figure 4.12 show the experimental results for Case D. In this case, an incomplete overflow situation does not occur. The blue color means a complete overflow situation where debris flow deposition height is lower than the Sabo dam elevation, and the red color means a free overfall situation where the debris flow deposition height is higher than the Sabo dam. In the experimental results, peak discharge is 981.36 cm³/s, peak flow depth is 2cm, and sediment concentration is around 32%.

To obtain more accurate simulation results, discharge coefficients are needed to considering other parameters. Therefore, discharge coefficient is calculated by single regression analysis with sediment concentration. The discharge coefficient is a dependent variable and sediment concentration is an independent variable in the regression model.

$$c_1 = f(C) \quad (4.5)$$

$$c_3 = f(C) \quad (4.6)$$

Table 4.3 shows the single regression analysis results in case of overflow situation by sediment concentration. From the table, R-square and P-value are important to estimate the regression equation. R-square is a statistical measure of how close the data are to the fitted regression line. In general, the higher the R-square, the better the model fits with data. P-value is a function of the observed data that is used for testing a statistical hypothesis. A low P-value(<0.05) indicates that statistically significant. Conversely, a larger P-value has no meaning between independent variable and dependent variable. In case of overflow situation, R square is equal to 0.613, and Adjusted R square is equal to 0.558. And, through the analysis of variance, p-value is equal to 0.012. So, this means that sediment concentration is also related with discharge coefficient. Therefore, discharge coefficient could be expressed as follows according to sediment concentration:

$$c_1 = -0.38029 + 0.037331C_{i-1/2} \quad (25\% < C_{i-1/2} < 35\%) \quad (4.7)$$

Table 4.4 shows the single regression analysis results in case of free overfall situation by sediment concentration. R square is equal to 0.039, and Adjusted R square is equal to 0.027. These values are not near to 1.0. However, through the analysis of variance, p-value is equal to 0.0414. So, statistical significance is confidence level. Therefore, regression equation could be

expressed as follows:

$$c_3 = 0.59751 + 0.003925C_{i-1/2} \quad (4.8)$$

Figure 4.13, and Figure 4.14 shows the relationship between discharge coefficient and sediment concentration in case of overflow situation and free overfall situation with trend line. It shows that sediment concentration C increases as discharge coefficient c_1 , and c_3 increases.

Equations 4.7, and 4.8 are limited equations in condition that sediment concentration is between 25% and 35%, because these equations are obtained under the condition that the sediment concentration is between 25% and 35%. When the sediment concentration is 0 in the overflow situation, c_1 becomes to minus value. In fact, sediment concentration equal to 0 means that clear water. Therefore, extrapolation was applied in case of overflow situation. When the sediment concentration equal to 0, discharge coefficients equal to 0.35. And, when the discharge coefficients equal to 0.35 in the equation 4.7, sediment concentration is 19.56%. So, when sediment concentration is less than 19.56%, discharge coefficient is 0.35. Also, when the sediment concentration is less than 25% or more than 35% in the free overfall situation, discharge coefficient was used equation 4.8 (Figure 4.15).

By applying the developed equations 4.7, and 4.8, simulation results are shown in Figure 4.16. In the simulation results which using equations of Takahashi et al.(1992), peak discharge is 929.9 cm^3 , peak flow depth is 1.63cm, and average sediment concentration is 29.6%. The simulation results which using equations of Egashira et al.(1993a) are similar with the simulation results which using equations of Takahashi et al.(1992). Peak discharge is $978.3 \text{ cm}^3/\text{s}$, peak flow depth is 1.75cm, and average sediment concentration is 31.2%. The simulation results in overflow situation and free overfall situation are in good agreement with experimental results. It means that discharge coefficient is affected by sediment concentration. In reality, there are some kinds of parameter to affect the debris flow discharge. If more parameter is considered, simulated results are more improved.

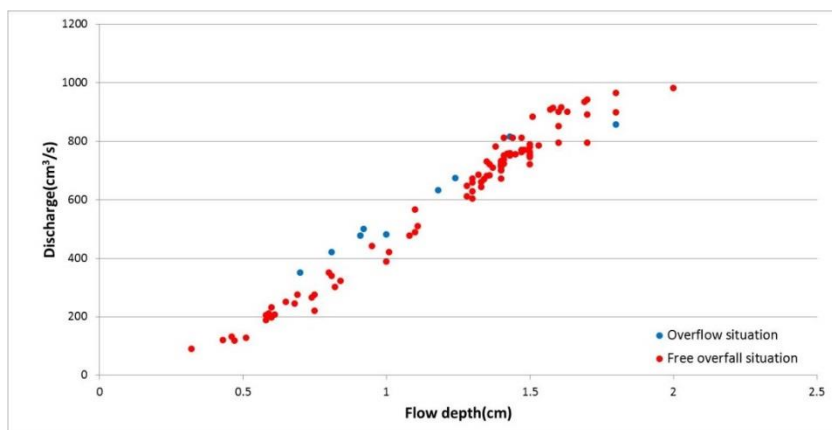
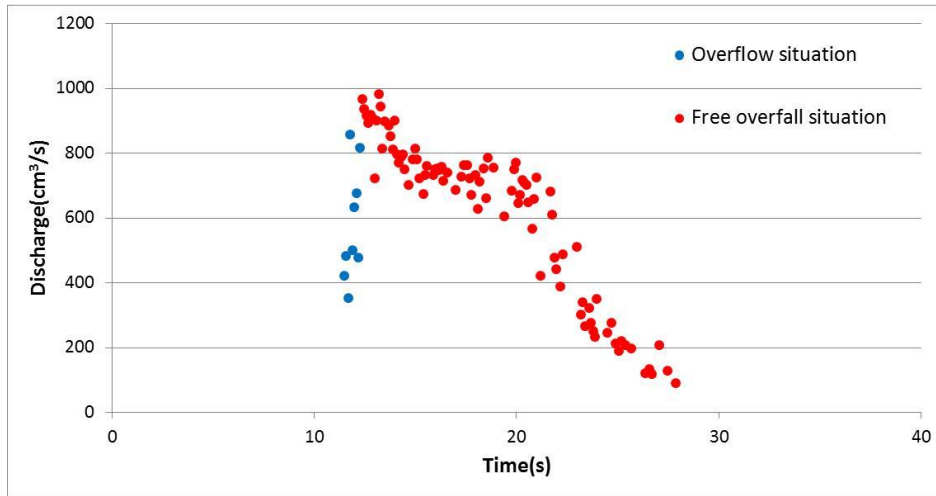
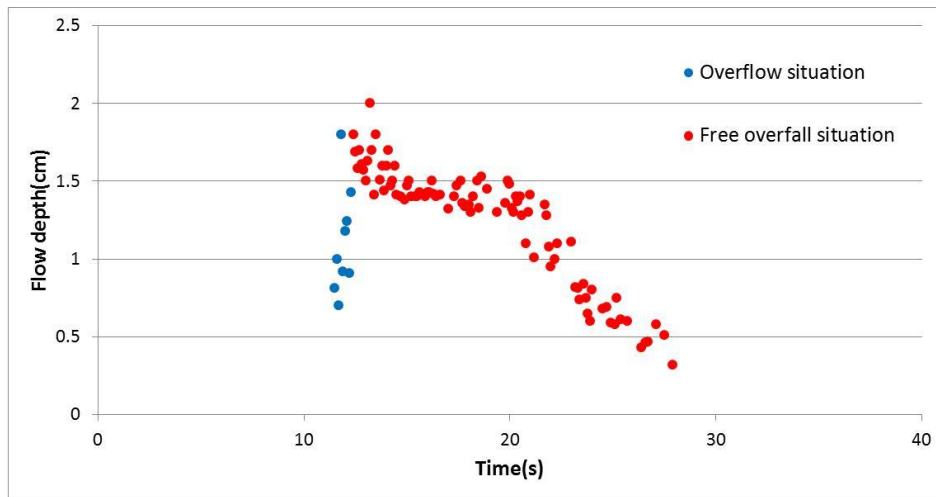


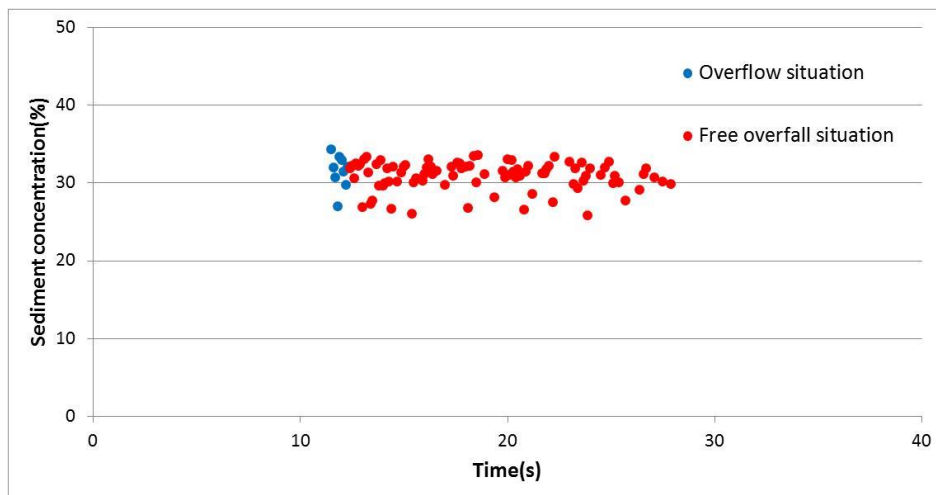
Figure 4.11 Relationship between flow depth and discharge (Case D-1)



(a) Debris flow discharge



(b) Flow depth



(c) Sediment concentration

Figure 4.12 Experimental results in Case D-1

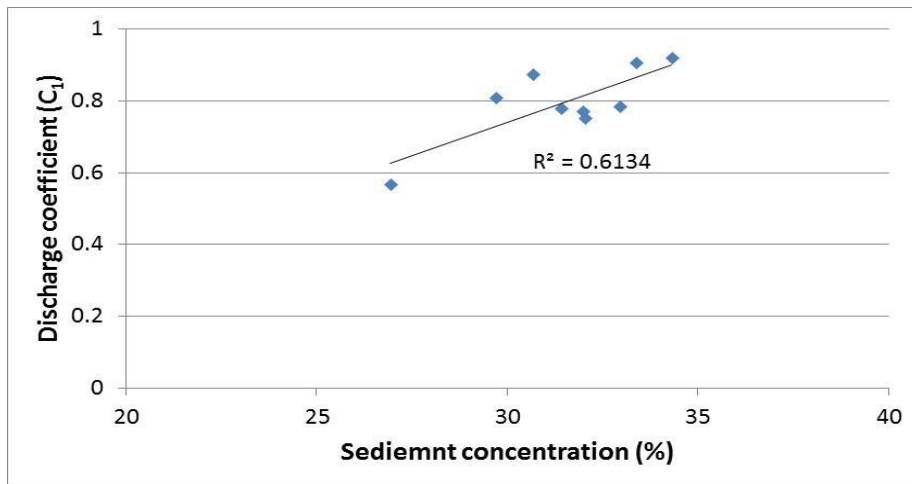


Figure 4.13 Relationship between discharge coefficient and sediment concentration in case of overflow situation (C₁)

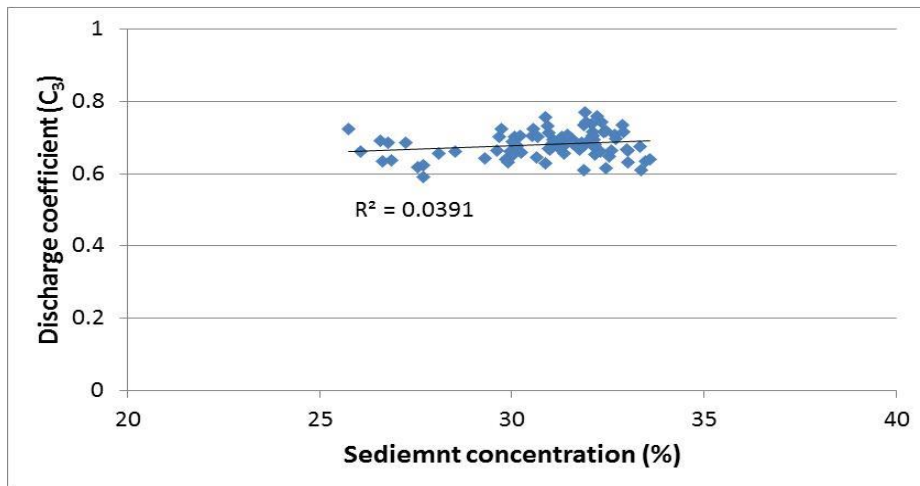


Figure 4.14 Relationship between discharge coefficient and sediment concentration in case of free overfall situation (C₃)

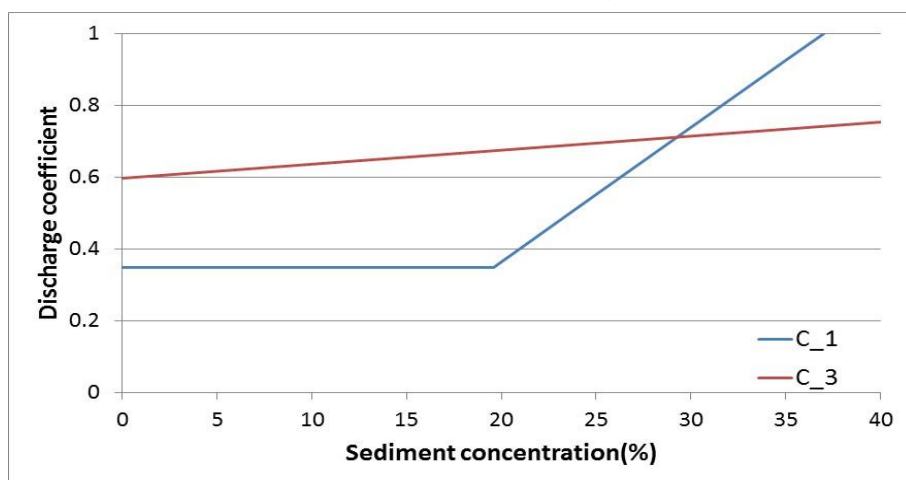


Figure 4.15 Discharge coefficient

Table 4.3 Regression analysis in case of overflow situation(Sediment concentration)

Regression Statistics	
Multiple R	0.783177
R Square	0.613366
Adjusted R Square	0.558133
Standard Error	0.069884
Observations	9

ANOVA

	df	SS	MS	F	Significance F
Regression	1	0.054235	0.054235	11.10499	0.012549
Residual	7	0.034187	0.004884		
Total	8	0.088421			

	Coefficients	Standard Error	t Stat	P-value	Lower 95%	Upper 95%	Lower 95.0%	Upper 95.0%
Intercept	-0.38029	0.35341	-1.07606	0.317584	-1.21597	0.455392	-1.21597	0.455392
Sediment concentration	0.03733	0.011202	3.332415	0.012549	0.010842	0.063821	0.010842	0.063821

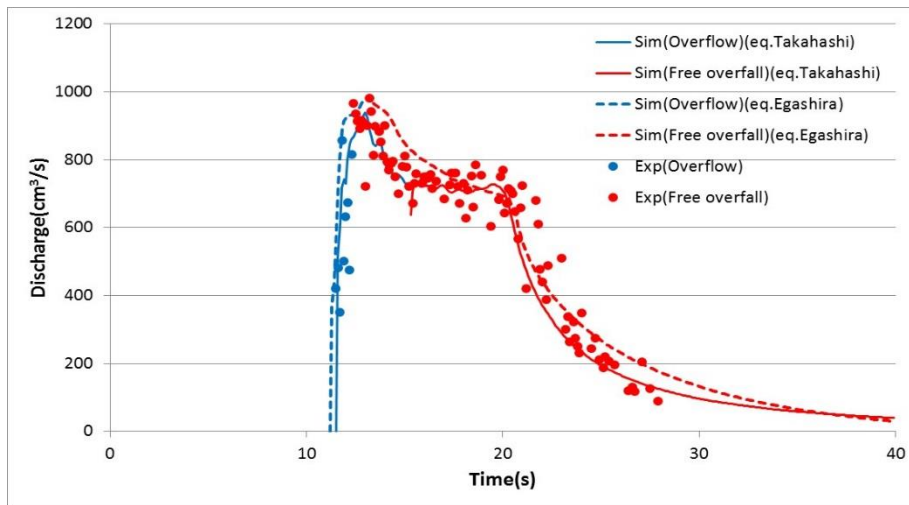
Table 4.4 Regression analysis in case of free overfall situation(Sediment concentration)

Regression Statistics	
Multiple R	0.197677
R Square	0.039076
Adjusted R Square	0.027357
Standard Error	0.036591
Observations	84

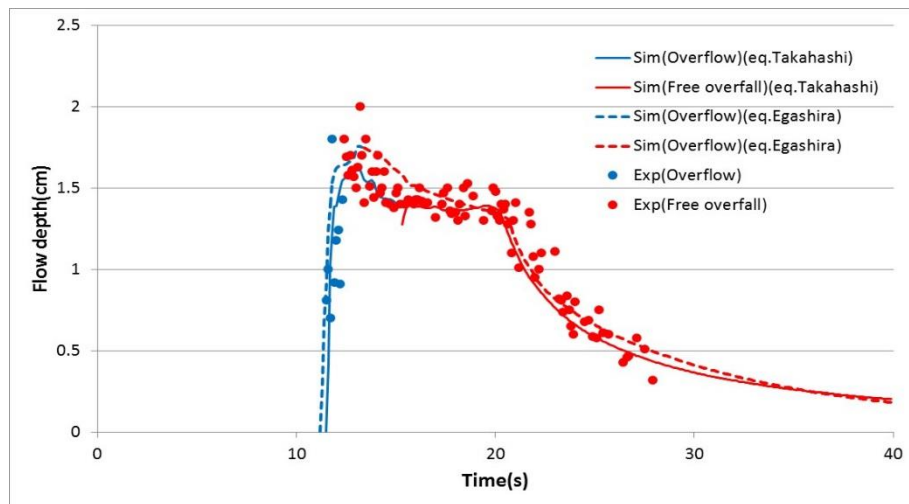
ANOVA

	df	SS	MS	F	Significance F
Regression	1	0.004465	0.004465	3.334536	0.071479
Residual	82	0.109791	0.001339		
Total	83	0.114256			

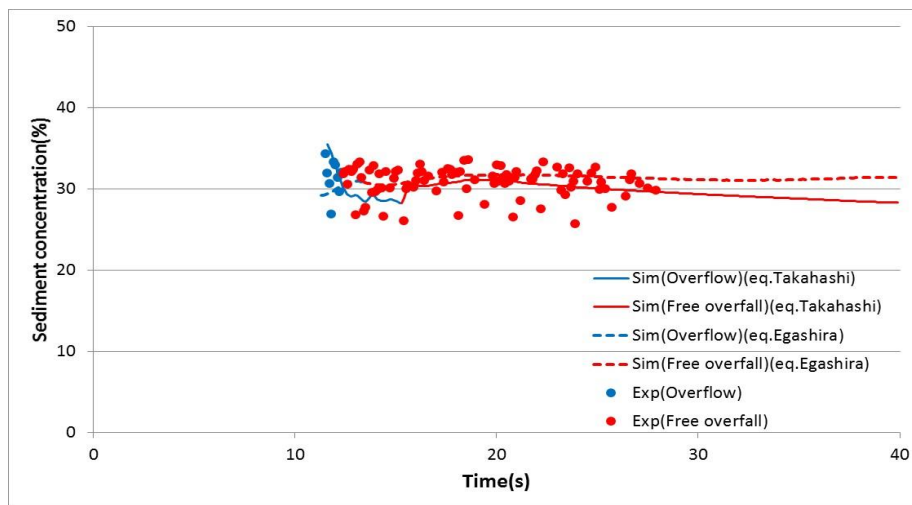
	Coefficients	Standard Error	t Stat	P-value	Lower 95%	Upper 95%	Lower 95.0%	Upper 95.0%
Intercept	0.559751	0.066553	8.410609	1.07E-12	0.427356	0.692146	0.427356	0.692146
Sediment concentration	0.003925	0.00215	1.826071	0.041479	-0.00035	0.008202	-0.00035	0.008202



(a) Debris flow discharge



(b) Flow depth

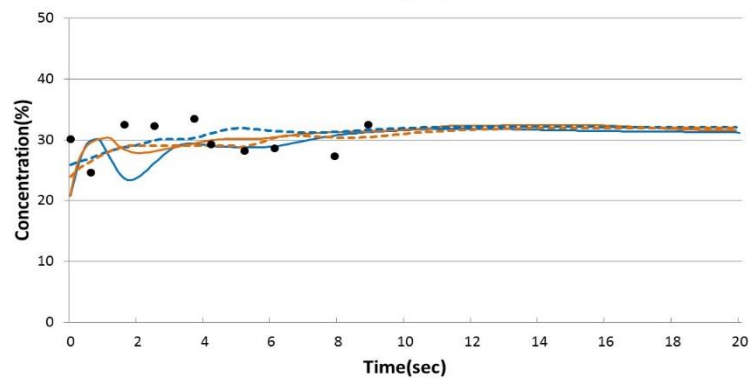
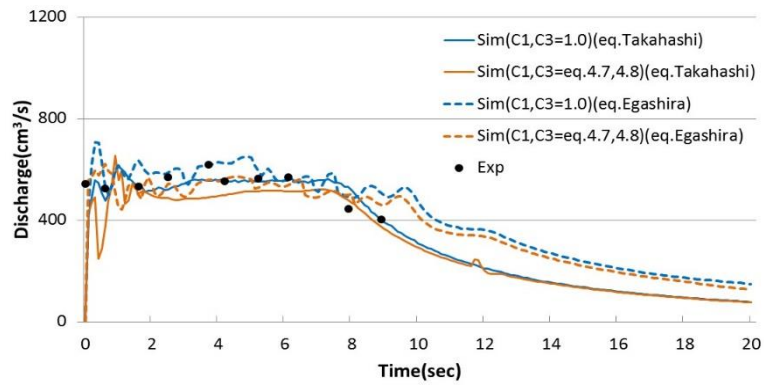


(c) Sediment concentration

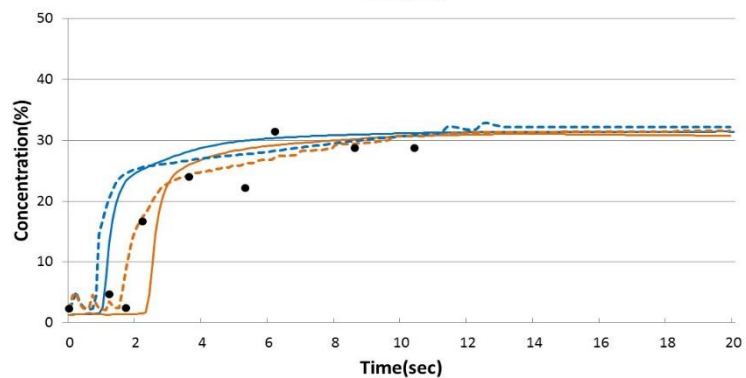
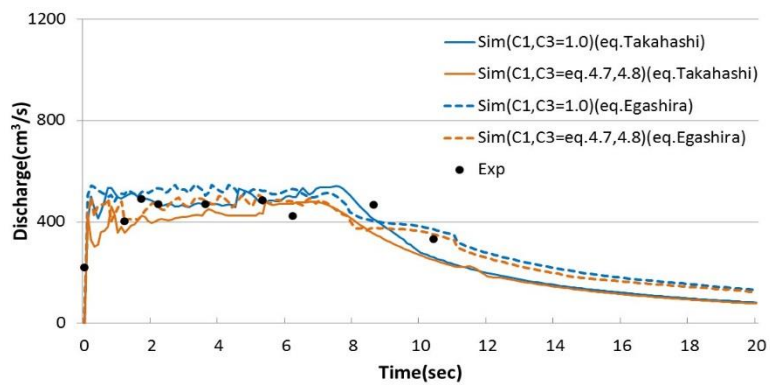
Figure 4.16 Applied discharge coefficient by sediment concentration (Case D-1)

Debris flow discharge and sediment concentration by arrangement of Sabo dam are calculated using equation 4.7, and equation 4.8. Figure 4.17, Figure 4.18 and Figure 4.19 show the debris flow discharge and sediment concentration. Time 0 means the debris flow's overflow time at each Sabo dams. Blue color means that discharge coefficients are equal to 1.0. Orange color means that discharge coefficients are derived from equations 4.7, and equation 4.8. Solid line means using Takahashi et al.(1992)'s equation, dotted line means using Egashira et al.(1992)'s equation. Black dot means experimental result.

From the discharge graph, the simulation results which using Takahashi et al.(1992)'s equation and Egashira et al.(1993a)'s equation are suited with experimental results. Although debris flow discharge results which using Takahashi et al.(1992)'s equation are underestimated compared with the results which using Egashira et al.(1993a)'s equation, both of results are in good agreement with experimental result. Also, in case of discharge coefficients are equal to 1.0 and in case of discharge coefficient using equation 4.7, and 4.8, both of results are in good agreement with experimental result. Even if the simulation results which using equation 4.7, and 4.8 are underestimated compared with the discharge coefficients are equal to 1.0. In other words, even if discharge coefficients are changed from 1.0 to equation 4.7 and 4.8, debris flow discharges are no significant difference. However, sediment concentration is different at lower Sabo dam. The simulation results that using equation 4.7 and equation 4.8 are better suited with experimental results. In case of discharge coefficients are used 1.0, sediment concentration is almost 0 during one second. And after that time, sediment concentration increases to 30%. In case of discharge coefficients using equation 4.7, and equation 4.8, sediment concentration is almost 0 during two seconds. And after that time, sediment concentration increases to 30%. As equations 4.7 and 4.8 are applied to the discharge coefficient in the simulation, sediment concentration at the lower Sabo dam are more matched with experimental results than in case of discharge coefficient equal to 1.0. At the lower Sabo dam, the reason why sediment concentration is almost 0 in the simulation results is that during debris flow is captured by Sabo dam, sediment is captured by Sabo dam and water overflow at the upper Sabo dam. At that time, this overflow is turbulent flow or immature debris flow. Figure 4.20 and 4.21 show the debris flow depth, deposition height, and sediment concentration just upstream of the lower Sabo dam in case of using Takahashi et al.(1992)'s equation and using Egashira et al.(1993a)'s equation. In this figure, Time 0 means that the debris flow's arrival time to the lower Sabo dam. Blue line means flow depth, red line means debris flow deposition height, and green line means sediment concentration. On average, flow depth is 1.5cm in the simulation results. However, flow depth just upstream of Sabo dam increases to height of Sabo dam because flow depth is captured by the Sabo dam until overflows occur. During increase the flow depth, sediment concentration is almost 0. This means that captured flow depth is not a debris flow. Turbulent flow is occurred at the beginning of overflow.

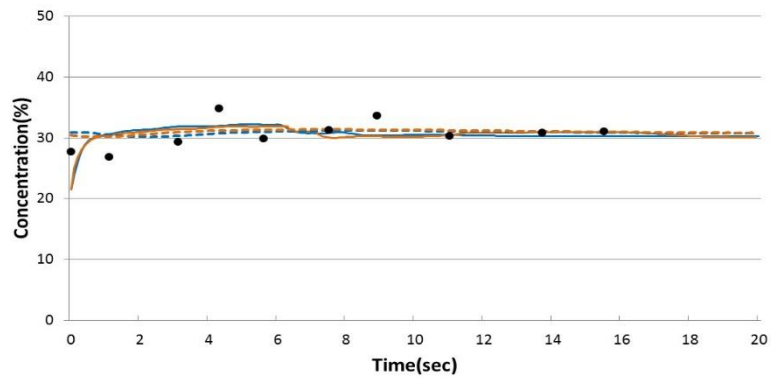
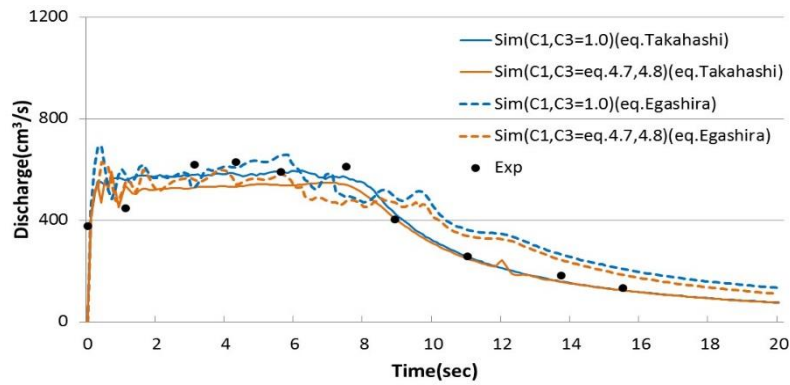


(a) Upper Sabo Dam

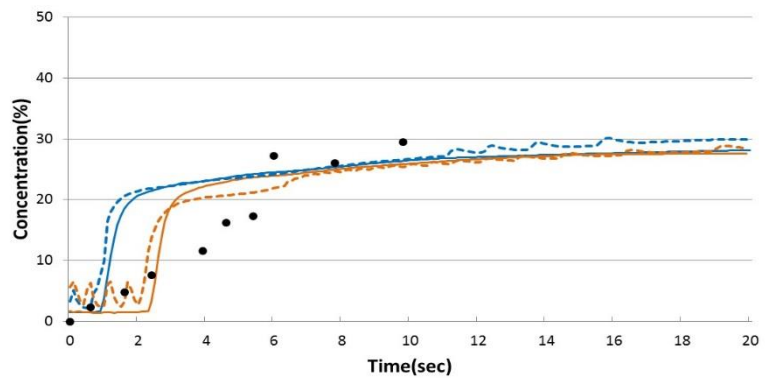
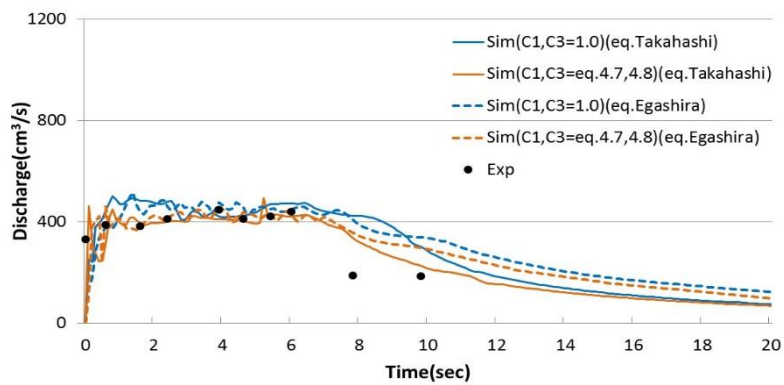


(b) Lower Sabo Dam

Figure 4.17 Debris flow discharge and sediment concentration using discharge coefficient equation that is determined by sediment concentration (Case C-1)

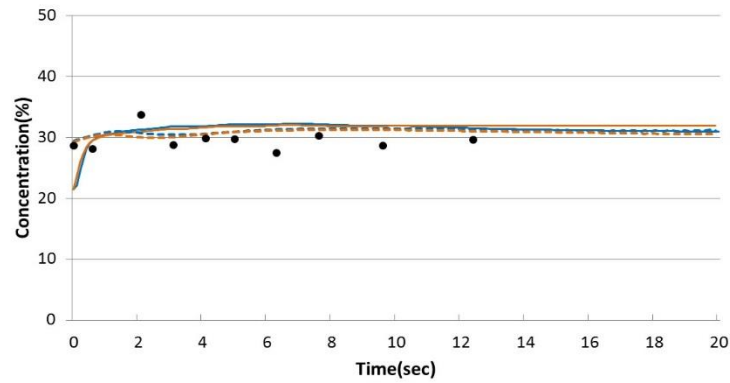
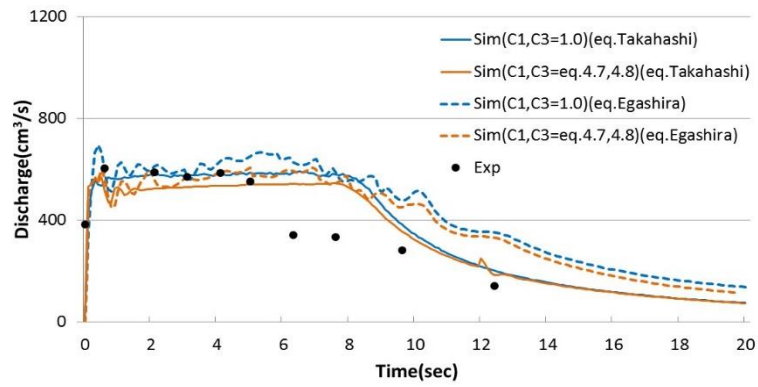


(a) Upper Sabo Dam

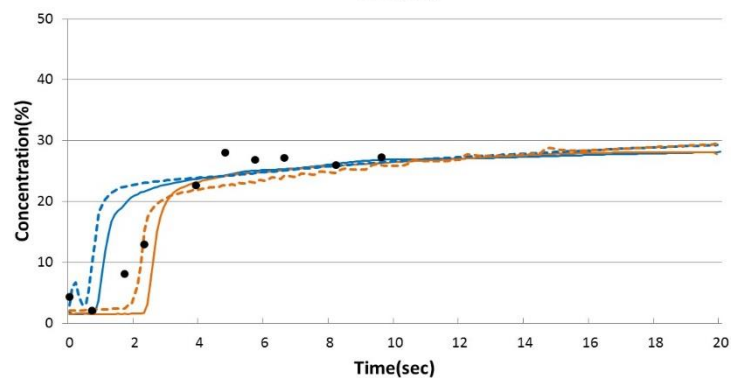
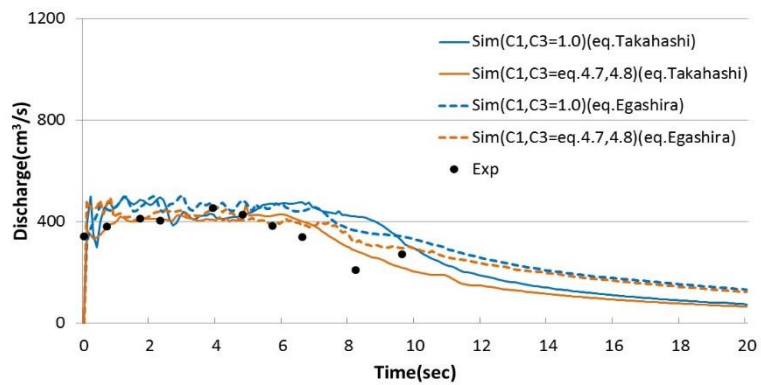


(b) Lower Sabo Dam

Figure 4.18 Debris flow discharge and sediment concentration using discharge coefficient equation that is determined by sediment concentration (Case C-2)

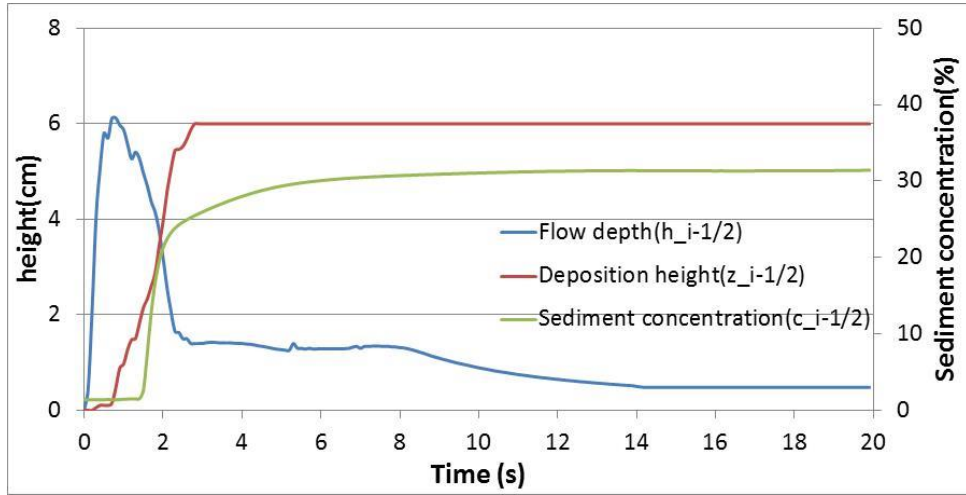


(a) Upper Sabo Dam

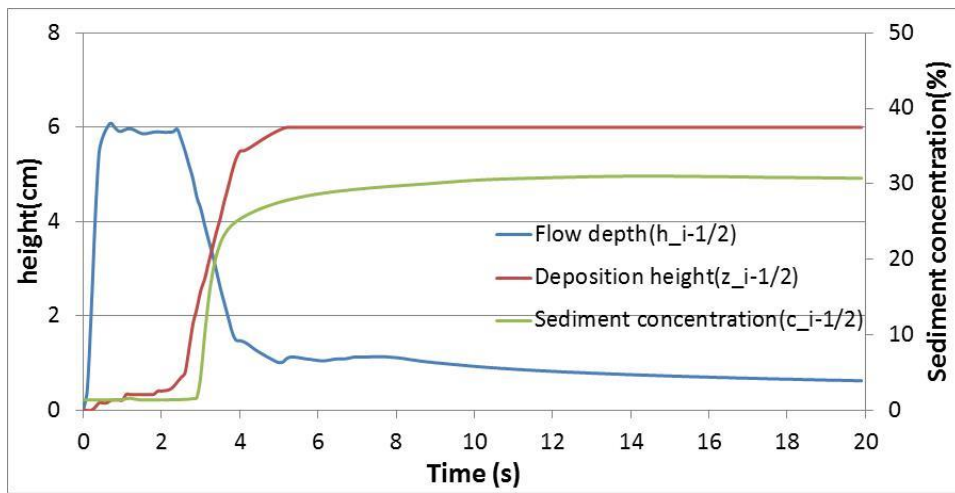


(b) Lower Sabo Dam

Figure 4.19 Debris flow discharge and sediment concentration using discharge coefficient equation that is determined by sediment concentration (Case C-3)

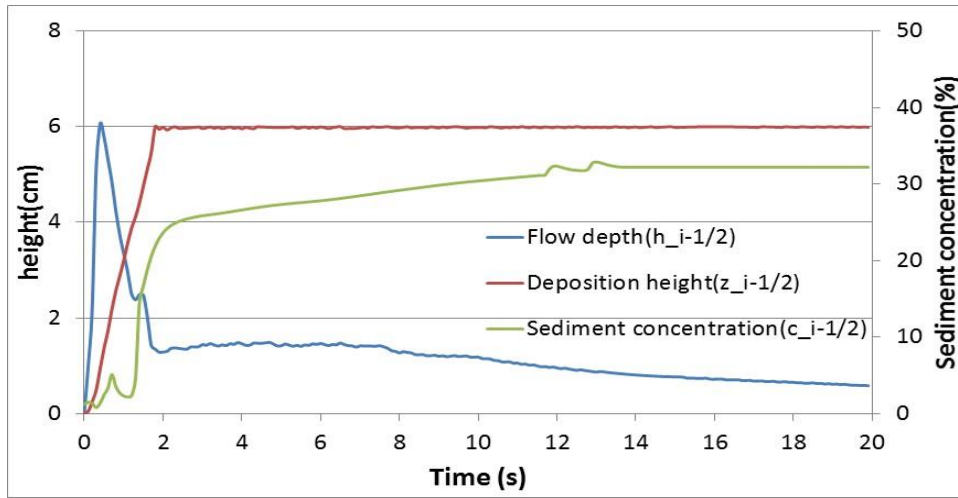


(a) Discharge coefficients are used 1.0

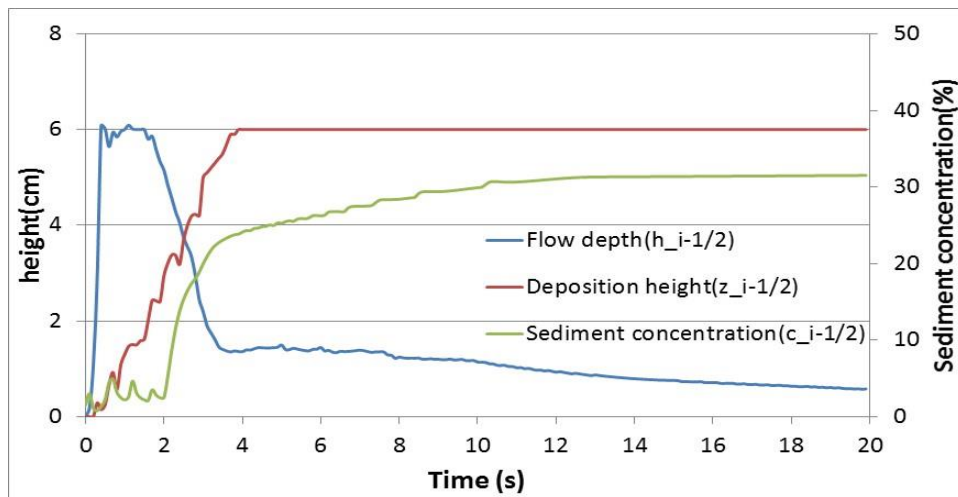


(b) Discharge coefficients are used equation 4.7, and equation 4.8

Figure 4.20 Debris flow depth, deposition height, and sediment concentration just upstream of lower Sabo dam.(Case C-1)(equation of Takahashi et al.)



(a) Discharge coefficients are used 1.0



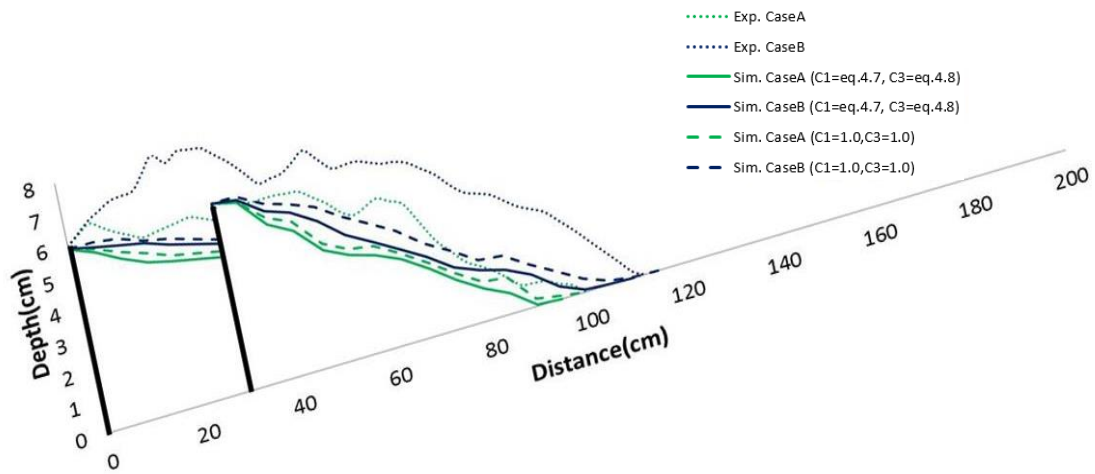
(b) Discharge coefficients are used equation 4.7, and equation 4.8

Figure 4.21 Debris flow depth, deposition height, and sediment concentration just upstream of lower Sabo dam.(Case C-1)(equation of Egashira et al.)

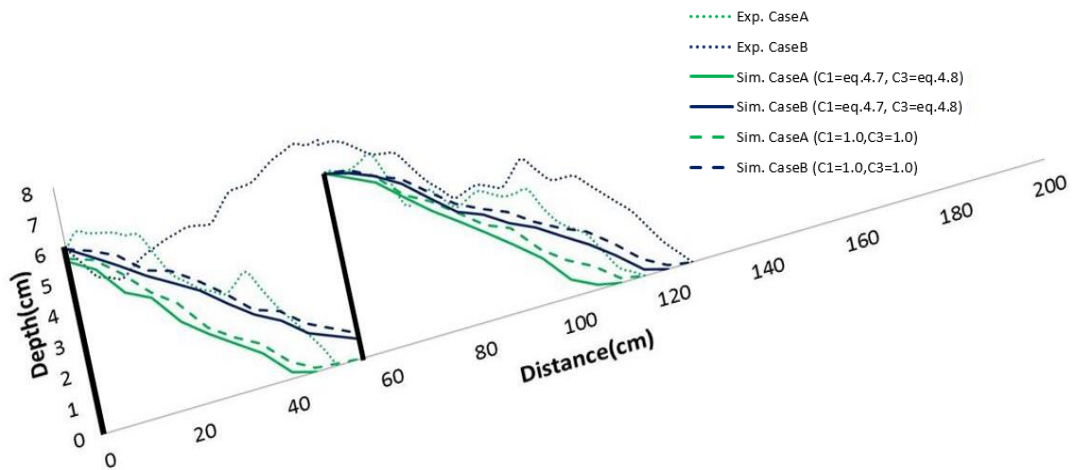
Though adjust the equations 4.7 and 4.8, debris flow deposition process are changed. Figure 4.22, and Figure 4.23 show the final debris flow deposition upstream of the Sabo dam by Takahashi et al.(1992)' equation, and Egashira et al.(1993a)'s equation in case A, and B. As equations 4.7 and 4.8 are applied to the discharge coefficient, deposition height and deposition length are underestimated compared with that in case of discharge coefficient equal to 1.0.

Thus, the simulation results using Takahashi et al.(1992)'s equation are more underestimated compared with experimental results. By contrast, the simulation results using Egashira et al.(1993a)'s equation are more suited with experimental results. However, debris flow deposition height at lower dam in Case B-1, and B-2 are underestimated compared with experimental results. This may due to the boundary conditions of the Sabo dam. In the experiment, as debris flow captured by the Sabo dam, bed gradient is changed gently. And then, debris flow velocity is decreased. This debris flow has greater deposition than erosion. In the simulation, the erosion and deposition velocity that have been given by Takahashi et al.(1992) are not described this state. However, the erosion and deposition velocity that have been given by Egashira et al.(1993a) are described this state. Because erosion and deposition velocity is described as debris flow velocity and bed gradient. However, the reason why although debris flow deposition height is underestimated at lower Sabo dam, Case B-1 and B-2 using Egashira et al.(1993a)'s equation is that calculation method of bed gradient just downstream of Sabo dam. Bed gradient is calculated at the center of the cell. This bed gradient is calculated by the average bed gradient at the in front of the cell and bed gradient at behind of the cell. However, bed gradient just downstream of Sabo dam is calculated by average bed gradient at the in front of the cell and its own bed gradient. In other words, bed gradient just downstream of Sabo dam is not affected by upstream of Sabo dam.

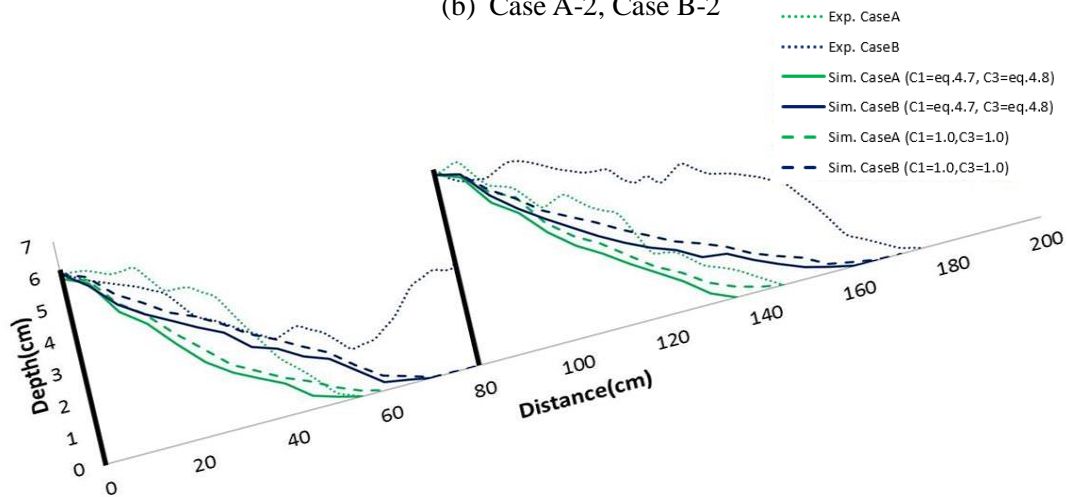
Figure 4.24, and Figure 4.25 show the debris flow deposition process in case C. Time 0 means the debris flow's arrival time to the upper Sabo dam. As apply the discharge coefficient equation 4.7 and 4.8 in the simulation, deposition process are under estimated compared with in case of discharge coefficient equal to 1.0. This means that debris flow deposition is slower when discharge coefficient is determined by equation 4.7, and 4.8 than that in the case of discharge coefficient equal to 1.0.



(a) Case A-1, Case B-1

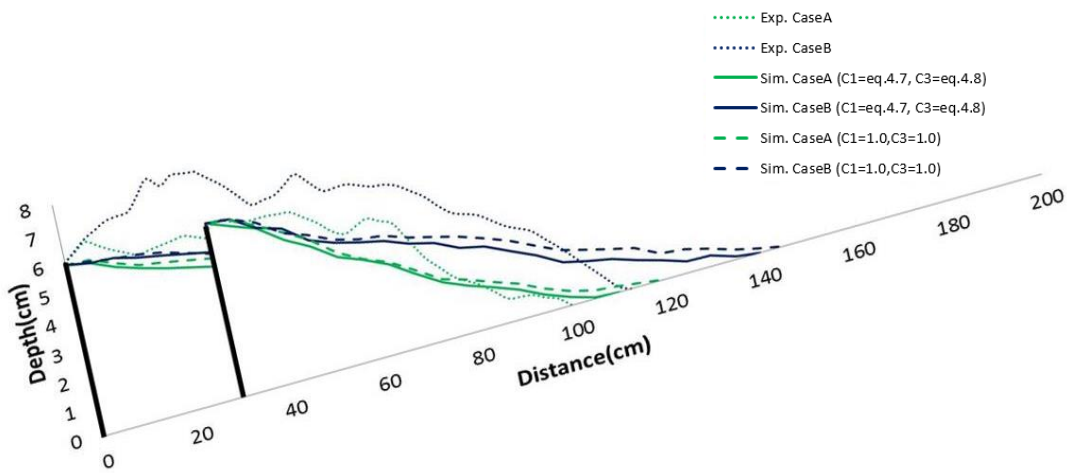


(b) Case A-2, Case B-2

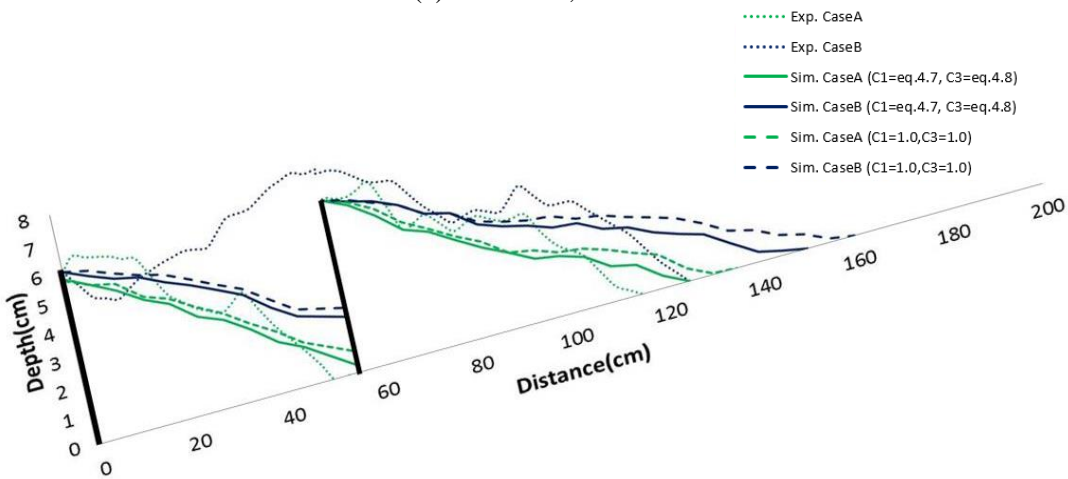


(c) Case A-3, Case B-3

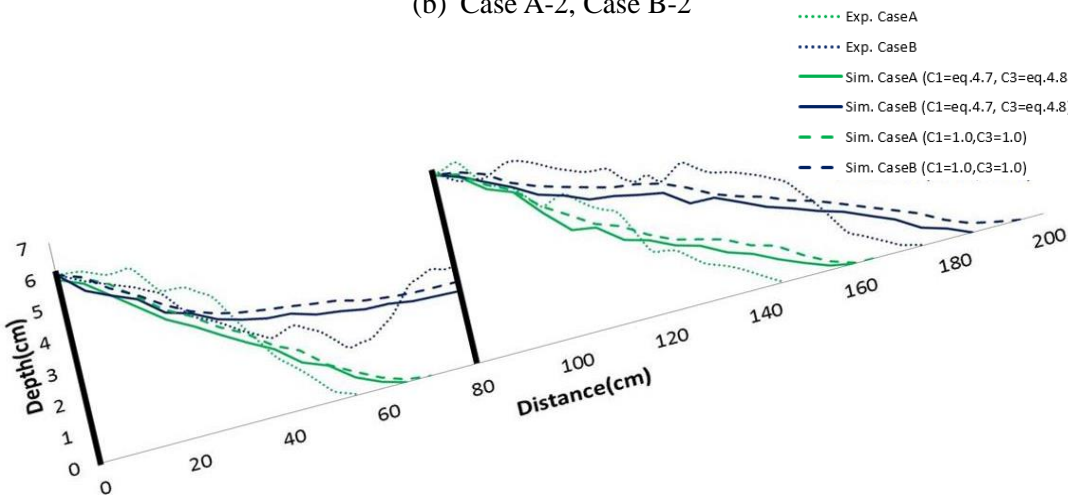
Figure 4.22 Final debris flow deposition upstream of the Sabo dam using discharge coefficient equation that is determined by sediment concentration (equations of Takahashi et al.)



(a) Case A-1, Case B-1

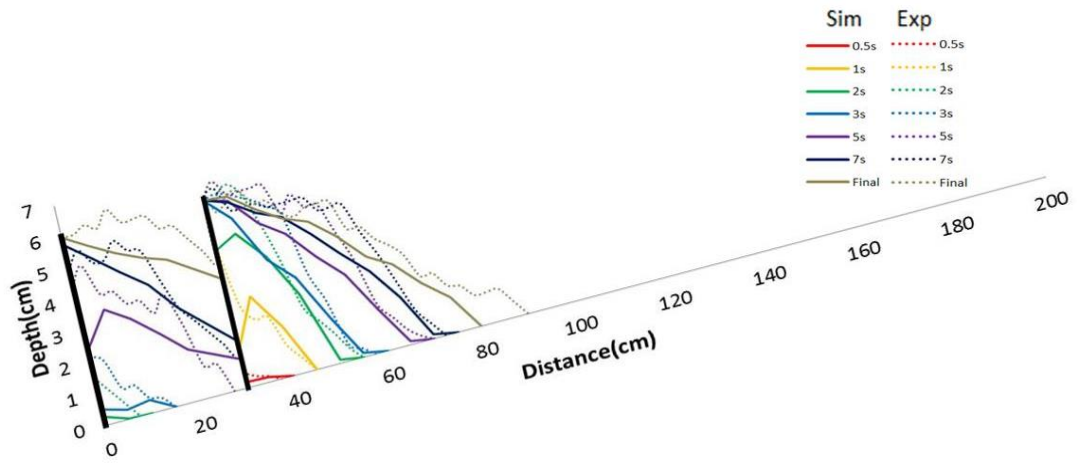


(b) Case A-2, Case B-2

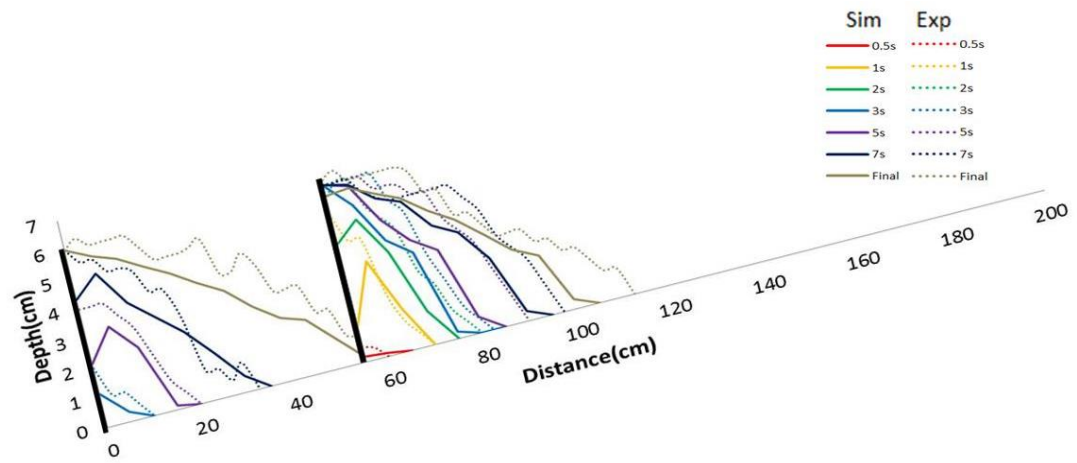


(c) Case A-3, Case B-3

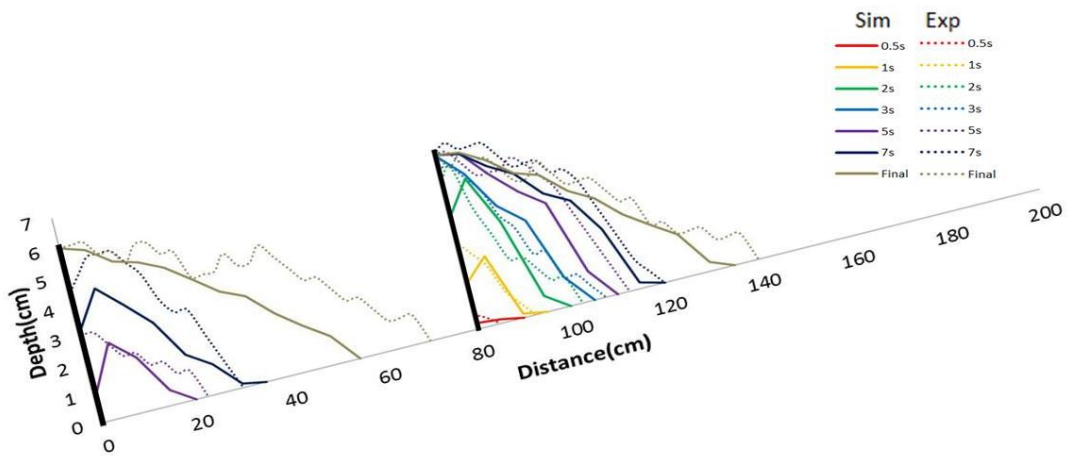
Figure 4.23 Final debris flow deposition upstream of the Sabo dam using discharge coefficient equation that is determined by sediment concentration (equations of Egashira et al.)



(a) Case C-1

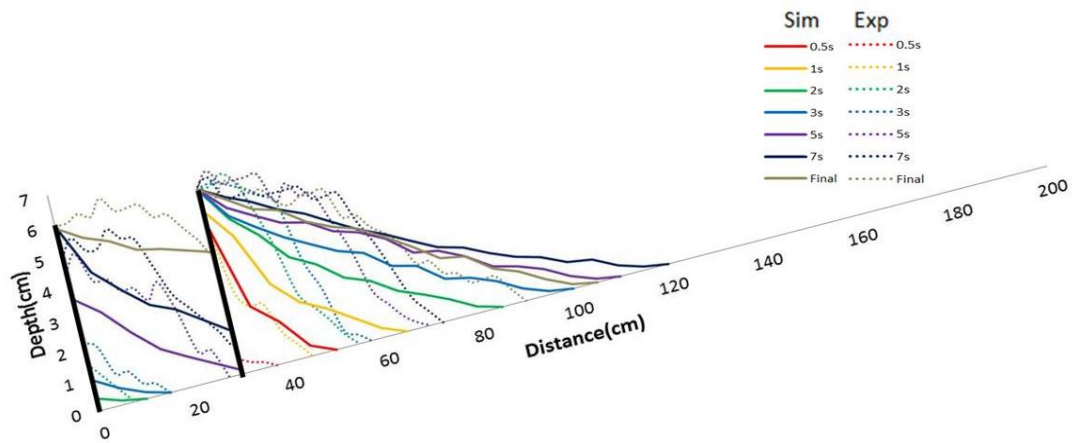


(b) Case C-2

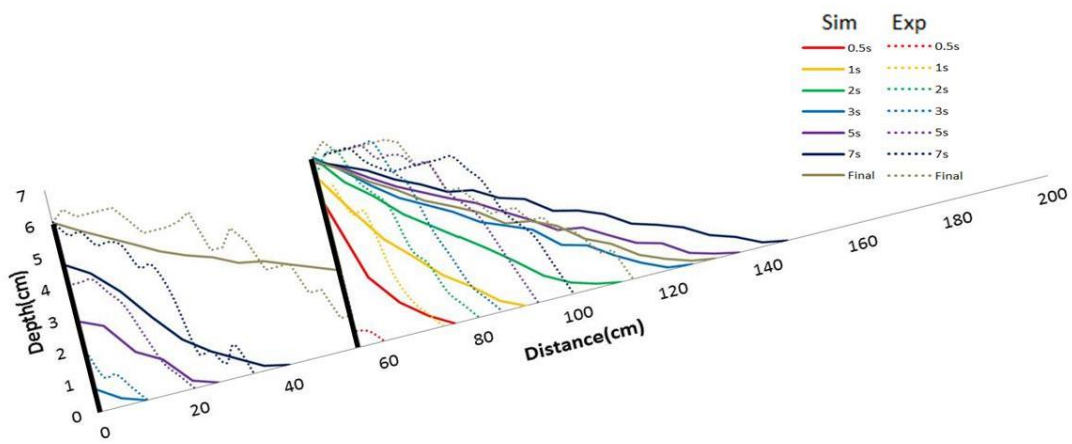


(c) Case C-3

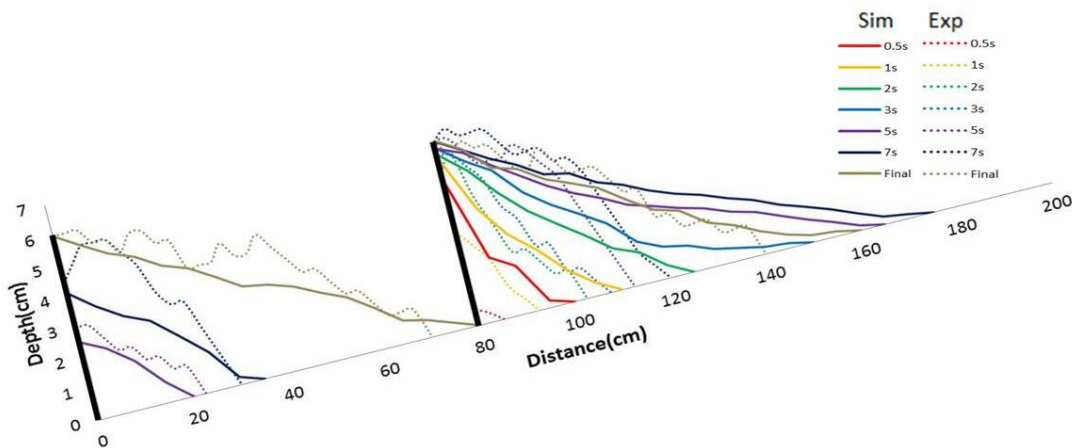
Figure 4.24 Debris flow deposition process upstream of the Sabo dam using discharge coefficient equation that is determined by sediment concentration (equations of Takahashi et al.)



(a) Case C-1



(b) Case C-2



(c) Case C-3

Figure 4.25 Debris flow deposition process upstream of the Sabo dam using discharge coefficient equation that is determined by sediment concentration (equations of Egashira et al.)

4.5 Summary

This chapter describes the discharge coefficient of the overflow equation and free overfall equation. Through RMSD analysis, the discharge coefficients are determined according to the position of Sabo dam and each equation. Also, based on the analysis of the experimental study, a new equations are obtained by sediment concentration. In the overflow situation and free overfall situation, discharge coefficient increases as sediment concentration increases.

As applying equation 4.7 and 4.8 the discharge coefficient, simulation results of debris flow discharge and sediment concentration at the Sabo dam were in good agreement with experimental result. In the debris flow deposition, simulation results using Takahashi et al.(1992)'s equation were underestimated. This could be adjusted by more feasible coefficient of erosion velocity and coefficient of deposition velocity. In contrast, simulation results using Egashira et al.(1993a)'s equation were overestimated. If the bottom of the bed is movable, more reliable results will be obtained.

CHAPTER 5

CONCLUSIONS

AND RECOMMENDATIONS

In this study, laboratory experiments and numerical simulations were conducted to study the debris flow reduction effect by arrangement of Sabo dams. A one-dimensional numerical model was developed to simulate the debris flow deposition upstream of a series of Sabo dams and to calculate the debris flow outflow discharge at the dam point. First, Takahashi et al's(1992) and Egashira et al's(1993a) debris flow deposition velocity models are applied to evaluate the debris flow capture capacity by arrangement of Sabo dams. Second, debris flow discharge at the Sabo dams is calculated by the overflow equation and free overfall equation. In fact, these equations are used for clear water at a weir. However, they are applicable to debris flow in the numerical model. Finally, the calculated overflow debris flow discharge was adjusted by the discharge coefficient. Discharge coefficients were determined by RMSD analysis and regression analysis considering the sediment concentration. The simulated results were compared with those obtained from the laboratory experiments. These conclusions are presented in the following.

5.1 Conclusions

The conclusions of this study are summarized as follows.

Debris flow depositions upstream of a series of Sabo dams

The debris flow deposition process was presented to investigate the debris flow reduction effect

according to the location of Sabo dams. The debris flow deposition upstream of a Sabo dam was investigated using the constitutive equations of Takahashi et al.(1997) and those of Egashira et al.(1997). The experiments were carried out in a fixed bed condition.

In the experimental results, the upper Sabo dam captured debris flow more than the lower Sabo dam. The sediment capture volume at the upper Sabo dam accounted for around 55%, and the lower Sabo dam accounted for about 45%, of the total captured volume. However, the distance between two Sabo dams was insufficient, and the upper Sabo dam was buried. This means that planned sediment gradient of the lower Sabo dam is close to bed gradient due to upper Sabo dam. In other words, a decrease in the distance between two Sabo dams leads to an increase in the equilibrium bed slope because of the upper Sabo dam.

The simulated results of debris flow deposition at a series of Sabo dams are in good agreement with the experimental results. However, some discrepancies are found in the shape of the deposition. The simulated results of Takahashi et al's(1992) equations were underestimated compared with the experimental results. In contrast, simulation results using Egashira et al's(1993a) equations were overestimated.

Debris flow discharge at a series of Sabo dams

A Sabo dam is a vertical obstruction over which debris must flow such as a weir. Therefore, to calculate debris flow discharge at the dam point, the overflow equation and free overfall equation are applied.

As debris flow goes by the Sabo dam, the total discharge of debris flow and peak discharge decreases. The greater the distance between two Sabo dams, the higher the rate of total discharge decrease. And the efficiency of the decrease rate of debris flow peak discharge at the lower Sabo dam is lower than at the upper Sabo dam. The sediment concentration also decreased as it passed the series of Sabo dams. However, the initial sediment concentration is lower than 5%. This means that debris flow that is not fully developed reaches the lower Sabo dam. In other words, the greater the distance between two Sabo dams, the easier it is for a fully developed debris flow to form. These simulated results of debris flow discharge and sediment concentration were consistent with the experimental results. Therefore, the overflow equations and free overfall equations were suitable for calculating debris flow discharge at the dam point.

Debris flow discharge coefficient

Laboratory experimental studies, RMSD analysis and regression analysis were carried out to determine the debris flow discharge coefficient. An incomplete overflow situation only occurred when the distance between two Sabo dams was 30cm. According to the distance between Sabo dam, position of Sabo dam, different discharge coefficients were calculated. The simulated results of debris flow discharge were in good agreement with the experimental results. However, the simulated results of sediment concentration were underestimated in comparison with the experimental results.

In the overflow equation and free overfall equations, discharge is calculated by flow depth. However, discharge coefficient is more affected by sediment concentration. So, discharge coefficient is suggested by calculating sediment concentration. Therefore, overflow debris flow discharge at the Sabo dam was evaluated sediment concentration compared with experimental studies. Finally, equation 4.7 and equation 4.8 are suggested to determined debris flow discharge.

5.2 Recommendations for Future researches

This study had led to an understanding of several aspects related to the estimation of debris flow discharge by arrangement of Sabo dams. Future work is required so as to improve the numerical model and experimental method. Several recommendations are discussed as follows.

- (a) Debris flow deposition upstream by arrangement of Sabo dams is described with the experimental results. In reality, debris flow deposition upstream of a Sabo dam is a very rapid deposition phenomenon. Therefore, the simulated results using Takahashi et al.'s(1992) equations are underestimated. They could be adjusted by erosion and deposition velocity coefficients, but they have limits. In contrast, the simulated results using Egashira et al.'s(1993a) equations are overestimated because the laboratory experiment was carried out on a fixed bed. If the bottom of the bed is movable, more reliable results will be obtained.
- (b) In this study, the closed-type Sabo dam is used. To suggest the best combination of a series of Sabo dams, a greater number of Sabo dams should be considered. And the open-type Sabo dam also should be considered.
- (c) In this study, a rectangular sand stopper was used to block the debris flow like a Sabo dam in the experiment. In the real field, closed-type Sabo dams have a crest. By changing the shape

of the Sabo dam in the experiment, overflow discharge will be improved.

- (d) To determine the discharge coefficient, flow depth and sediment concentration are considered. In fact, the discharge coefficient depends on many factors. It is necessary to investigate the parameters affecting the discharge coefficient.
- (e) Suggested equations for discharge coefficient have limitation that sediment concentration from 25% to 35%.
- (f) To investigate the effectiveness of a series of Sabo dams, it is necessary to consider the low land area that is the debris flow fan. To consider the debris flow fan, a two-dimensional numerical model is needed.
- (g) In this study, a one-dimensional numerical model was developed to investigate reduction effect by arrangement of Sabo dams. The model was verified only by using laboratory experimental results. In order to improve the model, it is necessary to verify the model actual field cases.

Reference

Armanini, A., Dellagiacom, F., and Ferrai L.: From the Check Dam to the Development of Functional Check Dams; Fluvial Hydraulics of Mountain Regions. Lecture Notes on Earth Sciences, Vol. 37, Springer, Berlin, 331-344, 1991.

Bagnold, R. A.: Experiments in a Gravity-Free Dispersion of Large Solid Spheres in a Newtonian Fluid Under Shear, Proc., Royal Soc. London, Ser. A, 225, pp.49–63, 1954.

Campbell, C. S.: Rapid Granular Flows. Ann. Rev. Fluid Mech, Vol. 22, pp.57-92, 1990.

Chatwin, S.C., J.W. Schwab and D. N., Swanston.: A Guide for Management of Landslide-Prone Terrain in the Pacific northwest 2nd, Land Management Hand book, No. 18, pp.153-155, 1994.

Chen, C. L.: Comprehensive Review of Debris Flow Modeling Concepts in Japan, Geol. Soc. Am. Rev. Eng Geol. Vol. VII, pp.13-29, 1987.

Di Silvio, G.: Soil Erosion and Conservation Part 2: Erosion Control Works. Lecture Notes, IHE, Delft, The Netherlands, 1991.

Egashira, S.: Mechanism of Sediment Deposition from Debris Flow (part 1), Journal of the Japan Society of Erosion Control Engineering, Vol. 46, No. 1, ser.186, pp.45-49, 1993a (in Japanese).

Egashira, S.: Review of Research Related to Sediment Disaster Mitigation, Journal of Disaster research, Vol. 2, No. 1, pp.11-18, 2007.

Evans, S., G.: Landslides and Surficial Deposits in Urban Areas of British Columbia: a review. Can. Geotech. J., 19: 269-288, 1982.

Frahoudi, J., Shahalami, H.5: Slope Effect on Discharge Efficiency in Rectangular Broad Crested Weir with Sloped Upstream Face. Int. J. Civ. Engng., V 3, N1, 2005.

Fujita, M., Mizuyama T., and Musashi Y.: Sediment Runoff Control by a Series of Sabo Dams. Proceedings of Hydraulic Engineering, Vol. 45, pp.697-702, 2001.

Gonzalez, C. A, Chanson, H.: Experimental Measurements of Velocity and Pressure Distributions on a Large Broad-Crested weir. Flow Measurement and Instrumentation 18:107-113, 2007.

Honda, N., Egashira, S.: Prediction of Debris Flow Characteristics in Mountain Torrents. In Proceedings of 1st International Conference on Debris-flow Hazards Mitigation, ASCE, pp.707-716, 1997.

Honda N., Egashira S.: Prediction of Debris Flow Characteristics in Mountain Torrents. In Proceedings of 1st International Conference on Debris-flow Hazards Mitigation, ASCE, pp.707-716, 1997.

HARRISON. A. J. M.: The Streamlined Broad-Crested Weir. Proc.-Inst. Civ. Eng., 38, pp.657–678, 1967.

Hunger, O., Evans, S. G., Bovis, M. J., and Hutchinson, J. N.: A Review of the Classification of Landslides of the Flow Type, Environmen. Eng. Geosci., No.78, pp.359-238, 2001.

Hunt, B.: Newtonian Fluid Mechanics Treatment of Debris Flows and Avalanches, J. Hydr. Engrg., ASCE, 120(12), pp.1350–1363, 1994.

Imran, J., Gary Parker, Jacques Locat, and Homa Lee.: 1D Numerical Model of Muddy Subaqueous and Subaerial Debris Flows, Journal of Hydraulic Engineering, ASCE, Vol. 127, No. 11, pp.959-968, 2001.

Iverson, R.M.: The Physics of Debris flows. Reviews of Geophysics, Vol. 35, Issue 3, pp. 245-296, 1997.

Johnson, A. M.: Physical Processes in Geology, Freeman, San Francisco, 1970.

Johnson, A. M., and McCuen, R. H.: Silt Dam Design for Debris Flow Mitigation. J. Hydraul. Eng., Vol. 115, No.9, pp.1293-1296, 1989.

Mizuyama, T., and Ishikawa, Y.: Technical Standard for the Measures Against Debris Flow (draft). Technical Memorandum of PWRI, No. 2632, 1988.

Nakagawa, H., Takahashi, T., Satofuka, Y. and Kawaike, K.: Evaluation of Efficiency of Sabo Facilities by Means of Numerical Simulation Methods, Annual Journal of Hydraulic Engineering, JSCE, Vol. 46, pp.665-670, 2002b (in Japanese).

Nakatani, K., Satofuka, Y., and Mizuyama, T. : Development of 'KANAKO', a Wide Use Debris Flow Simulator Equipped with GUI, Proc. of 32nd Congress of IAHR, Venice, Italy, CD-ROM, 10 pp., A2.c-182, 2007.

O'Brien, J. S. and Julien, P. Y.: Two-Dimensional Water Flood and Mudflow Simulation, J. Hydr. Engrg., ASCE, 119(2), pp.244-261, 1993.

Osanai, N., Mizuno, H., Mizuyama T.: Design Standard of Control Structures Against Debris Flow in Japan, Jurnal of Disaster Research, Vol. 5, no.3, 2010.

Osti, R., and Egashira, S.: Method to Improve the Mitigative Effectiveness of a Series of Check Dams Against Debris Flow, Hydrological processes, Vol.22, pp.4968-4996, 2008.

Shieh, C. L. and Tsai, Y. F.: Experimental Study on the Configuration of Debris-Flow Fan, in: Proceedings of the First International Conference on Debris-flow Hazards Mitigation: Mechanics, Prediction and Assessment, San Francisco, California, pp.133-142, 1997.

Stranb, S.: Schneltes Granulares Fliegen in Subaerischen Pyroklastischen Strömen. Dissertation an der Bayerischen Julius- Maximilians-Universit~it Wiirzburg, 1995.

Takahashi, T.: Mechanical Characteristics of Debris flow, J.Hydr. Div., ASCE, 104(8), pp.1153-1169, 1978.

Takahashi, T., Nakagawa, H., Harada, T. and Yamashiki, Y.: Routing Debris Flows with Particle Segregation, Journal of Hydraulic Engineering. ASCE, Vol. 118, No.11, pp.1490-1507, 1992.

Takahashi, T. and Nakagawa, H.: Flood/Debris Flow Hydrograph Due to Collapse of a Natural Dam by Overtopping, Journal of Hydrosience and Hydraulic Engineering, JSCE, Vol. 12, No. 2, pp.41-49, 1994.

Takahashi, T.: Debris flow: Mechanics, Prediction and Countermeasures. Taylor & Francis/Balkema, pp. 1-448, 2007.

VanDine, D., F.: Debris Flows and Debris Torrents in the Sourhern Canadian Cordillera. Can. Geotech. J., 22:44-68, 1985

VanDine, D. F. and Bovis, M.: History and Goals of Canadian Debris-Flow Research, Nat. Hazards, Vol.26(1), pp.67-80, 2002.

Varnes, D. J.: Slope Movement Types and Processes: in Landslides Analysis and control (Scguster, R.L. and Krizek, R.J. eds.), NAS Sp. Rep. 179:11-33, 1978.

List of Figures

Figure 1.1	Sediment-related disasters	1
Figure 1.2	Number of debris flow occurrences in Japan	2
Figure 1.3	Number of dead and missing in Japan	2
Figure 1.4	Debris flow at Hougawachi, Kumamoto Prefecture, Japan	4
Figure 1.5	Debris flow at Kuratsukuri, Miyama Town, Asuwa Gun, Fukui Prefecture Japan	4
Figure 1.6	Takahashis' classification of slope movements	6
Figure 1.7	Classification countermeasures against sediment hazards(Egashira., 2007)	7
Figure 1.8	Lateral walls(channel)	8
Figure 1.9	Debris flow captured by closed-type Sabo Dam . Oita Prefecture, Japan, 12 July, 2012.	9
Figure 1.10	Open-type Sabo Dam	10
Figure 1.11	Non-structure countermeasure	11
Figure 1.12	A series of Sabo Dam	13
Figure 2.1	Sediment storage capacity of a Sabo dams	16
Figure 2.2	Debris-flow-capturing process	16
Figure 2.3	Experimental flume	18
Figure 2.4	Experimental Sabo dam	19
Figure 2.5	Upstream deposited sediment	19
Figure 2.6	Particle size distribution of sediment materials	20
Figure 2.7	Upstream part of the flume	21
Figure 2.8	Experimental method	21
Figure 2.9	Sampler boxes	23

Figure 2.10	Experimental setup	23
Figure 2.11	Debris flow captured volume	24
Figure 2.12	Final debris flow deposition upstream of Sabo dams	25
Figure 2.13	Final debris flow deposition upstream of Sabo dams(picture)	26
Figure 2.14	Debris flow deposition process upstream of Sabo dams	27
Figure 2.15	Clear water discharge at the outlet flume without Sabo dam	28
Figure2.16	Debris flow discharge, sediment discharge, and sediment concentration without Sabo dam	29
Figure 2.17	Debris flow discharge at each Sabo dams	32
Figure 2.18	Sediment concentration at each Sabo dams	33
Figure 2.19	Sediment distributions	35
Figure 3.1	Coordinate of uniform debris flow	42
Figure 3.2	Ratio of the quasi-static skeletal pressure to the total pressure according to Takahashi et al. (1997) and Egashira et al. (1997)	46
Figure 3.3	Definition of the variables	47
Figure 3.4	Overflow situation	48
Figure 3.5	Free overfall situation	48
Figure 3.6	Definition of arrangement of variables on meshes	50
Figure 3.7	The way of advancing the calculation	51
Figure 3.8	Final debris flow deposition upstream of the Sabo dam (equations of Takahashi et al.)	55
Figure 3.9	Final Debris flow deposition upstream of the Sabo dam (equations of Egashira et al.)	56
Figure 3.10	Debris flow deposition process upstream of Sabo dam(equations of Takahashi et al.)	57

Figure 3.11	Debris flow deposition process upstream of the Sabo dam(equations of Egashira et al.)	58
Figure 3.12	Clear water discharge at the outlet flume without Sabo Dam	59
Figure 3.13	Debris flow discharge and sediment concentration at the outlet flume without Sabo Dam	60
Figure 3.14	Debris flow discharge of the Sabo dams (equation of Takahashi et al.)	62
Figure 3.15	Sediment concentration (equation of Takahashi et al.)	63
Figure 3.16	Debris flow discharge of the Sabo dams (equation of Egashira et al.)	64
Figure 3.17	Sediment concentration (equation of Egashira et al.)	65
Figure 4.1	Experimental set up	70
Figure 4.2	Debris flow hit the deposited sediment	70
Figure 4.3	Time changeable to debris flow deposition	71
Figure 4.4	Particle size distribution of sediment materials	71
Figure 4.5	Bottom of the flume	71
Figure 4.6	Definition of the variables	72
Figure 4.7	Bed elevation($z_{i-1/2}$)	73
Figure 4.8	Debris flow discharge and sediment concentration (Case C-1)	75
Figure 4.9	Debris flow discharge and sediment concentration (Case C-2)	76
Figure 4.10	Debris flow discharge and sediment concentration (Case C-3)	77
Figure 4.11	Relationship between flow depth and discharge (Case D-1)	79
Figure 4.12	Experimental results in Case D-1	80
Figure 4.13	Relationship between discharge coefficient and sediment concentration in case of overflow situation	81
Figure 4.14	Relationship between discharge coefficient and sediment concentration in	

	case of free overfall situation	81
Figure 4.15	Discharge coefficient	81
Figure 4.16	Applied discharge coefficient by sediment concentration (Case D-1)	84
Figure 4.17	Debris flow discharge and sediment concentration using discharge coefficient equation that is determined by sediment concentration (Case C-1)	86
Figure 4.18	Debris flow discharge and sediment concentration using discharge coefficient equation that is determined by sediment concentration (Case C-2)	87
Figure 4.19	Debris flow discharge and sediment concentration using discharge coefficient equation that is determined by sediment concentration (Case C-3)	88
Figure 4.20	Figure 4.19 Debris flow depth, deposition height, and sediment concentration just upstream of lower Sabo dam.(Case C-1)(equation of Takahashi)	89
Figure 4.21	Figure 4.19 Debris flow depth, deposition height, and sediment concentration just upstream of lower Sabo dam.(Case C-1)(equation of Egashira)	90
Figure 4.22	Final debris flow deposition upstream of the Sabo dam using discharge coefficient equation that is determined by sediment concentration (equations of Takahashi et al.)	92
Figure 4.23	Final debris flow deposition upstream of the Sabo dam using discharge coefficient equation that is determined by sediment concentration (equations of Egashira et al.)	93
Figure 4.24	Debris flow deposition process upstream of the Sabo dam using discharge coefficient equation that is determined by sediment concentration (equations of Takahashi et al.)	94
Figure 4.25	Debris flow deposition process upstream of the Sabo dam using discharge coefficient equation that is determined by sediment concentration (equations of Egashira et al.)	95

List of Tables

Table 1.1	Varnes' classification of slope movements	5
Table 2.1	Sediment material	19
Table 2.2	Experimental conditions	22
Table 2.3	Experimental conditions	22
Table 2.4	Debris flow and sediment peak discharge	31
Table 2.5	Sediment size distribution	34
Table 3.1	Varnes' classification of slope movements	38
Table 3.2	Flow conditions at Sabo dam	49
Table 3.3	Parameters for numerical simulation	54
Table 3.4	Debris flow peak discharge	66
Table 4.1	Experimental conditions	69
Table 4.2	Discharge coefficient by RMSD value	74
Table 4.3	Regression analysis in case of overflow situation(Sediment concentration)	82
Table 4.4	Regression analysis in case of overflow situation(Sediment concentration)	83

Curriculum Vitae

Name Namgyun KIM

Citizenship Republic of Korea

Date of Birth September 1, 1986

E-mail knkblue2@hanmail.net

Ph.D. Student (2011 ~ 2015)
Department of Civil and Earth Resources Engineering
Kyoto University, Kyoto, Japan

M. Sc. (2009~2011)
Department of Disaster Prevention Engineering
Gangwon National University, Samcheok, Republic of Korea

B.E. (2005~2009)
Department of Fire & Disaster prevention Engineering
Gangwon National University, Samcheok, Republic of Korea

Papers based on the Thesis

Kim, N., Nakagawa, H., Kawaike, K., and Zhang, H.: A study on improvement of capture capacity by the arrangement of sabo dam. *31st Annual meeting of Japan Society for Natural Disaster Science*, pp.73-74, September, 2012.

Kim, N., Nakagawa, H., Kawaike, K., and Zhang, H.: A study on debris flow deposition by the arrangement of sabo dam. *Annual Journal of Hydraulic Engineering*, JSCE, Vol. 57, pp.I_97-I_102, February, 2013.

Kim, N., Nakagawa, H., Kawaike, K., and Zhang, H.: Influence of a series of sabo dams on debris flow deposition. *Annals of the Disaster Prevention Research Institute*, Kyoto University, No. 56B, pp.531-538, June, 2013.

Kim, N., Nakagawa, H., Kawaike, K., and Zhang, H.: Numerical simulation on debris flow with a series of sabo dam. *32nd Annual meeting of Japan Society for Natural Disaster Science*, pp.3-4, September, 2013.

Kim, N., Nakagawa, H., Kawaike, K., and Zhang, H.: One dimensional numerical simulation on debris flow of sabo dam. *Annals of the Disaster Prevention Research Institute*, Kyoto University, No. 56B, pp.415-424, February, 2014.

Kim, N., Nakagawa, H., Kawaike, K., and Zhang, H.: A study on debris flow outflow discharge at a series of sabo dams. *Journal of Japan Society for Natural Disaster Science*, Vol. 33, Special Issue., pp.43-52, September, 2014.